Sur l'élaboration des composites SiC/Al par le procédé au K2ZrF6 bases physico-chimiques et incidence sur la résistance des fibres

Sylvie Schamm-Chardon

N° d'ordre : 302

THÈSE

PRESENTÉE A

L'UNIVERSITÉ DE BORDEAUX I

POUR OBTENIR LE GRADE DE

DOCTEUR

Spécialité : SCIENCES DES MATÉRIAUX

PAR

Sylvie SCHAMM

Ingénieur ENSCPB

SUR L'ÉLABORATION DES COMPOSITES SiC/Al PAR LE PROCÉDÉ AU K_2ZrF_6

BASES PHYSICO-CHIMIQUES ET INCIDENCE SUR LA RÉSISTANCE DES FIBRES

Soutenue le 7 juillet 1989, devant la commission d'examen :

MM.	P. HAGENMULLER	*Président*
	R. COHEN-ADAD	
	C. BERNARD	
	J. ETOURNEAU	
	B. BAUDELET	*Examinateurs*
	J. GRANNEC	
	R. NASLAIN	

-1989-

à Jean-Yves

Sans vous deux, qui avez su donner le meilleur de vous-mêmes à vos six enfants, cette thèse ne serait pas

Pour vous ma plus tendre affection

Cette étude a été réalisée au Laboratoire de Chimie du Solide du CNRS de l'Université de Bordeaux I. Je tiens à exprimer toute ma reconnaissance à Monsieur le Professeur P. HAGENMULLER pour m'avoir accueillie dans son Laboratoire et pour avoir accepté de présider le jury de cette thèse.

Monsieur le Professeur J. ETOURNEAU, Directeur actuel du Laboratoire de Chimie du Solide, m'a fait l'honneur d'examiner ce travail et de participer à mon jury de thèse; je l'en remercie vivement.

J'ai été très sensible à la bienveillance que m'a montrée Monsieur R. COHEN-ADAD, Professeur à l'Université de Lyon I, par ses remarques éclairées sur l'étude thermodynamique et en acceptant de juger ce mémoire. Qu'il veuille bien agréer mes respectueux remerciements.

Que Monsieur C. BERNARD, Directeur de Recherche au LTPCM de Grenoble, trouve ici l'expression de ma sincère gratitude pour son accueil chaleureux et les conseils fructueux qu'il m'a prodigués avec une égale patience.

Monsieur B. BAUDELET, Professeur à l'INP de Grenoble, a bien voulu juger cette étude; je le remercie et suis honorée de l'intérêt qu'il y a porté.

Monsieur le Professeur R. NASLAIN, Directeur du Laboratoire des Composites Thermostructuraux, a assuré la direction scientifique de cette thèse. Je suis heureuse de pouvoir lui exprimer ici ma gratitude pour m'avoir guidée de ses conseils et soutenue de ses encouragements au cours de ces années de recherches.

Monsieur J. GRANNEC, Professeur à l'Université de Bordeaux I, m'a fait bénéficier de sa compétence dans le domaine de la chimie des fluorures. Je lui en suis très reconnaissante ainsi que d'avoir accepté de participer à ce jury de thèse.

Je veux aussi remercier Monsieur L. RABARDEL, Ingénieur de Recherche au LCS, pour sa collaboration et pour m'avoir fait profiter des avantages du microcalorimètre différentiel à flux qu'il vient de développer.

Monsieur Y. LE PETITCORPS, Maitre de Conférences à l'Université de Bordeaux I, m'a accompagnée avec compétence, gentillesse et disponibilité pour une part de ce travail. Qu'il soit assuré de ma sincère amitié.

Que tous les membres du groupe 'Composites à Matrice Métallique' trouvent ici le témoignage de ma reconnaissance pour leur constante sollicitude; plus particulièrement, Monsieur J.M. QUENISSET pour les dicussions fructueuses que nous avons eues, Monsieur R. FEDOU pour sa contribution ainsi que Messieurs L. ALBINGRE et D. ROCHIER pour leur aide amicale.

Je ne voudrais pas oublier de nommer ceux du Laboratoire de Chimie du Solide qui ont contribué à la réalisation de ce travail : Monsieur G. LE FLEM pour son aide dans l'étude de divers travaux russes, Monsieur J.P. CHAMINADE pour m'avoir largement permis d'utiliser ses dispositifs de manipulation en atmosphère contrôlée, Monsieur M. LAHAYE pour les microanalyses X et Auger, Monsieur J.J. VIDEAU pour les analyses IR, Messieurs J.P. CAZORLA et L. TRUT pour les analyses X, enfin Messieurs J. LOZANO et J. VILLOT pour leur compétence technique.

Merci aussi à Mademoiselle C. DUPOUY, Monsieur E.Bouillon, Madame J. BRET ainsi que l'équipe MEA du CEMES-LOE de Toulouse dont j'ai le plaisir de faire partie actuellement sous la bienveillante direction de Monsieur J. SEVELY. Ils ont su me permettre de mener à bien la réalisation de ce mémoire.

Enfin, je citerai le Ministère de la Recherche et de la Technologie pour le soutien financier qu'il m'a apporté dans cette étude.

SOMMAIRE

CHAPITRE II

CHAPITRE III

INTRODUCTION GENERALE

INTRODUCTION GENERALE

L'idée d'associer des matériaux aux caractéristiques complémentaires au sein d'un même solide, appelé composite, en vue de lui conférer un ensemble de propriétés originales a permis de répondre aux exigences spécifiques des industries aéronautique et aérospatiale que ne pouvaient plus satisfaire les matériaux traditionnels. Depuis, les potentialités de cette technologie ont attiré l'attention et l'intérêt de beaucoup d'autres secteurs d'application tels que l'automobile et même les sports de haute compétition, le choix des constituants du composite pouvant être extrêmement varié. Cependant les composites, matériaux synthétiques qui supposent l'enrobage de l'un des constituants, le renfort, par l'autre, la matrice, sont des matériaux complexes. Aussi, bien que les plus anciens d'entre eux, les composites à matrice organique, aient rapidement connu un développement industiel, l'élaboration et les propriétés de leurs homologues à matrice métallique ou céramique, destinés à des applications respectivement à moyenne et à haute température, posent encore des problèmes tant fondamentaux que technologiques.

L'intérêt de l'approche composite est de permettre d'obtenir des matériaux à caractéristiques mécaniques spécifiques (rapportées à la densité du matériau) plus élevées que celles des métaux et des matières plastiques traditionnels. L'utilisation de renforts fibreux, caractérisés par une résistance à la rupture et un module d'Young élevés et disposés de manière uni- ou multi-directionnelle au sein d'une matrice, confère en plus à ces matériaux un caractère anisotrope, i.e. la possibilité de supporter des contraintes suivant des directions prédéfinies de forte sollicitation. L'emploi d'une matrice métallique plutôt que d'une matrice organique, outre le fait

qu'il permet d'étendre le domaine d'utilisation en température des composites à 350-600°C au lieu de 200°C, leur confère de nouveaux avantages. Ils ont une excellente tenue à l'environnement (absence de vieillissement aux UV, insensibilité à l'humidité) et ne dégazent pas sous vide. Leur résistance et leur rigidité sont plus élevées notamment dans la direction perpendiculaire aux fibres. Ils présentent une bonne conductivité thermique et électrique. Ces avantages justifient le regain d'intérêt que suscitent les matériaux composites à matrice métallique pour leur emploi comme matériaux structuraux dans le domaine aérospatial.

Ce travail concerne les matériaux composites à matrice métallique et plus spécifiquement les problèmes d'élaboration posés par le renforcement des alliages légers (i.e. à base d'aluminium) par des fibres longues de type céramique (SiC, C).

La mise en oeuvre de renforts fibreux au sein d'une matrice d'alliage léger peut se faire de deux manières différentes (1):

- la réalisation de **demi-produits** par imprégnation, généralement en continu, par l'aluminium liquide, des renforts fibreux sous forme de fils, de rubans ou de monocouches suivi de la mise en forme et de la consolidation des demi-produits par compression à chaud.
- l'**imprégnation de préformes** réalisées par tissage multidirectionnel de fibres longues multibrins selon des procédés proches des techniques de la fonderie et du forgeage.

Cependant aux températures d'élaboration des composites (i.e. 700-800°C), proches de la température de fusion de l'aluminium, les fibres de carbure de silicium (ou de carbone) sont mal mouillées par l'aluminium ($\theta \simeq 160°$). Le métal ne peut donc pas monter par capillarité entre les brins élémentaires d'une mèche ou dans les pores d'une préforme fibreuse multidirectionnelle. Le mouillage des fibres céramiques par l'aluminium liquide ($\theta \simeq 90°$) n'a lieu qu'à des températures plus élevées, de l'ordre de 900-950°C. Eusthatopoulos et coll. ont montré à ce sujet que la

présence d'une pellicule d'alumine à la surface de l'aluminium liquide empêchait le contact direct entre le métal et la céramique aux températures inférieures à 850-900°C et de ce fait retardait, en terme de température, la transition non mouillage-mouillage (2). Envisager l'élaboration des composites aux températures supérieures à 850°C, de façon à favoriser le mouillage, activerait thermiquement la formation du carbure d'aluminium Al_4C_3 qui peut avoir lieu dès 500°C par réaction directe entre l'aluminium et le carbone (3). Il en résulterait une dégradation excessive des fibres par dissolution dans l'aluminium, une fragilisation de la matrice et une sensibilité du matériau à la corrosion. Par ailleurs, les propriétés métallurgiques de l'aluminium en souffriraient.

De nombreuses méthodes ont été préconisées pour améliorer la mouillabilité des fibres céramiques par l'aluminium liquide. Elles font appel à deux types de technologies:

(i) le traitement préalable de la surface des fibres tels que le **traitement aux alcalins** (Na/Mg-Sn), les **dépôts métalliques** (Ni, Cu, Ag) et les **dépôts céramiques** (TiC, ZrC, composés Ti-B) (4)

(ii) l'**addition d'éléments d'alliage** spécifiques à l'aluminium (Li) (2,5)

Ces méthodes ont été le plus souvent établies de façon semi-empirique et les publications qui les décrivent (en général des brevets) contiennent peu d'informations sur leurs bases scientifiques. Grâce aux études réalisées sur le mouillage par les métaux liquides du carbone, des carbures et des métaux, il est possible d'expliquer les phénomènes physico-chimiques qui sous-tendent ces procédés (6,7). Dans tous les cas qui vont être cités, on remarquera que, en général, l'amélioration du mouillage est réalisée au détriment d'une fragilisation du composite et/ou du coût de mise en oeuvre.

(i) Les métaux liquides mouillent presque toujours les métaux solides et le degré de mouillabilité est d'autant meilleur que les deux métaux présentent une solubilité mutuelle ou forment un (ou des) composé(s) intermétallique(s) (6,7).

Le **traitement aux alcalins** qui a été essentiellement développé pour les fibres de graphite (à base Rayone ou PAN), consiste à immerger les fibres en continu et sous atmosphère d'argon, successivement dans un bain de Na à 550°C, dans un bain de Sn-2%Mg à 600°C et enfin dans le bain d'aluminium fondu (8). Le sodium formerait des composés d'intercalation avec le graphite (les ions positifs du métal s'insèrent entre les plans graphitiques de la fibre) et l'étain liquide à 600°C dissout le sodium (9). Ainsi, le dépôt intermédiaire du métal alcalin rend possible le mouillage de la fibre de graphite par l'étain. A son tour, l'aluminium liquide dissout le dépôt Na-Sn et mouille la fibre. L'expérience a cependant montré que l'infiltration des mèches par l'aluminium n'est complète qu'en présence de magnésium. Son rôle serait de stabiliser à la surface de la fibre le dépôt Na-Sn, devenu liquide pendant l'imprégnation par l'aluminium, grâce à la précipitation du composé intermétallique à haut point de fusion (772°C) qu'il peut former avec l'étain, Mg_2Sn. Cependant ni la formation du composé Mg_2Sn, ni celle de tout autre composé ternaire du type Na-Sn-Mg n'ont encore été démontrées (10). Les composites ainsi obtenus ont des propriétés mécaniques proches de celles théoriquement prévisibles grâce à la loi des mélanges. Malgré tout, la mise en oeuvre du procédé aux alcalins reste délicate (atmosphère contrôlée, produits inflammables).

Les **dépôts métalliques** de Ni, Cu, ou Ag sont en général réalisés par pulvérisation ionique, depôt électrolytique ou cémentation (4,11-14). Le nickel forme avec l'aluminium des composés intermétalliques stables tel que Al_3Ni. Mais bien que, en conséquence, le mouillage de la fibre soit excellent, le dépôt de métal et les composés intermétalliques qui se sont formés protègent mal la fibre contre toute attaque par l'aluminium (Al_4C_3) et les produits de réaction, Al_3Ni et Al_4C_3,

fragilisent la matrice. Par ailleurs, afin d'obtenir un bon mouillage de la fibre par l'aluminium, un dépôt continu, donc relativement épais (0,5 à 1 μm), doit être réalisé. Il en résulte une augmentation indésirable de la densité du composite pour les fractions volumiques élevées de fibres. La formation du composé intermétallique Al_3Cu et la forte solubilité de l'argent dans l'aluminium font aussi des revêtements respectivement de cuivre et d'argent des dépôts de choix pour promouvoir le mouillage des fibres céramiques par l'aluminium. Cependant, ces dépôts, de la même façon que le dépôt de nickel, conduisent à une mauvaise protection de la fibre, une fragilisation de la matrice et une densité élevée.

Contrairement aux dépôts métalliques, les **dépôts céramiques** protègent bien les fibres contre l'agression de l'aluminium liquide. Mais l'infiltration de mèches de carbone par du carbure de Ti ou de Zr à partir d'un mélange gazeux réactif (H_2+CH_4+$TiCl_4$ ou $ZrCl_4$) entre 700 et 1700 °C ne permet qu'une imprégnation partielle des mèches par l'aluminium liquide même en opérant sous une pression de 0,3 kPa bien que les carbures métalliques soient mieux mouillés par les métaux que les carbures covalents ou le carbone grâce à la formation de liaisons métal-métal à travers l'interface. Le plus efficace des revêtements céramiques est le codépôt de titane et de bore obtenu par réduction de vapeurs de $TiCl_4$ et BCl_3 en présence de vapeurs de zinc à 700°C. Ce revêtement qui pourrait être un mélange de Ti, B, TiB ou/et TiB_2 conduit à une bonne imprégnation des mèches par l'aluminium liquide. Il n'est, en revanche, plus efficace si les fibres sont exposées à l'air avant imprégnation.

Les traitements de surface précédents ne permettent en général que la réalisation de **demi-produits** (élaboration en continu sur mèches longues et sous atmosphère contrôlée). L'élaboration de pièces finies nécessite des opérations supplémentaires de consolidation et de mise en forme dont le coût de mise en oeuvre ne fait qu'accroître le prix de revient du matériau composite.

(ii) L'addition d'**éléments très électropositifs** tels Mg ou Ca mais surtout Li à l'aluminium permet d'obtenir un bon mouillage de SiC (ou C) bien que ce traitement ait été plutôt préconisé pour les fibres de Al_2O_3 (2,5). Les éléments plus électropositifs que l'aluminium se substituent à lui dans la couche d'alumine qui recouvre le métal liquide et diminuent sa compacité. L'aluminium liquide peut alors plus facilement diffuser à travers la couche d'oxyde et mouiller la céramique. Le lithium est particulièrement efficace dans la mesure ou il entraine une dislocation rapide du film d'oxyde (2). Cependant, l'imprégnation de préformes avec les alliages Al-Li ne peut se faire que sous vide de manière à éviter toute oxydation excessive du Li.

Ainsi, les méthodes développées précédemment pour améliorer le mouillage des renforts fibreux ((i) et (ii)), si elles ont fait preuve de leur efficacité au plan chimique, s'avèrent soit d'industrialisation délicate et coûteuse, soit dégradantes au plan mécanique.

Une méthode physique telle que le forgeage liquide (squeeze casting) est un autre moyen de compenser l'absence d'imprégnation spontanée des préformes céramiques par l'aluminium liquide. Elle consiste à appliquer une très forte pression, à l'aide d'un piston, sur le métal liquide qui a été préalablement coulé sur la préforme céramique placée dans un moule. Ainsi, d'une part, l'aluminium entre par force au sein du renfort, d'autre part, il se solidifie rapidement sous l'effet de la très haute pression (environ 100 MPa). En effet, la température de solidification de l'aluminium est augmentée (ΔT) proportionnellement à l'augmentation de la pression (ΔP, au dessus de la pression atmosphérique) conformément à l'équation de Clausius-Clapeyron :

$$\Delta T = \frac{T_f (V_l - V_s)}{H_f} \Delta P$$

où T_f, H_f, V_l, V_s sont respectivement la température de fusion à la pression atmosphérique, la chaleur latente de fusion, le volume spécifique de la phase liquide et le volume spécifique de la phase solide de l'aluminium (15). De plus, le gaz présent au sein de la préforme est chassé lors de l'application de la pression et remplacé par le métal liquide. Dans ce cas, le contact direct du métal sous pression avec les parois du moule de forgeage favorise l'évacuation rapide de la chaleur. Ce mode d'élaboration permet donc, en une seule opération, une imprégnation complète de préformes complexes, quelle que soit leur porosité résiduelle, tout en limitant le temps d'interaction fibre-matrice à haute température et en conduisant à une meilleure qualité métallurgique de l'aluminium. Les pressions utilisées restent cependant élevées. Elles peuvent être une source d'endommagement mécanique pour les préformes les plus rigides. De plus, elles nécessitent l'utilisation de presses de forte capacité lorsqu'il s'agit d'imprégner des pièces de taille significative. Leur mise en oeuvre devient alors coûteuse.

Toute technique simple permettant d'améliorer la mouillabilité du renfort ferait diminuer les pressions à appliquer et contribuerait à la limitation des coûts de production. C'est pour cette raison que J.P. Rocher et al., qui nous ont précédés dans cette étude, ont orienté leurs travaux vers la recherche d'un procédé de prétraitement spécifique qui puisse être utilisé pour des préformes complexes et autorise leur imprégnation par l'aluminium selon des techniques proches de celle utilisées actuellement en fonderie d'alliages légers (16). Le choix a été guidé par "l'idée de rechercher s'il existait, parmi les flux désoxydants déjà utilisés en fonderie d'alliages légers , des espèces chimiques qui seraient susceptibles de promouvoir le mouillage des fibres à base de C ou de SiC par les alliages d'aluminium". Sur ces bases, un procédé original d'élaboration des matériaux composites à matrice d'alliage léger a été développé avec succès et breveté (17). Dans son principe, il consiste à faire précipiter à la surface des fibres qui constituent le

renfort céramique des **microcristaux du fluorure K_2ZrF_6.** Ce dépôt s'effectue en imprégnant la préforme par une solution aqueuse du fluorure portée à ébullition. L'élimination du solvant s'opère ensuite par étuvage à 100°C. La préforme ainsi prétraitée peut alors être installée dans un moule de fonderie. L'ensemble moule-préforme est préchauffé, puis l'aluminium est coulé et pénètre la préforme spontanément par remontée capillaire (principe de la coulée par gravité).

L'intérêt et les avantages de ce procédé, communément appelé **procédé au K_2ZrF_6**, par rapport aux procédés précédemment décrits, résultent du fait qu'il:

- est de mise en oeuvre simple puisqu'il fait appel à des produits déjà rencontrés en fonderie d'aluminium et s'opère à l'air.
- ne nécessite aucune pression (dans le cas de nos préformes de laboratoire) hormis la pression métallostatique.
- s'applique à des préformes poreuses de différentes natures (C, SiC) et de différentes morphologies (tissu, feutre, 2DSiC(Nicalon)/SiC(CVI), 4DC/C).

Ce travail a été motivé par la volonté **(i)** d'expliquer la nette amélioration de la mouillabilité des préformes céramiques par l'aluminium en présence du fluorure K_2ZrF_6, **(ii)** d'étudier la compatibilité chimique entre renfort et fluorure et entre renfort et matrice en présence du fluorure, **(iii)** de mettre en évidence l'intérêt du procédé dans l'optique d'une transposition industrielle. Les moyens que nous avons utilisés et les résultats obtenus sont présentés dans les trois publications (chapitres I, II et III) et les deux annexes qui constituent le présent mémoire.

Le **premier chapitre** concerne l'établissement du diagramme de phases partiel du système ternaire réciproque $KF\text{-}AlF_3\text{-}Al_2O_3\text{-}K_2O$ afin de mettre en évidence l'éventuel effet fondant, vis à vis de l'alumine qui recouvre l'aluminium liquide et inhibe le mouillage des céramiques par le métal, des fluorures mis en jeu au cours du procédé au K_2ZrF_6, i.e. "$6KF,4AlF_3$". La mise en cohérence des

résultats du calcul thermodynamique obtenus grâce à la théorie CIS (Conformal Ionic Solution, Annexe I) et des résultats expérimentaux obtenus sur le comportement thermique des mélanges K_3AlF_6-Al_2O_3 a permis de tracer ce diagramme dans un domaine de compositions proches de la section K_3AlF_6-Al_2O_3 (Annexe II) .

Dans le **second chapitre**, nous avons tenté d'expliquer les fondements du procédé au K_2ZrF_6 à partir de considérations thermodynamiques et d'une approche numérique basée sur la modélisation de l'imprégnation de préformes poreuses. En particulier, la section verticale "6KF,4AlF_3"-Al_2O_3 extraite du diagramme de phases du système ternaire réciproque KF-AlF_3-Al_2O_3-K_2O établi au chapitre I, de même que les grandeurs thermodynamiques - variations d'énergie libre de Gibbs et d'enthalpie - associées aux réactions chimiques mises en jeu dans le procédé ont permis de comprendre l'efficacité du procédé en termes de mouillage. Par ailleurs, l'influence des paramètres physiques associés au procédé au K_2ZrF_6, i.e. l'exothermicité des réactions chimiques et l'abaissement de l'angle de contact, sur l'aptitude à l'imprégnation de préformes fibreuses (2DSiC(Nicalon)/SiC(CVI)) est étudiée grâce au modèle numérique.

Dans la **dernière partie**, une caractérisation mécanique en traction de monfilaments CVD de carbure de silicium après chaque étape du procédé au K_2ZrF_6, i.e. dépôt du fluorure, préchauffage à 650°C, incorporation dans l'aluminium, a été effectuée et les résultats ont été analysés de manière statistique sur la base d'une fonction de distribution de Weibull. L'observation des faciès de rupture primaire et de la surface des filaments, de même que les spectrométries X et Auger ont permis de mettre en évidence les causes et les modes de rupture. Ce type d'étude a été un moyen de mettre en évidence les compatibilités chimiques entre renfort, matrice et fluorure.

Cette étude a, en outre, fait l'objet de deux communications publiées:

- l'une dans le cadre des Journées Métallurgiques d'Automne de la Société Française de Métallurgie (Paris, 18-20 octobre 1988) (18)

- l'autre dans le cadre du troisième congrès européen sur les matériaux composites, ECCM3 (Bordeaux, 20-23 Mars 1989) (19).

BIBLIOGRAPHIE

(1) - J.P. Rocher, F. Girot, J.M. Quenisset, R. Pailler, R. Naslain, Mémoires Scientifiques de la Revue de la Métallurgie, Février 1986, 69

(2) - N. Eustathopoulos, J.C. Joud, P. Desré, J.M. Hicter, J. Mater. Sci. 9 (1974) 1233

(3) - S. Kohara, Proceedings of Japan-US Conference on Composite Materials, Tokyo 1981, ed. K.Kawata et T. Alasaka (Japan Society for Composite Materials, 1981), 224-231

(4) - M.F. Amateau, J. Comp. Mater. 10 (1976) 279

(5) - A.R. Champion, N.H. Krueger, H.S. Hartmann, A.K. Dhingra, Proceedings of the 2nd International Conference on Composites Materials, Toronto 1978, ed. B. Noton et al., 883-904

(6) - Yu.V. Naidich, Prog. Surf. Membr. Sci. 14 (1981) 353-484

(7) - F. Delannay, L. Froyen, A. Deruyttere, J. Mater. Sci. 22 (1987) 1-16

(8) - R.T. Pepper, E.G. Kendall, US Patent N°. 3,770,488 (1973)

(9) - H. Hansen, "Constitution of Binary Alloys", Mc Graw-Hill, New-York,(1958)

(10) - D.M. Goddard, J. Mater. Sci. 13 (1978) 1841-1848

(11) - R. Lignon, Rech. Aerospat. 1 (1974) 49

(12) - A. G. Kulkarni, B. C. Pai, N. Balasubramanian, J. Mater. Sci. 14 (1979) 592-598

(13) - D.G. Gelderloos, K. R. Karasek, J. Mater. Sci. Letters 3 (1984) 232-238

(14) - E. De Lamotte, K. Phillips, A.J. Perry, H.R. Killias, J. Mater. Sci. Letters 7 (1972) 346-349

(15) - T.W. Chou, A. Kelly, A. Okura, Composites 16(3) (1985) 187-206

(16) - J.P. Rocher, Thèse de doctorat, Université de Bordeaux I, n°888 (1985)

(17) - J.P. Rocher, X. Corretja, R. Pailler, J.M. Quenisset, R. Naslain, Brevet Européen 83.9012044, 14 Avril 1983

(18) - S. Schamm, J.P. Rocher, R. Naslain, Mémoires et Etudes Scientifiques de la Revue de Métallurgie, Septembre 1988, n°9, 483

(19) - S. Schamm, J.P. Rocher, R. Naslain, Developments in the Science and Technologie of Composites Materials, Actes ECCM 3 (A.R. Bunsell et al.), 20-23 Mars 1989, 157-163, Elsevier Applied Science, Londres et New-York

CHAPITRE I

INTRODUCTION AU CHAPITRE I

Le mauvais mouillage des fibres de SiC ou C par l'aluminium aux températures inférieures à 900°C résulte de la présence d'une pellicule d'alumine à la surface de l'aluminium liquide. A ces températures, la compacité de cette pellicule d'oxyde est telle qu'elle joue le rôle de barrière de diffusion entre le métal et la céramique, les empêchant de réagir.

Le **procédé au K_2ZrF_6** a été développé dans l'espoir que les fluorures qu'il met en jeu se comportent comme des flux désoxydants vis-à-vis de l'aluminium. Ces fluorures ont été décrits par Lundin, qui a utilisé un traitement semblable pour favoriser le mouillage de feuillards d'acier par l'aluminium, comme étant les produits de la réaction entre l'aluminium et le fluorure K_2ZrF_6 selon

$$3\ "2KF,ZrF_4" + 4\ Al \rightleftharpoons "6KF,4AlF_3" + 3\ Zr$$

Le processus de mise en oeuvre de cette réaction au travers de la pellicule d'alumine est expliqué au chapitre II.

L'amélioration du mouillage des substrats de SiC et C par l'aluminium, en présence du fluorure K_2ZrF_6 , dès la température de fusion du métal, ayant effectivement été mise en évidence (Thèse J.P. Rocher), nous nous sommes attachés à démontrer l'effet fondant du mélange de fluorures "$6KF,4AlF_3$" sur la pellicule d'alumine aux températures inférieures à 900°C. Pour cela, le diagramme de phases du système $KF–AlF_3–Al_2O_3$ devait être établi afin d'examiner l'allure des surfaces liquidus dans le domaine de composition, "$6KF,4AlF_3$"-quelques % Al_2O_3 (mol), correspondant aux conditions expérimentales du procédé. Une première approche expérimentale du comportement thermique des mélanges $K_3AlF_6–Al_2O_3$ (K_3AlF_6 est un des constituants du mélange "$6KF,4AlF_3$") ayant mis en évidence

l'existence d'un nouveau composé, Al_2O_3-β (K_2O. nAl_2O_3, n=5,11), l'étude a du être étendue au système plus complexe $KF–AlF_3–Al_2O_3–K_2O$. Etant donné le nombre très important de résultats expérimentaux nécessaires pour établir le diagramme de phases d'un tel système, nous avons préféré l'aborder grâce au **calcul thermodynamique**.

Le calcul du diagramme de phases d'un système, basé sur le principe de la minimisation de son énergie libre de Gibbs totale, suppose que soient connues les énergies libres de Gibbs de sa phase liquide et des différents composés solides qu'il contient. Le système $KF–AlF_3–Al_2O_3–K_2O$ appartient à la famille des systèmes dits réciproques car les espèces qui le constituent vérifient la relation d'échange

$$KF + \frac{1}{6} Al_2O_3 \rightleftharpoons \frac{1}{2} K_2O + \frac{1}{3} AlF_3$$

En conséquence, il est ternaire et est appelé **système ternaire réciproque**. Grâce à cette particularité, sa phase liquide a pu être modélisée sur la base de la théorie CIS (Conformal Ionic Solution) dont le seul paramètre ajustable, Z, a pu être fixé en faisant coïncider les résultats du calcul avec les résultats expérimentaux que nous avions obtenus lors de l'étude des mélanges $K_3AlF_6–Al_2O_3$. L'application de la théorie CIS aux systèmes ternaires réciproques est présentée à l'annexe I. Les données thermodynamiques impliquées dans le modèle et nécessaires au calcul du diagramme de phases, i.e. les grandeurs thermodynamiques des sous-systèmes unaires KF, AlF_3, Al_2O_3, K_2O et binaires $KF–AlF_3$, $AlF_3–Al_2O_3$, $Al_2O_3–K_2O$, $K_2O–KF$ du système ternaire réciproque, ont été soit retrouvées dans la bibliographie, soit calculées en mettant en cohérence les diagrammes de phases expérimentaux de la bibliographie avec les diagrammes de phases que l'on peut calculer grâce à des modèles. La méthodologie utilisée est présentée à l'annexe II. Finalement, le programme d'optimisation "Mélange 16" mis au point au L.T.P.C.M./Grenoble dans l'équipe de C. Bernard a permis de mener à bien les

calculs de minimisation et de tracer point par point le diagramme de phases du système $KF–AlF_3–Al_2O_3–K_2O$. Ce diagramme peut être représenté dans un plan étant donnée la réciprocité du système.

L'utilisation des résultats de ce calcul en ce qui concerne l'allure des courbes liquidus dans la section verticale "$6KF,4AlF_3$"–Al_2O_3 est discutée au chapitre II.

Soumis à "Calphad"

PARTIAL PHASE DIAGRAM OF THE TERNARY RECIPROCAL SYSTEM $KF–AlF_3–Al_2O_3–K_2O$

S. SCHAMM, L. RABARDEL, J. GRANNEC, R. NASLAIN
Laboratoire de Chimie du Solide du CNRS, Université de Bordeaux I
351, Cours de la libération, 33405 -Talence, France

C. BERNARD AND O. RELAVE
Laboratoire de Thermodynamique et Physico-Chimie Métallurgiques
associé au CNRS (UA 29), ENSEEG/INPG, Domaine Universitaire
38401- Saint-Martin-d'Hères, France

ABSTRACT

A K_2ZrF_6 treatment improves the wettability of SiC (or C) fibers by aluminum alloys. A possible mechanism involves the formation of K_3AlF_6 followed by the dissolution of the alumina film. DTA analyses of $K_3AlF_6–\alpha–Al_2O_3$ mixtures show that a temperature invariant transition occurs at 1132 K, the solid containing trace amounts of $KAlF_4$ and β–alumina at room temperature. Part of the ternary reciprocal system $KF–AlF_3–Al_2O_3–K_2O$ is calculated, the Gibbs free energy of the liquid being described according to the CIS theory. The $K_3AlF_6–Al_2O_3$ isopleth section is given. It is characterized by a liquidus with a deep minimum at 1132 K and 11.6 wt.% alumina.

1 - INTRODUCTION

The ability of ceramic fibers to be more or less wetted by liquid metals, e.g. light alloys, is a key parameter in the processing of metal matrix composites via liquid routes. It is now well established that both silicon carbide and carbon fibers are not spontaneously wetted by liquid aluminum alloys at the temperatures commonly used in light alloy casting (i.e. 973-1073 K). This drawback has been overcome by applying either a suitable coating to the fibers (e.g. TiC or TiB_2) or a high pressure to the liquid (squeeze casting). Recently, a new fiber treatment has been suggested by J.P. Rocher et al., which has the advantage of requiring a simple procedure (1,2). In its principle, it consists in immersing the fiber preform in an aqueous solution of K_2ZrF_6. After drying, the fiber preform is effectively wetted ($\theta \simeq 70°$) by aluminum alloys at a temperature slightly above their liquidus. The chemistry of the process could be related to the following overall equation:

$$3\ "2KF,ZrF_4" + 4\ Al \rightleftharpoons "6KF,4AlF_3" + 3\ Zr \qquad [1]$$

as proposed in a similar way by H. Lundin, who used the treatment to enhance the wetting ability of steel sheets by aluminum, and as discussed in another study of the authors (3,4). The fluorides which are formed could act as fluxes to dissolve the alumina film which covers the liquid and prevents wetting from taking place (5,6). However, the detailed mechanism of the wetting enhancement and the nature of the chemical species involved remains unknown.

The aim of the present contribution was initially to establish the phase diagram of the ternary $KF–AlF_3–Al_2O_3$ system with the attention focussed on the liquidus surfaces and invariant points in composition domains of interest for the understanding of the K_2ZrF_6 fiber treatment. As a matter of fact, in a preliminary experimental approach of the thermal behavior of $K_3AlF_6–\alpha–Al_2O_3$ mixtures

(K_3AlF_6 is one of the fluorides which may result from equation [1]), based on DTA, calorimetric experiments, X-ray and IR analyses, a new phase, i.e. β–alumina (K_2O, nAl_2O_3 with n = 5, 11) was observed in the solid after cooling at room temperature. Therefore, the study has to be extended to the more complex $KF–AlF_3–Al_2O_3–K_2O$ ternary reciprocal system. Regarding the amount of work which would have been necessary to establish the phase diagram experimentally, an approach based on thermodynamic calculations was preferred. A statistical model, derived from the Conformal Ionic Solution (CIS) theory, already used for reciprocal molten salt systems (7-9), was chosen to describe the liquid phase and the calculations were performed with the software MELANGE 16 (10).

2 - THERMAL BEHAVIOR OF K_3AlF_6–α–Al_2O_3 MIXTURES

The fluoride K_3AlF_6 which is one compound of the mixture "$6KF,4AlF_3$" (fig.7) was thought to play a key role in the wetting enhancement mechanism (its equivalent for sodium, the cryolite Na_3AlF_6, is used to dissolve alumina in the electrolytic preparation of aluminum) (4).

Many experimental studies have been devoted to the $α–Al_2O_3–Na_3AlF_6$ phase diagram which is usually presented as a simple eutectic (with T_E=1233-1236 K and X_E = 10-11,5 wt.% α–alumina) (fig.1) (11). Similarly, the corresponding $α–Al_2O_3–Li_3AlF_6$ phase diagram is given as a simple eutectic (with T_E = 1048-1058 K and X_E = 0,7-2 wt.% α–alumina) (11). Moreover, the general features of the liquidus of the $α–Al_2O_3–Na_3AlF_6$ system are not strongly modified when Li_3AlF_6 is added, the T_E and X_E values being progressively shifted towards those for $α–Al_2O_3–Li_3AlF_6$ (fig.2) (12). Since, in the same manner, the addition of K_3AlF_6 to $α–Al_2O_3–Na_3AlF_6$ simply results in a decrease in T_E and an increase in X_E, as shown in fig.3, one could reasonably assume that the $α–Al_2O_3–K_3AlF_6$ system would

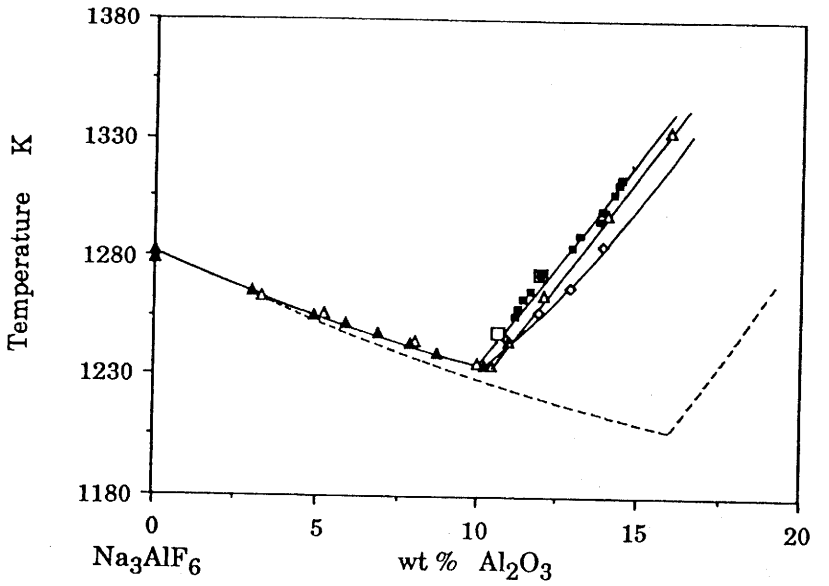

Figure 1:

Phase diagram of the quasi-binary system Na_3AlF_6-Al_2O_3 (11)

-- Abramov: TA, high cooling rate
▲ Fenerty et al.: TA, low cooling rate
◇ Fenerty et al.: visual observations
△ Foster: quenching technique
▪ Chin et al.: saturation measurements
□ Henry et al.: saturation measurements

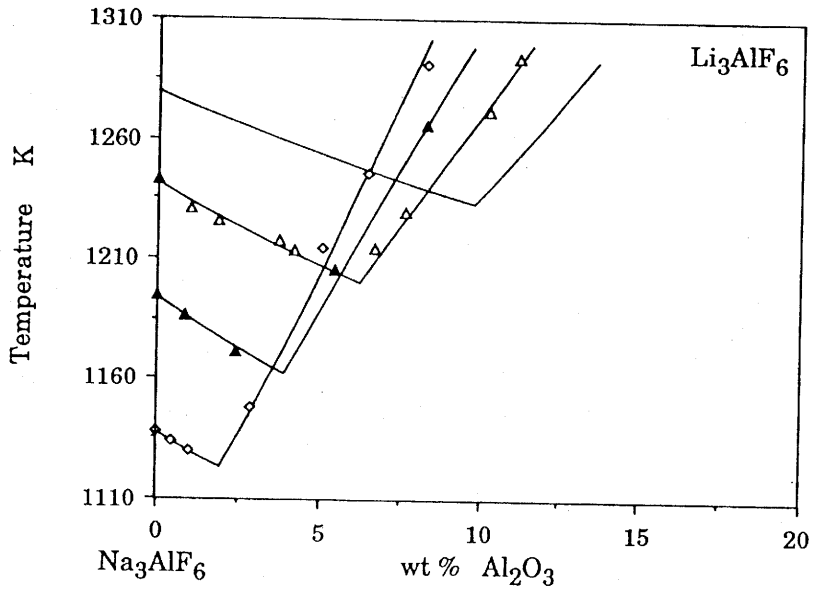

Figure 2:

Liquidus diagrams for Na_3AlF_6-Al_2O_3 with

– 0
△ 10
▲ 20
◇ 30

wt % Li_3AlF_6 given on alumina-free basis (12)

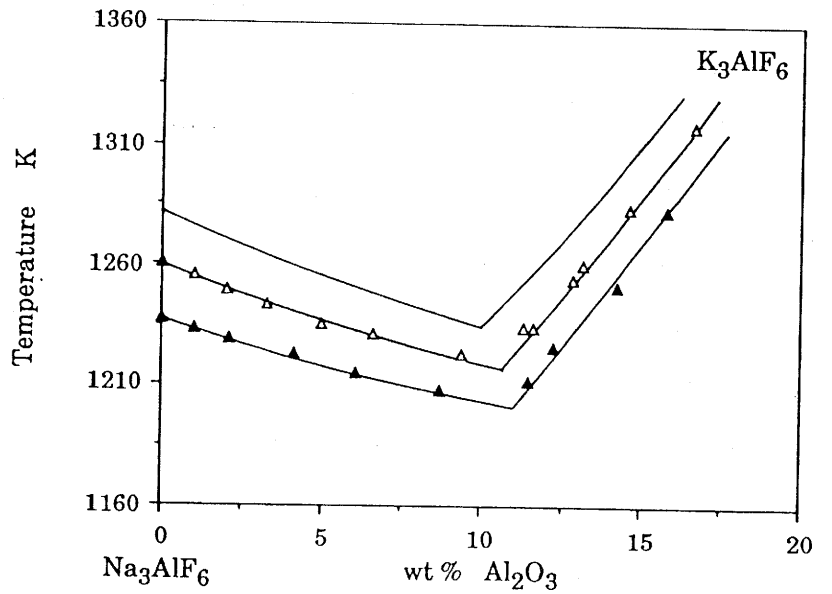

Figure 3:

Liquidus diagrams for Na_3AlF_6-Al_2O_3 with

– 0
△ 10
▲ 20

wt % K_3AlF_6 given on alumina-free basis (12)

behave as a simple eutectic system with T_E (K_3AlF_6) < T_E (Na_3AlF_6) and X_E (K_3AlF_6) > X_E (Na_3AlF_6).

Several authors have already studied the liquid phase of the α–Al_2O_3–K_3AlF_6 system (13-17). Almost all of them reported a "minimun" on the liquidus curve which falls in the same domains of temperature and composition (i.e. 1083-1113 K and 21-24 wt.% alumina, respectively). Only A.I. Belyaev mentioned somewhat different data (i.e. 1183 K and 14-14,5 wt.% alumina) (14). Finally, the recent study due to R.V. Chernov et al. presented this minimum as an eutectic invariant (17).

Regarding the lack of reliable data in this field, we have in a first step, studied the phase equilibria taking place in the α–Al_2O_3–K_3AlF_6 system on the basis of calorimetric experiments as well as X-ray diffraction (XRD) and infracted (IR) analyses of the solid phases.

2.1 - Experimental

Potassium cryolite has been prepared in the solid state according to a chemical reaction corresponding to the following equation :

$$3\,KF + AlF_3 \rightleftharpoons K_3AlF_6 \qquad [2]$$

by heating, at 823 K for 15 hours under an atmosphere of argon, a stoichiometric mixture of potassium and aluminum fluorides. KF was a commercial product, anhydrous and with a low content of cation impurities. AlF_3 was prepared according to a two-step procedure : (i) a treatment in a platinum crucible of AlF_3,nH_2O by NH_4,HF followed after grinding by (ii) an annealing treatment of the powder performed in a platinum crucible at 873 K in a stream of gaseous HF (18). The chemical analysis of the potassium cryolite resulted in the following data : K: 32.7; Al: 10.3 and F: 57.0 at.% (vs 30 ; 10 and 60 at. % theor.). Its temperature and enthalpy of melting were found to be 1260 K and 125 ± 2.5 $kJ.mol^{-1}$ respectively and

are in a reasonable agreement with the literature (T_m(K) = 1268 (19) ; 1269 (20) ; 1273 (21) and ΔH_m (kJ.mol^{-1}) = 115.5 (20) ; 122.6 ± 1.7 (21)).

α–alumina was obtained by heating in air (at 1473K for 16 hours) a commercial χ–alumina powder (whose total content in cation impurities was less than 10 ppm)

The α–Al_2O_3–K_3AlF_6 samples were prepared according to a two-step procedure : (i) one gram of mixture was prepared from α–Al_2O_3 and K_3AlF_6 powders, in a dry glove box, and then annealed at 1023 K for 24 hours in a platinum crucible, under an atmosphere of dry argon, (ii) after grinding in the dry glove box, 80 mg samples were set in platinum tubes which were sealed under argon with a microtorch.

The thermal analysis experiments were performed with a microcalorimeter designed by L. Rabardel and which is described elsewhere (22). The apparatus was calibrated in both temperature and energy with pure tin and gold. The accuracy of the measurements was thought to be ± 2 K and 1.5 % kJ.mol^{-1} respectively. The DTA curves were recorded both during heating and cooling at a rate of 4 K.min^{-1}. Regarding the tendency of the potassium cryolite–α–alumina melts to remain supercooled, only the data obtained on heating will be considered in the following.

The XRD spectra were recorded with a Cu-Kα diffractometer according to a conventional procedure. The IR spectra were recorded with a double beam dispersive spectrometer (PE 983) and a data processing computer. The powder samples were first mixed with Nujol and then set within a film cell between two cesium iodide plane crystals.

2.2 - Results and discussion

The thermal behaviors of α–Al_2O_3–K_3AlF_6 mixtures containing respectively 0 ; 5.0 ; 15.3 ; 17.9 ; 21.0 ; 23.2 ; 25.0 ; 30.1 and 90.0 wt % alumina were experimentally

studied. The thermal transitions which have been observed suggest, at least in a first approximation, the occurence of a temperature invariant transition within the whole composition range (fig.4 ; Table 1). The tentative corresponding phase diagram is given in fig.5. It clearly shows the invariant at 1132 K as well as the liquidus curve on the K_3AlF_6 rich side whereas it was not observed on the α–alumina rich side. It was thought that the slope of the liquidus curve joining the invariant point and the melting point of pure alumina should be very sharp since ΔT = 1195 K for ΔX = 69 wt % alumina and consequently : (i) the liquidus could be located at temperatures exceeding the limit of the apparatus (all experiments were limited in temperature at 1300 K) and (ii) the heat of melting could not be detected due to the low fraction of crystals melting per unit of temperature increase. It is noteworthy that N.W.F. Phillips et al. (23) and later on M. Rolin (24) found no thermal deviation on cooling curves corresponding to the primary crystallization of alumina in the α–Al_2O_3–Na_3AlF_6 system, even at a low cooling rate (i.e. 0.5 $K.min^{-1}$).

The Tammann diagram corresponding to the invariant transition has been also plotted in fig.5. From a linear extrapolation of the data (table 1), it appears that the invariant point composition is 21±1 wt.% alumina, a value which is in rather fair agreement with the liquidus curve drawn for the K_3AlF_6–rich mixtures.

However, the results of the XRD analyses performed on the DTA samples after cooling and grinding (in the dry glove box) show that small amounts of β–alumina and $KAlF_4$ were present while α–alumina was not observed for composition ranging from 21 to 30 wt % alumina. The same conclusion could also be drawn for the 17.9 wt % alumina sample (although there is some uncertainty about β–alumina). Furthermore, for 90.0 wt % alumina, $KAlF_4$ was no longer observed whereas β–alumina was still present and α–alumina recovered. Finally, the only crystalline phase detected in the 5.0 and 15.3 wt % alumina samples (i.e. on the left of the invariant point) was K_3AlF_6.

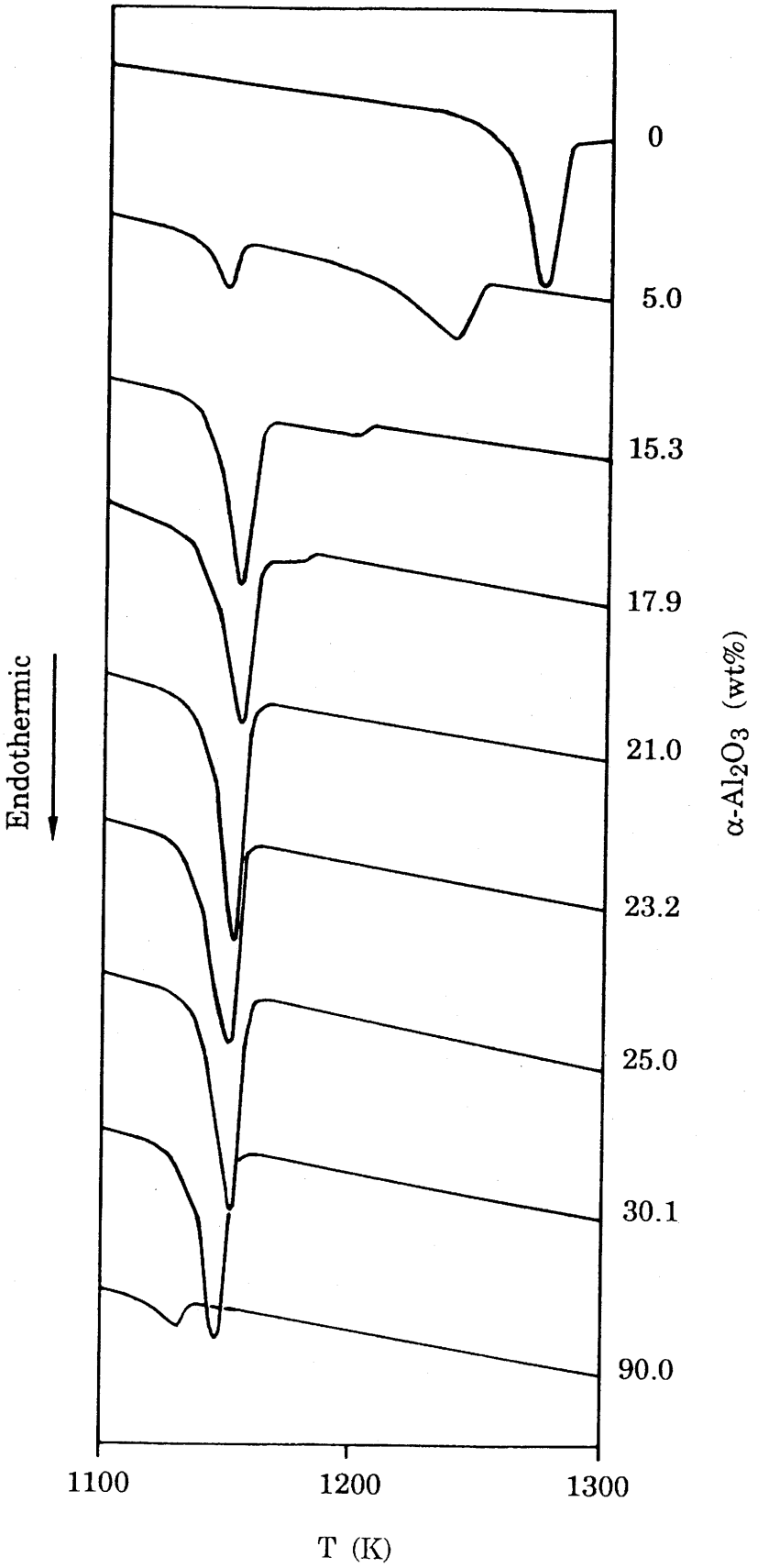

Figure 4: DTA curves of the α–Al_2O_3–K_3AlF_6 mixtures recorded on heating the samples in sealed platinium tubes

α–Al_2O_3 (wt %)	5.0	15.3	17.9	21.0	23.2	25.0	30.1	90.0
T (eutectics) (K)	1131	1136	1134	1133	1136	1138	1131	1118
T(liquidus) (K)	1232	1189	1167	-	-	-	-	-
ΔH (liquidus) ($J.mol^{-1}$)	-30740	-108930	-121730	-159050	-147010	-138500	-128240	-9520

Table 1: DTA data for the α–Al_2O_3–K_3AlF_6 mixtures

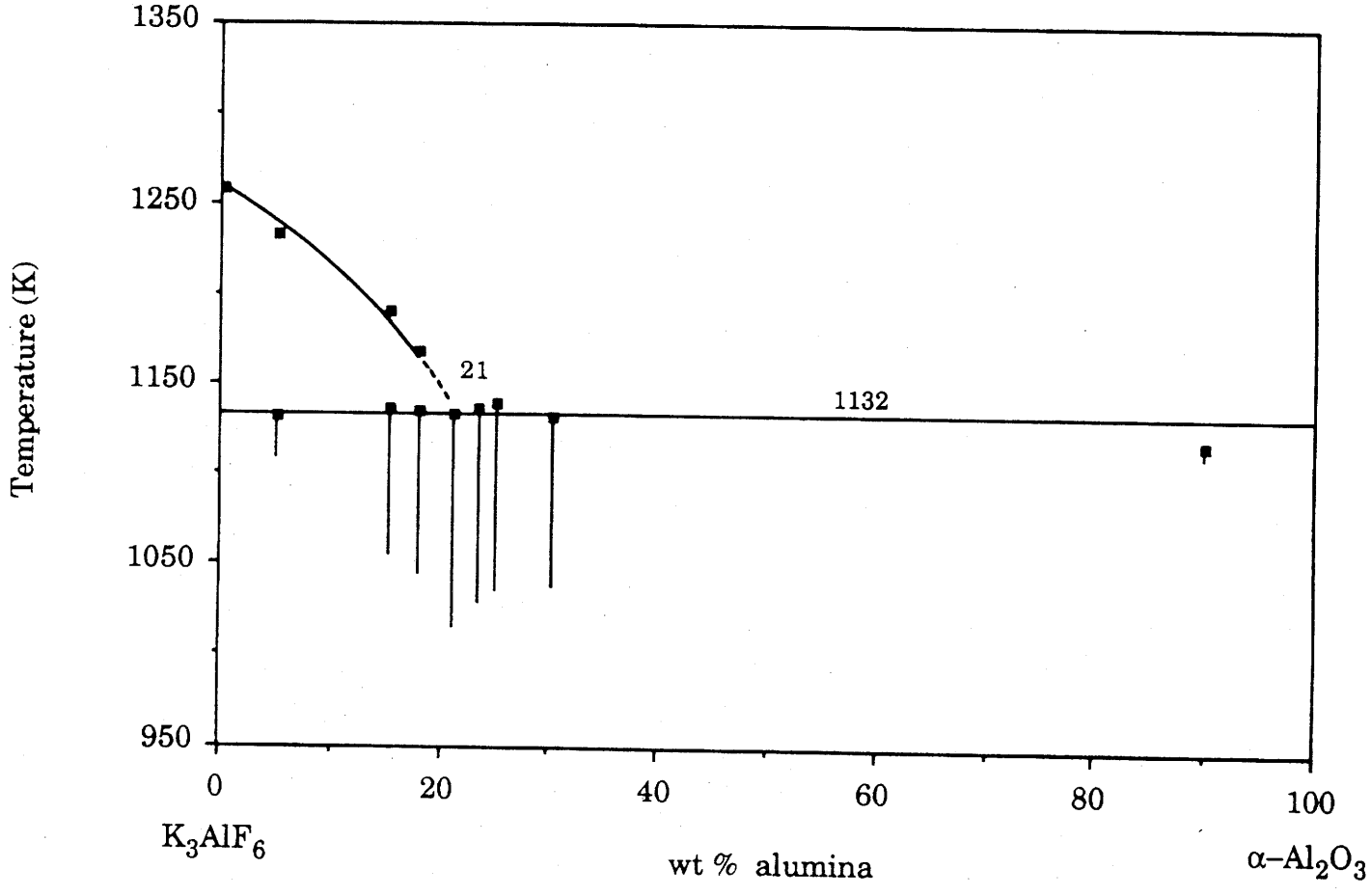

Figure 5: Tentative phase diagram of the K_3AlF_6–Al_2O_3 system based on DTA data

In the alumina–sodium cryolite system, H. Ginsberg and A. Böhm reported that for alumina concentrations less than 12.5 wt %, the XRD-patterns of samples slowly cooled from 1273 K exhibited only the cryolite lines whereas corundum lines were observed when the alumina concentration was increased. However, for alumina concentrations less than 12.5 wt % and after an aluminum sulfate extraction (to recover the alumina) : β– and γ– aluminas were identified by XRD in the slowly cooled samples while only β–alumina was present in the quenched specimens (25). J. Brynestad et al. also mentioned that β–alumina was present in samples quenched from 1273 K (26). P.A. Foster reported the occurence, in quenched alumina–sodium cryolite mixtures, of large amounts of what he called a m-alumina (m for mullite-type) as well as a small amount of zeta-alumina, regardless of the overall alumina content of the mixtures. Moreover, quenching experiments from below the liquidus led to mixtures of m-alumina and corundum for compositions on the high alumina side of the eutectic while only m-alumina was observed for those on the low alumina side (27). It is noteworthy that A. Grant Elliot et al. mentioned later a λ–phase in the $NaAlO_2$–Al_2O_3 system, with a formula $Na_2O.xAl_2O_3$ (x = 3-12), whose XRD pattern is similar to that of m-alumina (28).

The occurrence of β–alumina in the K_3AlF_6–Al_2O_3 samples submitted to DTA and corresponding to alumina-rich compositions, has been confirmed by IR spectrometry analyses, as shown in fig.6. Starting from pure K_3AlF_6 (characterized by two absorption lines at 570 and 390 cm^{-1} according to (29)), the addition of increasing amounts of alumina gives rise, for x ≥ 17.9 wt % alumina, to new sharp IR absorption lines at 1050 ; 860 ; 760 ; 710 ; 600 ; 460 ; 380 and 310 cm^{-1} different from those of α–alumina (30) and which have been assigned to potassium β–alumina (on the basis of the IR-spectrum reported for the related sodium phase (31)).

From the results of the XRD and IR data, it thus appears that the α–Al_2O_3–K_3AlF_6 system does not behave as a true quasi-binary system (at least for X > 18-20 wt % alumina). The important conclusions which can be drawn from the

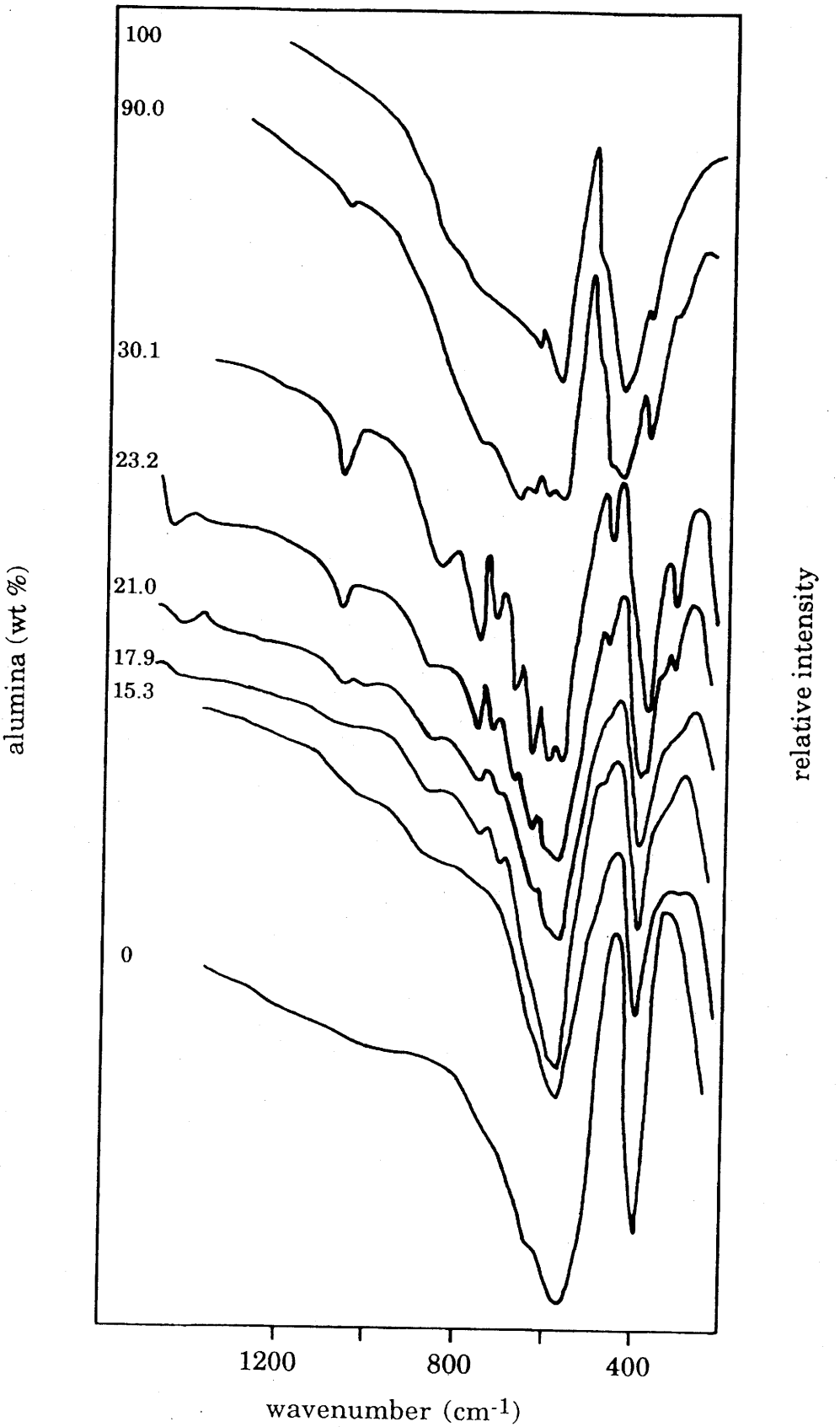

Figure 6: I.R. spectra of the K_3AlF_6–α–Al_2O_3 mixtures

experimental study are : (i) the occurrence of a temperature invariant transition at 1132 K and (ii) that of β–alumina in some of the materials after cooling at room temperature. It is worthy of note that β–alumina type phases have been also mentioned for the related α–Al_2O_3–Na_3AlF_6 system although it has been generally considered up to now as a true quasi-binary system.

3 - PARTIAL CALCULATION OF THE PHASE DIAGRAM OF THE TERNARY RECIPROCAL SYSTEM KF–AlF_3–Al_2O_3–K_2O

On the basis of the identification of β–alumina and $KAlF_4$ in the samples submitted to DTA analysis, the study was extended to the more complex system KF–AlF_3–Al_2O_3–K_2O (K_3AlF_6 and $KAlF_4$, are compounds from the KF–AlF_3 binary system whereas α–and β– aluminas belong to the Al_2O_3–K_2O binary system). The calculation of the phase diagram required the knowledge of the Gibbs free energies of the liquid phase and of the various involved compounds. One of the major difficulties of such a calculation lied in the modelling of the liquid phase.

The nature of the chemical species that may be present in the cryolite–alumina molten mixtures has been the subject of different studies (11). On the basis of cryoscopic measurements, S.H.K. Ratkje has established that oxyfluoride species $Al_2OF_{2x}^{4-2x}$ are present besides the previously well-identified Na^+, F^-, AlF_6^{3-} and AlF_4^- ions in the liquid phase corresponding to NaF-rich compositions in the NaF–AlF_3–Al_2O_3–Na_2O system (11). For the related KF–AlF_3–Al_2O_3–K_2O system, a similar conclusion has been drawn. In addition, the occurence of the $AlOF_y^{1-y}$ oxyfluoride species has been suggested (32).

Till now, no model has been proposed to describe analytically a liquid phase made of a mixture of oxides and fluorides. However, M. L. Capoor et al. and H. Gaye et al. have described the liquid phase of oxide-based systems in terms of a model assuming the occurence of Mi-O-Mj cells (where Mi and Mj are the related cations)

while M. Blander, M.L. Saboungi and their coworkers have applied the so-called Conformal Ionic Solution (CIS) to molten salts (7-9, 33, 34).

The CIS theory is suited to systems referred to as reciprocal systems, the simplest being made of two monovalent cations A^+ and B^+ associated with two monovalent anions C^- and D^- with the following double exchange equilibrium :

$$AC + BD \rightleftharpoons AD + BC \qquad [3]$$

It clearly appeared that the $KF–AlF_3–Al_2O_3–K_2O$ system could be regarded as a reciprocal system since the four ionic species obey the following double exchange equilibrium :

$$KF + \frac{1}{6} Al_2O_3 \rightleftharpoons \frac{1}{2} K_2O + \frac{1}{3} AlF_3 \qquad [4]$$

On the basis of this feature, the CIS theory which is briefly described below was used to : (i) define the composition coordinates and (ii) calculate the Gibbs free energy of the liquid . It is based on the application of the statistical mechanics to molten salts and can be used to predict the main features of the phase diagram from limited experimental data. Its previous application to various ionic systems, e.g. Li,K/F,Cl (35) ; $Na,Sr/Cl,NO_3$; $Na,Ba/Cl,NO_3$; $Li,K/Cl,CrO_4$; $Li,K/Br,CrO_4$; Na,Ba/F,Cl (9) as well as to the molten salts used in the Hall-Héroult processing of aluminum (i.e. the $LiF-NaF-AlF_3$ (36) ; $LiF-NaF-CaF_2$; $NaF-AlF_3-CaF_2$ and $LiF-AlF_3-CaF_2$ (37) systems) has led to a good agreement between the experimental and calculated phase diagrams. Moreover, the model has been used to consider composition domains which would have been difficult to study experimentally (9, 37).

3.1 - The CIS theory

In the CIS theory, molten salts are assumed to be totally ionized and only anion-cation interactions are taken into account. The model is only suited to

reciprocal molten salt systems involving ions of the same electrical charge, like the A^+, B^+, C^-, D^- system mentioned above.

The molar Gibbs free energy of the liquid defined relative to the elements A, B, C, D in their standard states can be expressed as a function of temperature, T, and ionic fraction, X_A, X_B, X_C, X_D, according to the following equation :

$$\Delta G_m = G_m - X_A G^\circ_A - X_B G^\circ_B - X_C G^\circ_C - X_D G^\circ_D \qquad [5]$$

which can be rewritten as :

$$\begin{aligned}\Delta G_m = {} & RT\,(X_A \mathrm{Ln} X_A + X_B \mathrm{Ln} X_B + X_C \mathrm{Ln} X_C + X_D \mathrm{Ln} X_D) \\ & + X_A X_C\, \Delta G^\circ_f\,(AC) + X_A X_D\, \Delta G^\circ_f\,(AD) + X_B X_C\, \Delta G^\circ_f (BC) + X_B X_D\, \Delta G^\circ_f (BD) \\ & + X_A \Delta G^E\,(AC\text{-}AD) + X_B \Delta G^E\,(BC\text{-}BD) + X_C \Delta G^E\,(AC\text{-}BC) + X_D \Delta G^E\,(AD\text{-}BD) \\ & - X_A X_B X_C X_D [\Delta G^\circ(3)]^2 / 2ZRT \qquad [5']\end{aligned}$$

The first term of equation [5'] is the entropy of configuration related to the ideal mixing of the ions, the ionic fractions being defined by :

$$X_A = \frac{N_A}{N_A+N_B} = 1-X_B \qquad \text{for the cations} \qquad [6]$$

$$X_C = \frac{N_C}{N_C+N_D} = 1-X_D \qquad \text{for the anions} \qquad [6']$$

where N_A, N_B, N_C and N_D are the number of moles of ions A^+, B^+, C^- and D^-. The following terms of equation [5'] correspond to the excess Gibbs free energy related to the ion mixing. The contribution of the compounds AC, AD, BC and BD is taken into account through the standard Gibbs free energies of formation of their liquid phases, ΔG°_f , whereas that of the binary systems AC–AD; AD–BD; AC–BC and BC–BD is expressed on the basis of the excess Gibbs free energies of the binary mixture of the related salts ΔG^E. Finally, the last term of equation [5'] takes into account the fact that ion mixing does not take place in a random manner since the

ions obey the double exchange relation [3]. $\Delta G°(3)$ is the standard molar Gibbs free energy change of the metathetical reaction [3] and Z is an adjustable parameter.

3.2 - Extension of the CIS theory to the $KF–AlF_3–Al_2O_3–K_2O$ system

The CIS theory has been already empirically extended to reciprocal systems made of ions bearing different electrical charges (which is actually the case for the $KF–AlF_3–Al_2O_3–K_2O$ or K^+, Al^{3+}/ O^{2-}, F^- system) by M.L. Saboungi and M. Blander (9). In equation [5'], the ionic fractions Xi : (i) should be replaced by the so-called equivalent (ion) fractions Yi (that will be defined later on) in the expression of the excess Gibbs free energy of mixing whereas (ii) they are kept in the ideal term. This procedure has been successfully applied by T. Förland to various binary systems (38).

Considering the ternary reciprocal system $KF–AlF_3–Al_2O_3–K_2O$ regarded as consisting of the unsymetrically charged K^+, Al^{3+}, O^{2-} and F^- ions with the double exchange relation [4], the Gibbs free energy of formation per equivalent of the liquid phase relative to the pure elements K, Al, O, F in their standard states can be expressed according to the following equation :

$$\Delta G_m = RT\,(N_K \mathrm{Ln}X_K + N_{Al}\mathrm{Ln}X_{Al} + N_O\mathrm{Ln}X_O + N_F\mathrm{Ln}X_F)/N$$
$$+Y_KY_F\,\Delta G_f^\circ\,(KF)+Y_{Al}Y_F\,\Delta G_f^\circ\,(AlF_3)/3+Y_{Al}Y_O\,\Delta G_f^\circ\,(Al_2O_3)/6 + Y_KY_O\,\Delta G_f^\circ\,(K_2O)/2$$
$$+Y_{Al}\,\Delta G^E(AlF_3\text{-}Al_2O_3)+Y_K\,\Delta G^E(KF\text{-}K_2O)$$
$$+Y_O\,\Delta G^E(K_2O\text{-}Al_2O_3)+Y_F\,\Delta G^E(KF\text{-}AlF_3)$$
$$-\,Y_KY_{Al}Y_OY_F\,[\Delta G°(4)]^2/2ZRT \qquad [7]$$

where N_K, N_{Al}, N_O and N_F are the number of moles of K^+, Al^{3+},O^{2-} and F^- ions (with $N = 3N_{Al} + N_K = 2N_O + N_F$ to satisfy the condition of charge balance), the Xi

and Yi fractions being defined by :

$$X_{Al} = \frac{N_{Al}}{N_{Al} + N_K} = 1 - X_K \quad \text{and} \quad X_O = \frac{N_O}{N_O + N_F} = 1 - X_F$$

$$Y_{Al} = \frac{3N_{Al}}{3N_{Al} + N_K} = 1 - Y_K \quad \text{and} \quad Y_O = \frac{2N_O}{2N_O + N_F} = 1 - X_F$$

4 - THERMODYNAMIC DATA AND PARAMETERS

In order to calculate the $KF–AlF_3–Al_2O_3–K_2O$ phase diagram in the composition domain considered here (i.e. in the vicinity of the $K_3AlF_6–Al_2O_3$ section), according to the procedure described above, the thermodynamic data for the compounds and related binary systems should be known. Some of them were available but others had to be either set in a coherent basis or even estimated.

4.1 - Thermodynamic data of the compounds

The compounds KF, AlF_3, K_3AlF_6 and $KAlF_4$, on one hand, $\alpha–Al_2O_3$, $\beta–Al_2O_3$ and $KAlO_2$ (i.e. $K_2O.Al_2O_3$), on the other hand, were considered in the calculations. Regarding the uncertainty of the nature and composition of β–alumina (which is presented either as stoichiometric compounds $K_2O.11Al_2O_3$ (β–phase) and $K_2O.5Al_2O_3$ (β"–phase) or as a phase with an extended range of composition K_2O,nAl_2O_3 with $5 < n < 10$), this phase has been treated, in the following, as a compound of formula $K_2O.9Al_2O_3$ (39, 40).

The thermodynamic data for KF, AlF_3, K_3AlF_6, K_2O and $\alpha–Al_2O_3$ were taken from the last issue of the JANAF (41). However, both the enthalpy and entropy of melting of K_2O were not avaible (K_2O is not stable on heating under a pressure of one atmosphere). Therefore, those of the neighboring Na_2O compound, which were available, have been taken into account. R.P. Beyer et al. have measured the heat

capacity of $KAlO_2$ at constant pressure up to 1400 K, their data have been used here (42). Furthermore, the enthalpy of formation and entropy at 298 K are those which have been estimated by T. B. Lindemer and T. M Besmann (43).

For β–alumina and $KAlF_4$, no thermodynamic data were available from literature. Their enthalpies of formation and entropies at 298 K were estimated on the basis of $\Delta G_f^\circ = A + BT$ equations from the related binary phase diagram. The heat capacities were calculated using the Neumann-Kopp rule.

4.2 - Binary systems

In the CIS theory, the excess Gibbs free energy of mixing of the binary mixture of the salts i and j, i.e. the ΔG^E terms in equation [7], is written as :

$$\Delta G^E (i\text{-}j) = YiYj [a + b (Yi\text{-}Yj) + cYiYj]$$

The parameters a, b and c were calculated after having set the ΔG_f°, the experimental data concerning the binary phase diagram i-j and the ΔG^E in a coherent basis.

(1) $KF–K_2O$ and $AlF_3–Al_2O_3$

These two binary phase diagrams are unknown. Since it was not possible, therefore, to depict accurately the behavior of their liquid phase, they were considered as obeying the law of ideal mixtures with the consequence that a = b = c = 0 in the CIS theory. The $KF–K_2O$ and $AlF_3–Al_2O_3$ binary edges of the $KF–AlF_3–Al_2O_3–K_2O$ phase diagram lie rather far from the $K_3AlF_6–Al_2O_3$ section which is of interest here. Thus, it was thought that the above assumption may not have a strong effect on the main features of the liquidus in the vicinity of the $K_3AlF_6–Al_2O_3$ section.

(2) $KF–AlF_3$

The $KF–AlF_3$ binary phase diagram has been studied experimentally by various authors (44-49). A compilation of the invariants of the diagram is given in table 2. It clearly appears that the data are in good agreement.

Only one study, that of B. Phillips et al., is based on experiments performed on AlF_3-rich samples heated in sealed tubes (48). However, the melting point of AlF_3 which was given (i.e.1263K) seems too low. Therefore, the JANAF data have been used to model the behavior of the liquid phase (41).

On the basis of the thermodynamic data calculated for $KAlF_4$ i.e. ΔH_f° = -2132.82 kJ. mol^{-1} and S° = 125.1 $J.mol^{-1}.K^{-1}$ at 298 K and of the following expression for $\Delta G^E(KF–AlF_3)$ (in $J.eq^{-1}$) :

$$Y_K Y_{Al} [-138100.82 + (39729.43 + 37.79T)(Y_K - Y_{Al}) + 149651.33\, Y_K Y_{Al}]$$

the $KF–AlF_3$ phase diagram has been computed. As shown in fig.7, the calculated phase diagram is coherent with the phase diagram drawn experimentally by B. Phillips et al. (with the discrepancy already mentioned for the AlF_3-rich compositions).

(3) $K_2O.Al_2O_3–Al_2O_3$

Only the composition domain ranging from $K_2O.Al_2O_3$ to pure alumina has been considered in the $K_2O–Al_2O_3$ binary system. The corresponding phase diagram has been calculated (39) and drawn experimentally in the 1473-1973 K temperature range (40). The two diagrams, although they exhibit the same general features, are characterized by invariant transitions differing in temperature, as shown in table 3.

Authors	T_f KF	T_e/X_e	T_f K_3AlF_6	T_e/X_e	T_p/X_p	T_f AlF_3
Pushin et al.	1158	1110/0.075	1308	843/0.40	-	-
Fedotiev et al.	1153	1113/0.068	1298	843/0.45	853/0.475	-
Dergunov	1129	1093/0.07	1285	-	-	-
Barton et al.	1129	-	1269	833/0.45	848/0.45	-
Phillips et al.	1129	1113/0.07	1258	833/0.45	847/0.5	1263
Jenssen	1131	1093/0.07	1273	833/0.45	853/0.5	-
Our calculation	1131	1107/0.04	1258	839/0.455	847/0.49	2523

Table 2: Invariants of the KF–AlF_3 binary phase diagram

X_e, X_p: eutectic, peritectic compositions (mole fraction)
T_f, T_e, T_p: fusion, eutectic, peritectic temperatures (K)

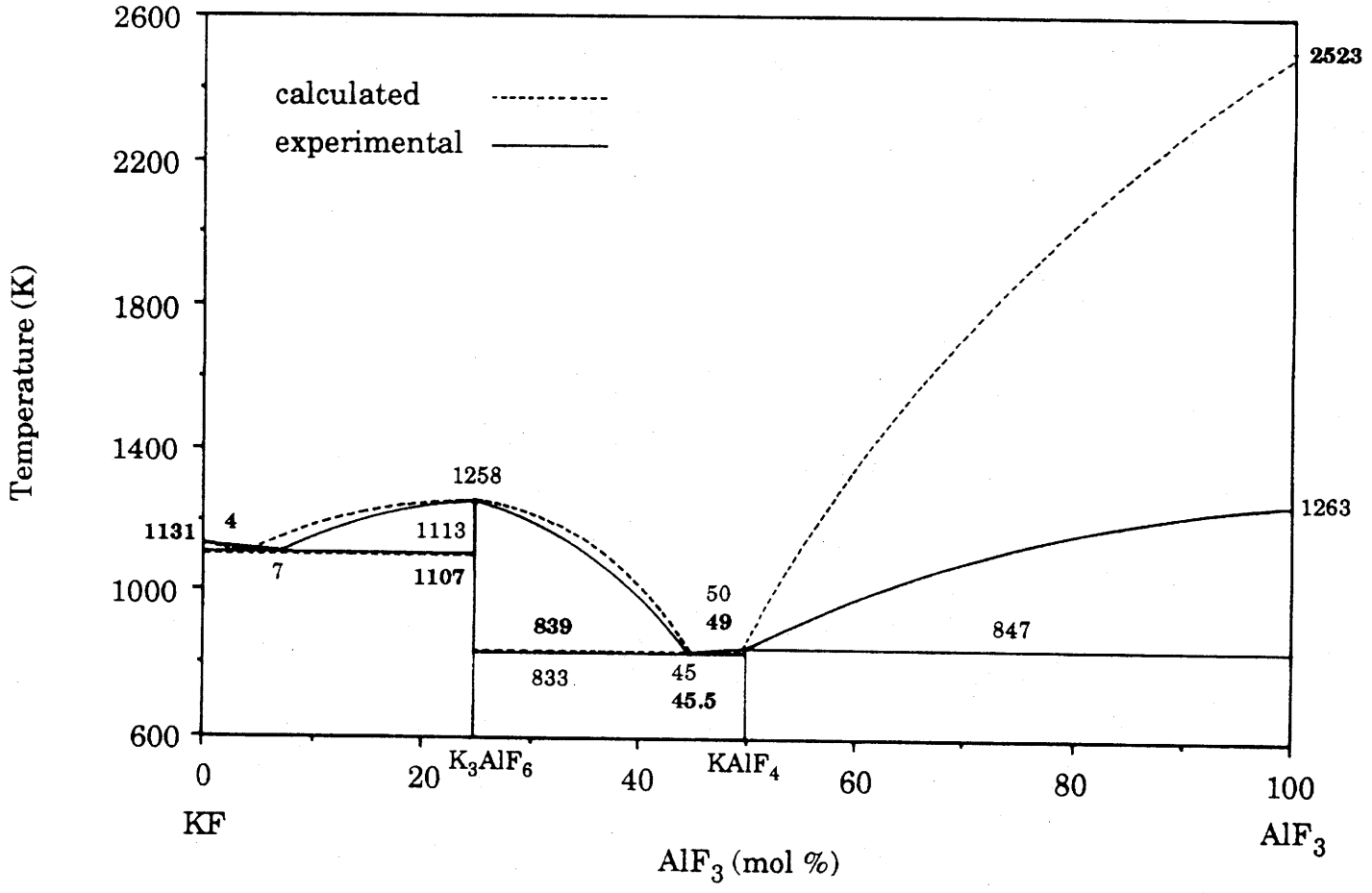

Figure 7: Calculated and experimental (23) phase diagrams of the KF-AlF_3 binary system

Authors	T_f $KAlO_2$	T_e/X_e	T_p/X_p	T_f Al_2O_3
Eliezer et al.:				
extended β–phase	1968	1905/0.6	2150/0.83	2327
two β–compounds	1968	1843/0.65	2150/ -	2327
Moya et al.	2533	1723/0.62	2150/ -	2327
Our calculation	1968	1876/0.658	2150/0.847	2327

Table 3: Invariants of the $K_2O.Al_2O_3$–Al_2O_3 binary phase diagram

X_e, X_p: eutectic, peritectic compositions (mole fraction)

T_f, T_e, T_p: fusion, eutectic, peritectic temperatures (K)

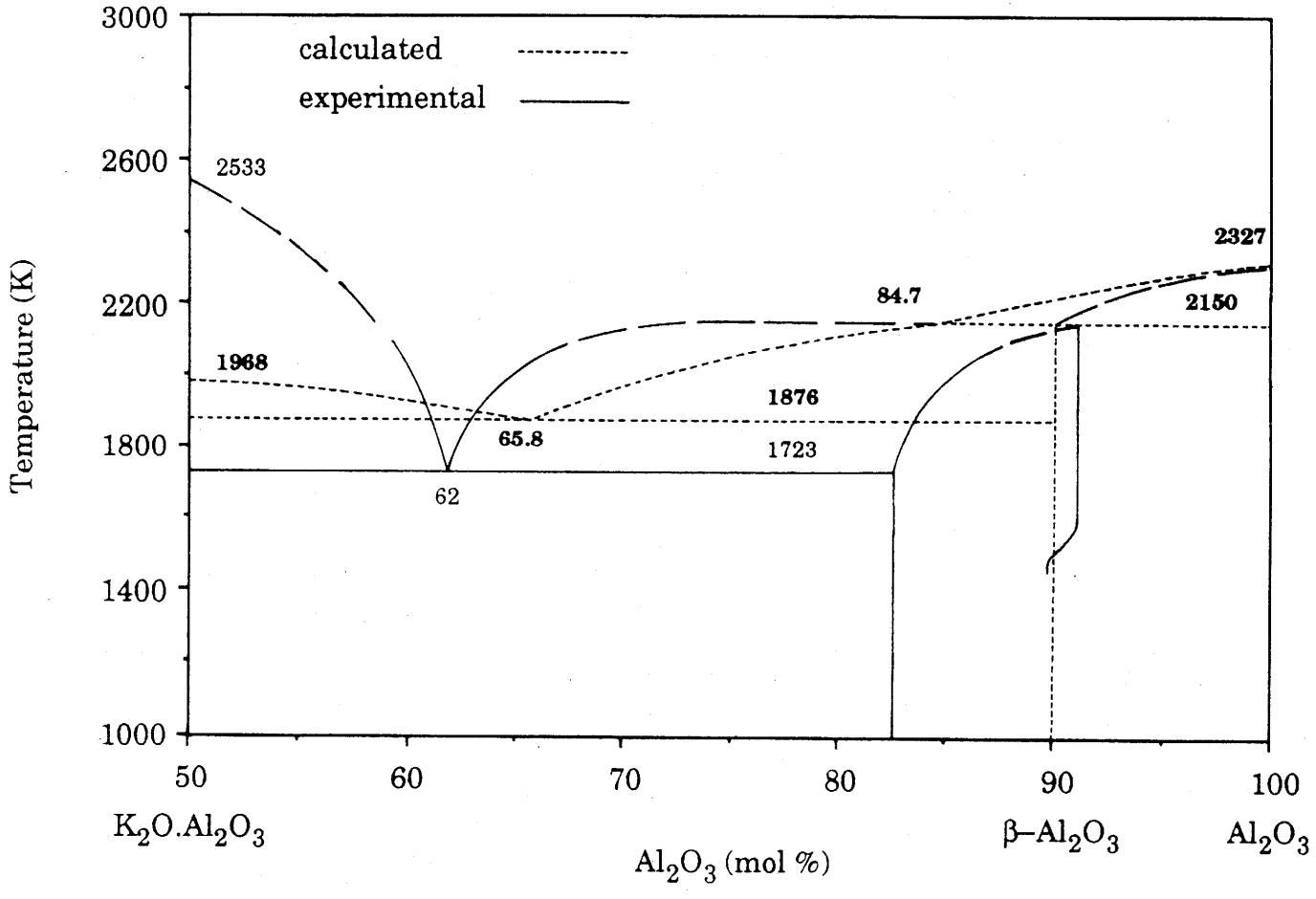

Figure 8: Calculated and experimental (40) phase diagrams of the $K_2O.Al_2O_3$-Al_2O_3 binary system

On the basis of the thermodynamic data retained for $K_2O.9Al_2O_3$ at 298 K i.e. ΔH_f°= -15681.2 kJ mol^{-1} and S° = 593.8 $J.mol^{-1}.K^{-1}$ and of the following equation used for ΔG^E (K_2O–Al_2O_3) in the CIS theory :

$$Y_K Y_{Al} (-128957.14) \text{ in } J.eq^{-1}$$

there is an acceptable compromise between the calculated phase diagram and the diagram drawn experimentally by J.S. Moya et al.(40) (fig.8).

4.3 - The liquid phase in the ternary reciprocal KF–AlF_3–Al_2O_3–K_2O system

The only adjustable parameter in [7] is Z. In the CIS theory, the value which is usually taken for Z is 6. However, M.L. Saboungi already mentioned that this value did not lead to a good agreement between calculated and experimental results when $\Delta G/RT$ (in - $\Delta G^2/2ZRT$ of the CIS theory) is large with respect to one and thus she suggested to consider Z has an adjustable parameter (9). In the present study, $\Delta G/RT$ is of the order of 18, this high value justifies the fact that Z has been regarded as an adjustable parameter in our calculations.

To take into account the temperature invariant observed at 1132 K, a Z value of 12.5 has to be retained. It is worthy of note that the calculations were run for a constant pressure (i.e. 1 atm) whereas the experiments were performed at constant volume (i.e. in sealed tubes). It was assumed that the pressure actually reached in such experiments was not high enough to modify significantly the phase diagram, in the condensed state, drawn for p = 1atm.

5 - CALCULATED KF–AlF_3–Al_2O_3–K_2O PHASE DIAGRAM

The phase diagram was calculated, for a composition range close to the K_3AlF_6–Al_2O_3 section, by minimizing the total Gibbs free energy of the system, at a constant pressure of 1 atm and for different temperatures, the composition being

defined with the internal variables Y_{Al} and Y_O (with $Y_K = 1-Y_{Al}$ and $Y_F = 1-Y_O$ as mentioned above). The calculations were run with the software MELANGE 16 (10).

The nature and relative proportion of the phases present at equilibrium thus obtained were used to draw the phase diagram in a plane square where the coordinates are the equivalent fractions Y_{Al} and Y_O (fig.9). Due to its reciprocal character (based on equation [4]), the system has only three independant components and the pressure has been fixed (i.e. to 1 atm as said above). Therefore, according to the phase rule the number of degrees of freedom is $v = 4 - \varphi$ (φ being the number of phases at equilibrium). Considering the liquidus of the phase diagram : (i) a surface (v = 2) represents an equilibrium L $\rightleftharpoons$ S (referred to as L+S) ,(ii) the intersection of two surfaces, i.e. a line (v = 1) represents a three phase equilibrium (referred to as $L + S_1 + S_2$) and finally (iii) the intersection of two lines, i.e. a point (v = 0) represents a four phase equilibrium (referred to as $L + S_1 + S_2 + S_3$).The composition, temperature and solid phases at equilibrium corresponding to the various invariant points of fig 9 are listed in table 4.

As shown in fig.9, the part of the phase diagram which has been calculated is self-consistent and has some common features with that experimentally drawn by P.A. Foster for the related $NaF–AlF_3–Al_2O_3–Na_2O$ system (fig.10) (50).(The outlines of a reciprocal system in equivalent and mole fractions respectively are the same (51)). The main difference lies in the fact that the $Na_3AlF_6–\alpha–Al_2O_3$ section reported in the literature is generally considered as a quasi-binary section (11) whereas the $K_3AlF_6–\alpha–Al_2O_3$ section calculated in the present study is not, as already suggested from the experimental data discussed above.

It is worthy of note that the hypothesis according to which the sodium cryolite–alumina system might not exhibit a simple binary eutectic transition but rather a reaction point (of peritectic-type) at the minimum of the two liquidus curves where the three solid phases $\alpha–Al_2O_3$; $\beta–Al_2O_3$ and Na_3AlF_6 might be in

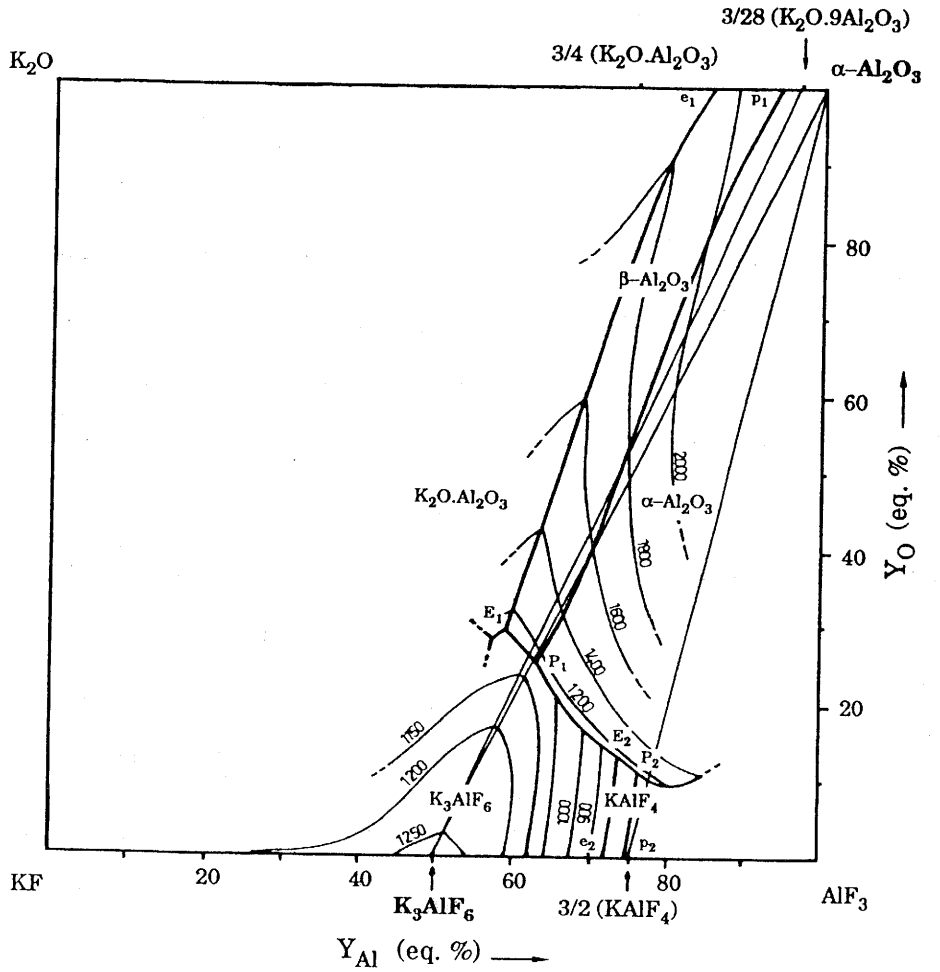

Figure 9:

Phase diagram of the ternary reciprocal system $KF–AlF_3–Al_2O_3–K_2O$ calculated in the vicinity of the $K_3AlF_6–\alpha–Al_2O_3$ section

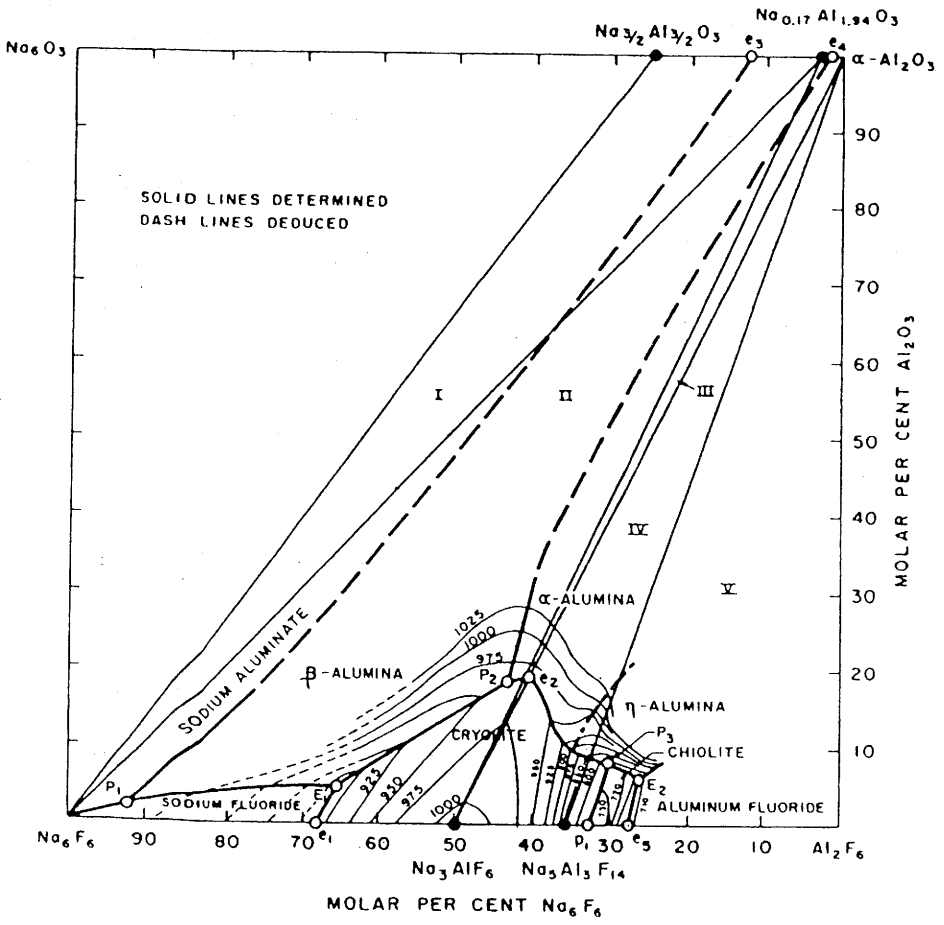

Figure 10:

Phase diagram of the ternary reciprocal system $NaF–AlF_3–Al_2O_3–Na_2O$ (50)

Point	Y_{Al} (eq.%)	Y_O	T(K)	Solid phases
e_1	85.2	100	1876	$KAlO_2$, β–Al_2O_3
p_1	94.3	100	2150	β–Al_2O_3, α–Al_2O_3
e_2	71.5	0	839	K_3AlF_6, $KAlF_4$
p_2	74.2	0	847	$KAlF_4$, AlF_3
E_1	58.6	28.8	1110	$KAlO_2$, K_3AlF_6, β–Al_2O_3
P_1	62.7	25.0	1132	β–Al_2O_3, K_3AlF_6, α–Al_2O_3
E_2	73.3	13.0	793	α–Al_2O_3, K_3AlF_6, $KAlF_4$
P_2	75.8	10.7	816	α–Al_2O_3, $KAlF_4$, AlF_3

Table 4: The invariants compositions, temperatures and related equilibrium solid phases

equilibrium with the liquid, has been already discussed by P.A. Foster, on the basis of the study of A.A. Kostjukov and finally was not retained (52, 53).

6 - ON THE ISOPLETH SECTION K_3AlF_6–α–Al_2O_3

The vertical section K_3AlF_6–α–Al_2O_3 which gives the phase relationships corresponding to the addition of α–alumina to potassium cryolite has been derived from the calculated phase diagram (fig.9) and is shown in fig.11. Consider the compositions along the line joining A (K_3AlF_6) and B(α–Al_2O_3) in fig.12 (fig.12 is a schematic representation of fig.9 to allow a more convenient definition of the points I, P_1, K and J) whose liquidus temperatures are given by the crossing of AB with the isothermal lines. The minimum of the corresponding liquidus curve occurs at point I (i.e. at 11.6 wt % α–Al_2O_3 and 1132 K) in fig.12. This minimum lies on the univariant line L+K_3AlF_6+β–Al_2O_3 and cannot be regarded as an eutectic point since the K_3AlF_6–α–Al_2O_3 section is not a simple binary system. The reason is that the composition of the primary phase formed from the melt between I and J (J lies at the crossing of the segment AB and the univariant line L + α–Al_2O_3 + β–Al_2O_3, at 21.9 wt % α–Al_2O_3 and 1640 K, fig.12), i.e. β–alumina, is not located in the AB section. The liquids whose compositions lie between the K-cryolite vertex A and the liquidus minimum I give rise to a K_3AlF_6 primary precipitation whereas those whose compositions fall between J and the α–alumina vertex B give rise to a precipitation of α–alumina as a primary phase and β–alumina as a secondary phase (the β–alumina vertex C being out of the AB vertical section). These transformations on cooling continue until the liquid becomes saturated both with respect to K_3AlF_6 and α–Al_2O_3 at point K (intersection of AB and CP_1, from the convex quadrilateral $ACBP_1$; at 13.9 wt % α–alumina and 1132 K), an invariant

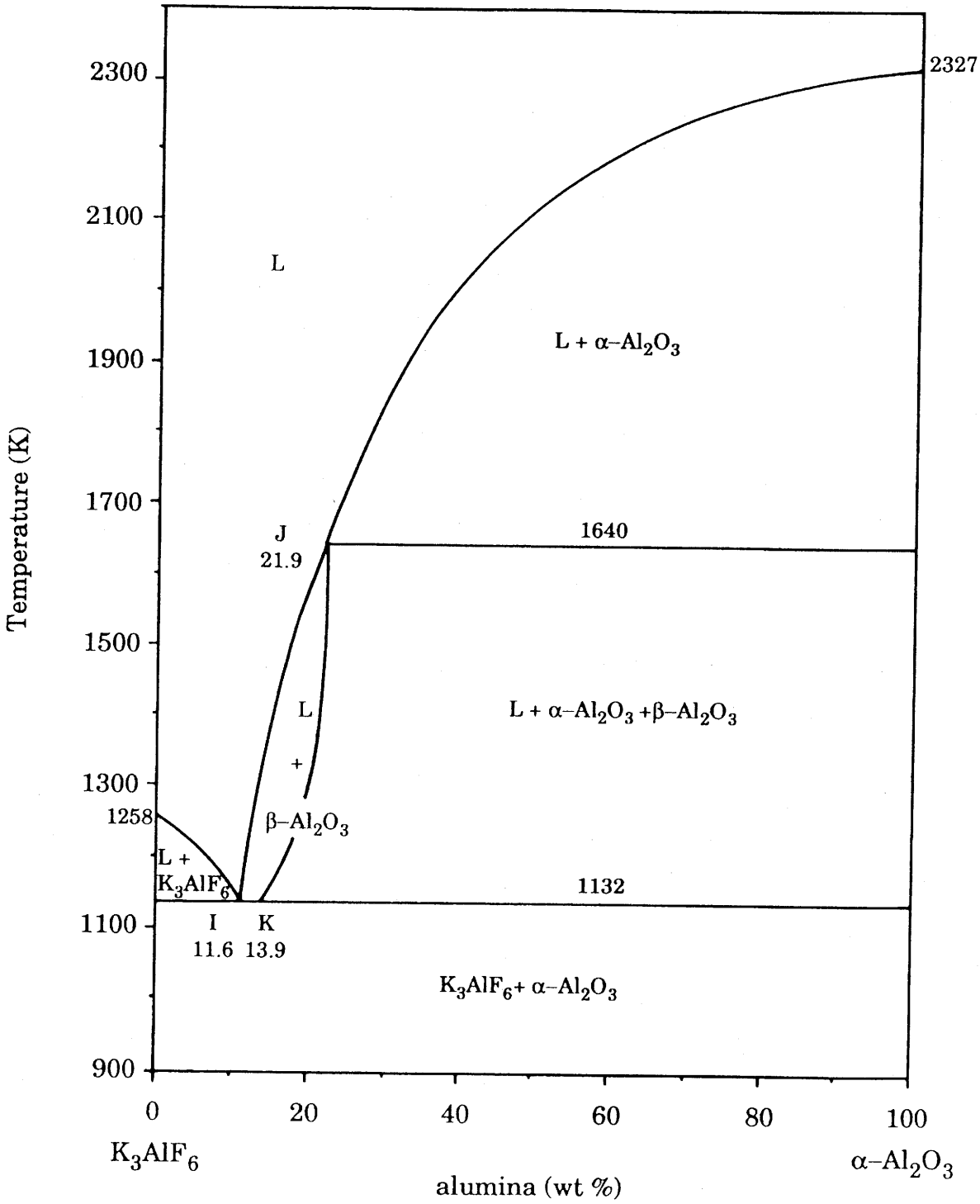

Figure 11: The K_3AlF_6–α–Al_2O_3 isopleth section of the $KF–AlF_3–Al_2O_3–K_2O$ phase diagram

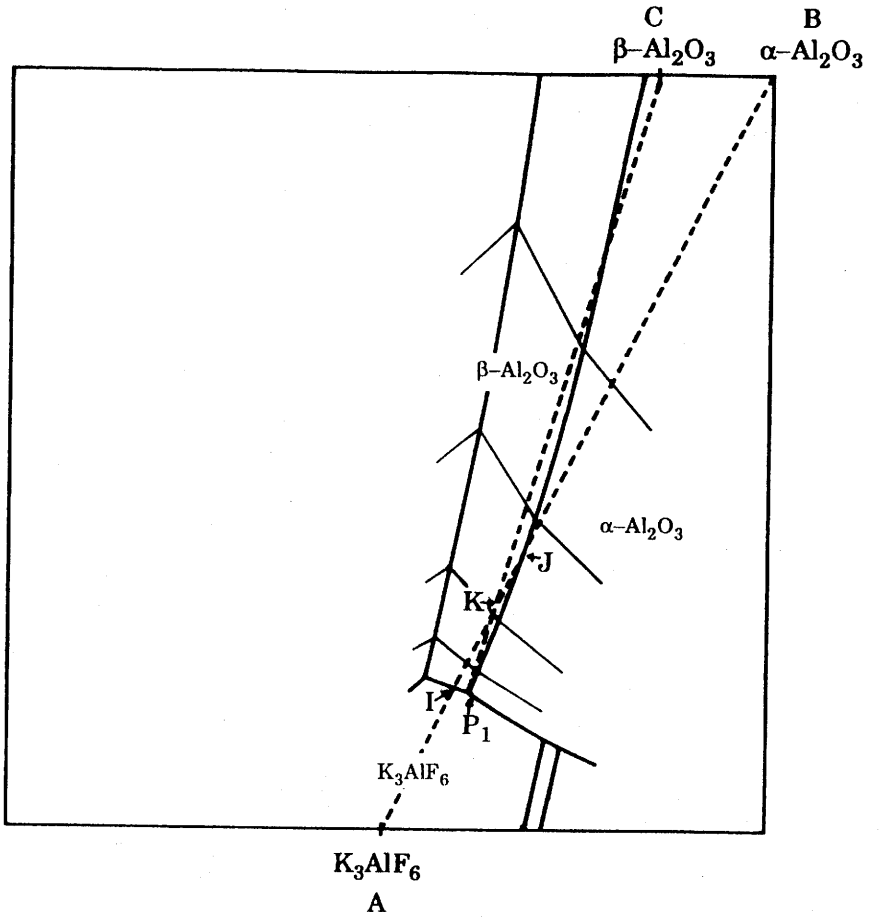

Figure 12: Schematic representation of the diagram of figure 9 to allow a more convenient definition of the points I, P_1, K and J

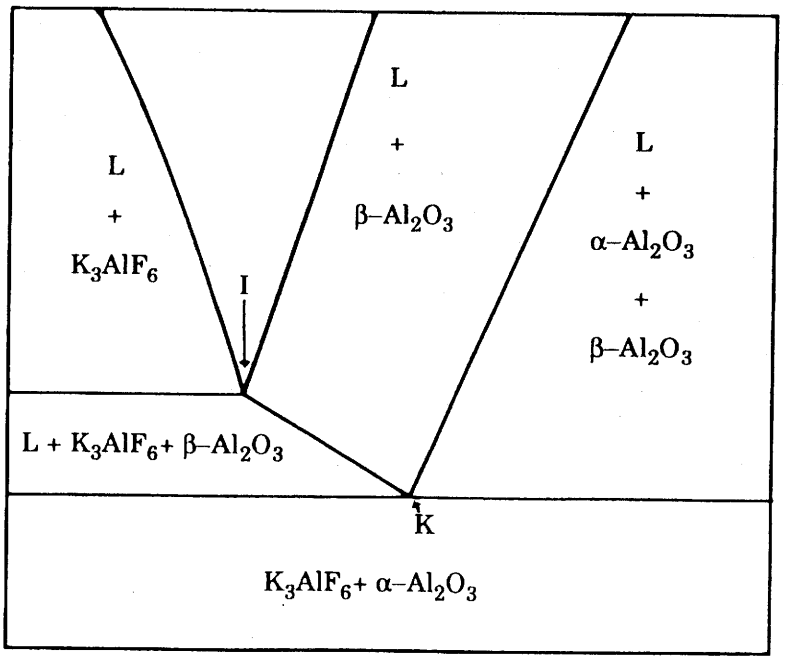

Figure 13: Phase relationship near the minimum of the liquidus in the vertical section K_3AlF_6–α–Al_2O_3 (schematic)

point corresponding to the peritectic-type following transition :

$$L + \beta\text{–}Al_2O_3 \rightleftharpoons K_3AlF_6 + \alpha\text{–}Al_2O_3 \qquad [9]$$

The secondary crystallization of β–alumina for compositions below the minimum of the liquidus I and of K_3AlF_6 for compositions between those of points I and K, as shown from fig.12 and 13, could not be evidenced from the calculations due to the fact that T_K and T_I were unresolved experimentally (the temperature invariant transition introduced in the calculations was 1132 K).

Thus, the main results of the experimental study can be justified, at least qualitatively, on the basis of fig.11. It appears from the above discussion that the first peak of complex shape observed on the DTA curves on heating (fig.4), for alumina concentrations less than 21 wt %, corresponds to the superposition of transition [9] and of the following transition :

$$L + K_3AlF_6 \rightleftharpoons \beta\text{–}Al_2O_3 \qquad [10]$$

and to the transition [10] only for alumina-rich compositions, whereas the second peak is associated to the end of melting (i.e. to the crossing of the liquidus surface). Therefore, the use of the Tammann drawing which has been made in fig.5 could be, at least formally, questioned.

Futhermore, on the basis of fig.11, it is not surprising that the liquidus could not be observed by DTA for the alumina-rich compositions, as already mentioned, since the temperature of the end of melting raises very rapidly above the T_I-T_K horizontal line, as soon as the alumina concentration is higher than those corresponding to points I, K (the liquidus temperature being well above the limit of the DTA equipment which has been used).

There is an apparent discrepancy between the calculations and the experimental results for the nature of the solids below the 1132 K invariant

transition. According to the calculations a mixture of α–Al_2O_3 and K_3AlF_6 should be present whereas K_3AlF_6, β–Al_2O_3 and $KAlF_4$ have been identified by X-ray and IR analyses for alumina concentrations ranging from 17.9 to 30.0 wt %. From the thermodynamic data which have been selected, it appears that although a mixture of K_3AlF_6, β–Al_2O_3, $KAlF_4$ is less stable than a mixture of K_3AlF_6, α–Al_2O_3 of the same composition, the difference in their total Gibbs free energies is very small. This apparent discrepancy could be due to : (i) an insuffisant accuracy in the calculations (e.g. related to the thermodynamic data which have been estimated or the assumptions which have been made) and/or (ii) the fact that equilibrium state may not have been reached in the DTA experiments. Thus, a new DTA analysis was performed on a 30.1 alumina wt % K_3AlF_6–α–Al_2O_3 sample. On cooling, the sample was annealed for 48 hours at 1090 K (and even for 240 hours in a further experiment) and then analyzed by X-ray diffraction and IR spectometry with the following main results :

(i) α–Al_2O_3 was indeed identified from the X-ray diffraction patterns in addition to β–Al_2O_3, $KAlF_4$ and K_3AlF_6 whereas the number and relative intensities of the diffraction lines of β–Al_2O_3 and $KAlF_4$ were found to have significantly decreased for the sample annealed for 240 hours with respect to those of the sample annealed for only 48 hours.

(ii) similarly the intensities of the main IR absorption lines attributed to β–Al_2O_3 were observed to have decreased as a function of the annealing time (fig.14).

Therefore, these complementary experimental data suggest that there may exist a transition between the metastable K_3AlF_6–$KAlF_4$–β–Al_2O_3 system commonly observed after cooling at room temperature and the stable K_3AlF_6–α–Al_2O_3 system, characterized by slow kinetics. The slow rate of transition could be the result of : (i) the fact that the transition takes place in the solid state and (ii) the small difference in energy between the two states which has been evidenced from the thermodynamic calculations.

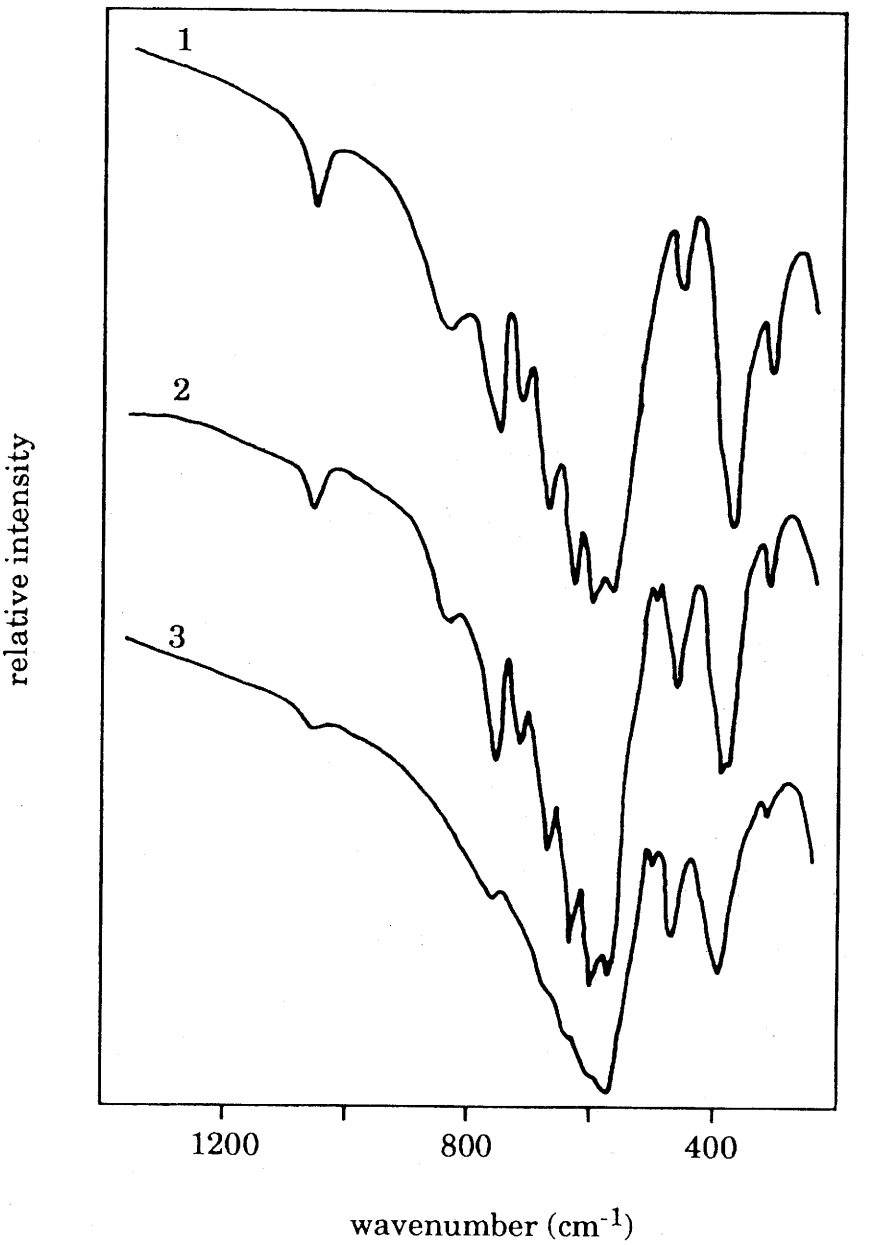

Figure 14 : I.R. spectra of the 30 wt % Al_2O_3 samples

1-DTA sample

2-after annealing 48 hours

3-after annealing 240 hours

7 - CONLUSION

The aim of this study was to draw, at least parly, the complex $KF–AlF_3–Al_2O_3–K_2O$ phase diagram, from a minimum of experimental data, utilizing an approach based on thermodynamic calculations and the CIS theory for the liquid phase.

The main features of the experimental study have been explained, at least qualitatively, from the calculated phase diagram. The main discrepancies, particularly that concerning the invariant point compositions could be due to : (i) the thermodynamic data which have been selected (some of them had to be estimated) and (ii) the fact that only two of the four edge binary systems were known.

The use of the $KF–AlF_3–Al_2O_3–K_2O$ phase diagram, calculated in the present study, for the understanding of the mechanisms of the enhancement of the wetting of SiC(or C) based ceramics by liquid aluminium alloys, will be presented in a detailed manner elsewhere (4).

ACKNOWLEDGEMENTS

The authors are indebted to professor R. Cohen-Adad for his advices concerning the interpretation of some of the features of the complex $KF–AlF_3–Al_2O_3–K_2O$ phase diagram, to J.J. Videau for the IR characterization of the materials and to J.P. Chaminade for his technical assistance.

REFERENCES

(1) - J.P. Rocher, X. Corretja, R.Pailler, J.M Quenisset and R. Naslain, *European Patent* **83.9012044,** April 14, 1983

(2) - J.P. Rocher, J.M. Quenisset , R. Naslain, *J. Mat. Sci. Letters*, **4**, 1527 (1985)

(3) - H. Lundin, *U.S Patent* **2, 686, 354,** August 17, 1954

(4) - S. Schamm, R. Fedou, J. P. Rocher, J. M. Quenisset, R. Naslain, to be submitted to Metallurgical Transactions

(5) - J.P. Rocher, J.M. Quenisset and R. Naslain, submitted to *J. Mater. Sci.*

(6) - N. Eustathopoulos, J.C. Joud, P. Desré, *J. Mater. Sci.* **9**, 1233 (1974)

(7) - M. Blander, S.J. Yosim, *J. Chem. Phys.* **39** (10), 2610 (1963)

(8) - M.L. Saboungi, *J. Chem. Phys.* **73** (11), 5800 (1980)

(9) - M.L. Saboungi, M. Blander, *J. Amer. Ceram. Soc.* **58** (1-2),1 (1974)

(10) - J.N. Barbier, C. Bernard, *Calphad XV*, Fulmer Grange UK (1986)

(11) - K. Grjotheim, C. Krohn, M. Malinovsky, K. Matiasovsky, J. Thonstad, 2nd Edition, *Aluminium Electrolysis-Fundamentals of the Hall-Héroult Process,* Aluminium-Verlag GmbH, Düsseldorf (1982)

(12) - D.A. Chin, E.A. Hollingshead, *J. Electrochem. Soc.* **113** (7), 736 (1966)

(13) - K.P. Batashev, A.I. Zhurin, *Metallurg.* **12,** 67 (1935)

(14) - A.I. Belyaev, *Legkie Metally*. **5** (3), 15 (1936)

(15) - V.P. Mashovets, *Elektrometallurghia alyuminia*, ONTI, Moscow, Leningrad (1938)

(16) - G.G. Babayan, *Armjanskii Khimicesky Zhurnal.* **20** (9), 692 (1967)

(17) - R.V. Chernov, M.I. Kostyuk, G.N. Novitskaya, *Fiz.-Khim.Svoitva Rasplavl. Tverd. Elektrolitov* , 103 (1979)

(18) - J. Grannec, L. Lozano, *Inorganic Solid Fluorides,* p.17, P. Hagenmuller Ed., Academic Press, New-York (1985)

(19) - K. Grjotheim, J.L. Holm, M. Malinovsky and S.A. Mikhaid, *Acta Chem. Scand.* **25,** 1695 (1971)

(20) - Y. Yoshida, T. Matsushima, *Keikinzoku.***19,** 488 (1969)

(21) - J. Holm, F. Gronvold, *Acta Chem. Scand.* **A27**, 2040 (1973)

(22) - L. Rabardel, to be published

(23) - N.W.F. Phillips, R.H. Singleton, E.A. Hollingshead, *J. Electrochem. Soc.* **102** (11), 648 (1955)

(24) - M. Rolin, *Bull. Soc. Chim. France,* 1201 (1960)

(25) - H. Ginsberg, A. Böhm, *Z. Elektrochem.* **61** (2), 315 (1957)

(26) - J. Brynestad, K. Grjotheim, F. Gronvold, J.L. Holm, S. Urnes, *Discussions Faraday Soc.* **32,** 90 (1961)

(27) - P.A. Foster, Jr., *J. Electrochem. Soc.* **106** (11), 971 (1959)

(28) - A. Grant Elliot, R.A. Huggins, *J. Am. Ceram. Soc.* **58** (11-12), 497 (1975)

(29) - M.J. Reisfeld, *Spectrochimica Acta* **29A,** 1923 (1973)

(30) - R.S. Krishnan, *Proc. Indian Acad. Sci.*. **26A**, 450 (1947)

(31) - R. D. Armstrong, P.M.A. Sfierwood, R.A. Wiggins, *Spectrochimica Acta.* **30A**, 1213 (1974)

(32) - S.H.K. Ratkje, *Electrochim. Acta.* **21**, 515 (1976)

(33) - M.L. Capoor, M. G. Frohberg, *Proc. Chem. Met. of Iron and Steel Symposium,* p.10, The Iron and Steel Institute Ed., England, (1971)

(34) - H. Gaye, J. Welfringer, *Second Int.Symp.on Metallurgical Slags and Fluxes,* p. 357, The Metallurgical Society of AIME Ed. (1984)

(35) - M. Blander, L.E. Topol, *Inorg. Chem.* **5** (10), 1641 (1966)

(36) - M.L. Saboungi, P.L. Lin, P. Cerisier, A.D. Pelton, *Met. Trans. B.* **11B**, 493 (1980)

(37) - P.L. Lin, A.D. Pelton, M.L. Saboungi, *Met. Trans. B.* **13B**, 61 (1982)

(38) - T. Forland, *Norg. Tek. Vitenskapsakad.*, **Ser. 2**, 4 (1957)

(39) - I. Eliezer, R.A. Howald, *High Temp. Sci.* **10**, 1 (1978)

(40) - J.S. Moya, E. Criado, S. De Aza, *J. Mat. Sci.* **17,** 2213 (1982)

(41) - Chase et al., *J. Phys. Chem.* , Ref. Data. **14** (1) (1985)

(42) - R.P. Beyer, M.J. Ferrante, R.R. Brown, *J. Chem. Thermodynamics* **12,** 985 (1980)

(43) - T.B. Lindemer, T.M. Besmann, *J. Nucl. Mat.* **100**, 178 (1981)

(44) - N.A. Pushin, A.V. Baskov, *Zh. Russ. Fiz Khim. Obshch.* **135,** 82 (1913)

(45) - P.P. Fedotiev, K. Timofeff, *Z. Anorg. Allgem. Chem.* **206**, 263 (1932)

(46) - E.P. Dergunov, *Dokl. Akad. Nauk. SSSR.* **60** (7), 1185 (1948)

(47) - C.J. Barton, L.M. Bratcher, W.R. Grimes, Unpublished Work referenced in *Phase Diagrams of Nuclear Reactor Materials* edited by R.E. Thoma, US At. Energy Comm. ORNL 2548 (1959)

(48) - B. Phillips, C.M. Warshaw, I. Mockrin, *J. Am. Ceram. Soc.* **49** (12), 631 (1966)

(49) - B. Jenssen, Thesis, The University of Trondheim, NTH Trondheim (1969)

(50) - P.A. Foster, *J. Amer. Ceram. Soc.* **58** (7-8), 288 (1975)

(51) - L.J. Gauckler, H.L. Lukas, E.-Th. Henig and G. Petzow, *Calphad* **2** (4), 349 (1978)

(52) - P.A. Foster, Jr., *J. Chem. Eng. Data.* **9** (2), 200 (1964)

(53) - A.A. Kostjukov, *Metallurgie des Aluminiums,* vol I, VEB Verlag Teknik, Berlin (1956)

CHAPITRE II

INTRODUCTION AU CHAPITRE II

Afin de mettre en évidence les phénomènes physico-chimiques qui sont impliqués dans le procédé au K_2ZrF_6, une double analyse a été effectuée. D'une part, l'amélioration du mouillage des préformes céramiques par l'aluminium en présence du fluorure K_2ZrF_6 est interprétée grâce à des considérations thermodynamiques. D'autre part, l'influence des paramètres physiques associés au procédé sur l'aptitude à l'imprégnation de préformes céramiques poreuses est étudiée sur la base d'une approche numérique.

Le calcul des variations d'énergie libre de Gibbs et d'enthalpie des deux réactions principales associées au procédé au K_2ZrF_6, i.e. :

$$3\ "2KF,ZrF_4" + 4\ Al \rightleftharpoons "6KF,4AlF_3" + 3\ Zr$$

et

$$9\ Al + 3\ Zr \rightleftharpoons 3\ Al_3Zr$$

montre qu'elles sont effectivement favorisées d'un point de vue thermodynamique et qu'elles sont **très exothermiques** (700°C). L'**élevation locale de température** causée par cette source de chaleur a pu être estimée grâce à une approche numérique basée sur la modélisation de l'imprégnation de préformes poreuses appliquée au cas des renforts du type 2D-SiC(Nicalon)/SiC(CVI) imprégnés avec succès par J.P. Rocher et al. La température au sein d'un tel renfort, prétraité par le fluorure, préchauffé à 650°C et sur lequel l'aluminium liquide a été versé, pourrait atteindre environ 800°C. A cette température, l'analyse de la section verticale "$6KF,4AlF_3$"-Al_2O_3, extraite du diagramme de phases du système ternaire réciproque KF-AlF_3-Al_2O_3-K_2O présenté au chapitre I, montre que **le mélange de quelques % de Al_2O_3 (mol) avec "$6KF,4AlF_3$" forme une phase liquide homogène très fluide**. L'alumine serait donc dissoute et la phase liquide formée, en s'éloignant de

l'interface Al/SiC vers la surface du métal liquide, rendrait possible le contact réel entre le métal et la céramique vers 800°C. Dans ces conditions, l'aluminium mouille le carbure de silicium.

Grâce au modèle numérique cité précédemment et développé par J. M. Quenisset et al. dans le cas du forgeage liquide appliqué à des préformes unidirectionnelles imprégnées parallèlement ou perpendiculairement à la direction des fibres, l'influence de l'**exothermicité** des réactions chimiques sur la profondeur maximale qu'il est possible d'imprégner, de même que l'influence de l'**abaissement de l'angle de contact** sur les pressions nécessaires à appliquer à l'entrée des préformes pour imprégner jusqu'à la profondeur maximale sont discutées.

Soumis à "Metallurgical Transactions"

THE K_2ZrF_6 WETTING PROCESS. EFFECT OF SURFACE CHEMISTRY ON THE ABILITY OF A SiC-FIBER PREFORM TO BE IMPREGNATED BY ALUMINUM

S. SCHAMM[1] , R. FEDOU[2], J.P. ROCHER[3], J.M. QUENISSET and R. NASLAIN[2]
Laboratoire de Chimie du Solide du CNRS, Université de Bordeaux I
351, Cours de la Libération, F-33405 Talence

ABSTRACT

SiC-ceramic materials, either as flat substrates or porous fiber preforms are spontaneously wetted by aluminum at 700-800°C when they have been pretreated with an aqueous solution of K_2ZrF_6. The wetting enhancement effect results from exothermic chemical reactions occuring at the SiC/Al interface. The first phenomenon thought to occur is a dislocation of the alumina film covering liquid aluminum due to a reaction of Al_2O_3 with K_2ZrF_6. Then alumina is totally dissolved, at low temperatures, by potassium/aluminum mixed fluorides, giving rise to a very fluid cryolitic liquid spreading out on the surface of liquid aluminum and to the true SiC/Al interface. Simultaneously, a large evolution of heat occurs

Present addresses :
1 CEMES-Laboratoire d'Optique Electronique du CNRS
29 rue J. Marvig, F-31055 Toulouse cédex
2 Laboratoire des Composites Thermostructuraux
Europarc, 3 avenue L. de Vinci, F-33600 Pessac
3 Société Européenne de Propulsion
BP 37, F-33165 Saint Médard-en-Jalles

mainly due to the reduction of K_2ZrF_6 by aluminum and the formation of Al_3Zr. The impregnation of 2D-SiC/SiC preforms by aluminum is modelled and the effect of both the contact angle decrease and local temperature rise, on the impregnation of the preforms, e.g. by gravity casting, is established.

Key-words *WETTING, METAL MATRIX COMPOSITE, SILICON CARBIDE, FIBER PREFORM, ALUMINUM, K_2ZrF_6.*

1 - INTRODUCTION

The elaboration of aluminum matrix composites (AMCs) according to processing techniques deriving from those already used in light alloy casting is made difficult by two main problems : (i) most ceramic fibers (e.g. C or SiC-based fibers) are poorly wetted by liquid aluminum at the casting temperatures of light alloys (i.e. 700-800°C) with the result that preforms of complex fiber architectures are only partially infiltrated by the metal and (ii) these fibers react with aluminum above about 500°C to form a layer of Al_4C_3 crystals lowering the fiber strength, rendering the matrix brittle and increasing the sensitivity of the material to aqueous corrosion (1, 2).

Various solutions have been proposed to enhance the wetting ability of ceramic fibers by liquid aluminum. Generally speaking, they are based on two different approaches : (i) surface treatments of the fibers including coating by metals (Cu, Ag, Ni) or ceramics (Ti-B, Ti-C, Zr-C) as well as treatments by alkali metals (e.g. Na-K/Sn-Mg) (3) and (ii) addition of specific alloying elements to aluminum (Li, Ca, Mg) (4, 5).

The **metal coatings** poorly protect the fibers against the attack by aluminum and the resulting intermetallic compounds ($NiAl_3$) or carbides embrittle the matrix. Furthermore, in order to achieve a good wetting of the fibers by aluminum, the coating has to be continuous and thus rather thick (typically about 1 μm) yielding a significant increase in the material density when the volume fraction of fibers is high (usually 0.4 to 0.5). The wetting by liquid aluminum of fibers coated with a **ceramic deposit**, e.g. a titanium or zirconium carbide, is rarely excellent even under a pressure of a few atmospheres. A Ti-B deposit, which is probably the best ceramic coating in this field, no longer promotes the wetting if it is in contact with the ambiant atmosphere prior to the impregnation step. In the alkali metal process, the surface treatment has to be performed in an inert atmosphere. Finally, all the

surface treatment processes are usually limited to the preparation of semi-products (e.g. composite wires or tapes). Therefore, the elaboration of near net shape parts implies additional and costly steps, such as hot-pressing.

In a similar manner, the impregnation of a porous fiber preform by liquid **Al-Li alloys** has to be conducted under vacuum (or a low pressure of an inert gas) in order to make easier the penetration of the liquid metal in the pore network and avoid an excessive oxidation of lithium.

Regarding the drawbacks of the various techniques presented above, the processing of AMCs is usually performed according to a **squeeze casting technique** in which a high pressure (about 100 MPa) is applied to the liquid with a piston. Under such conditions, the liquid is forced to flow in the pore network of the preform, the pressure compensating the absence of wetting and capillary rise of the metal. Furthermore, since pressure is maintained during cooling, it contributes to close the micropores in the material and yields a matrix of higher microstructural and mechanical quality. However, squeeze casting would be a costly processing technique for parts of large dimensions mainly due to the size of the pressing equipments (6).

A new wetting treatment, which permits the spontaneous impregnation of ceramic porous preforms (made of C or SiC-based fibers) by liquid aluminum alloys at low temperatures (i.e. at a temperature slightly above the liquidus), has been proposed by Rocher et al. (7). In its principle, it consists of a treatment, applied directly to the preform, according to which **K_2ZrF_6 microcrystals** are precipitated on the fiber surface, from an **aqueous solution** at a temperature close to the boiling point . After elimination of the solvent by drying, the treated preform can be totally inpregnated with a liquid aluminum alloy at about 800°C by simple gravity casting. The process was successfully applied to various kinds of preforms including 2D-SiC(Nicalon)/SiC(CVI) preforms (8).

The aim of the present contribution is to discuss the mechanims which may be at the origin of the observed wetting enhancement of the ceramic fibers as well as to show the effect of the K_2ZrF_6 treatment on the impregnation ability of the preform by liquid aluminum. The experimental results and thermodynamic calculations that will be used have been presented elsewhere and will be only briefly recalled for the purpose of discussion (9, 10).

2 - ORIGIN OF THE WETTING ENHANCEMENT

2.1 - Experimental results recall

The efficiency of the K_2ZrF_6-process, in terms of wetting improvement, has been established by Rocher et al. on the basis of both preform impregnation experiments at laboratory scale and sessile drop experiments (9). Their main results will be briefly recalled and compared to those reported by other authors, for the purpose of discussion.

When **a preform made of SiC-based fibers*** is first treated with an aqueous K_2ZrF_6 solution at about 80°C, in order to obtain a deposit of a few mg of K_2ZrF_6 per cm^2 after evaporation of the solvent, and then put in contact with the surface of a bath of liquid aluminum in air, the following phenomena are observed : (i) the preform rapidly turns red due to an evolution of heat and (ii) simultaneously, the liquid metal climbs by capillary effect in the preform, the liquid front remaining roughly parallel to the preform-bath contact plane.

Sessile drop experiments were performed under a good vacuum (residual pressure : 10^{-4} to 5.10^{-4} Pa) with plan substrates of graphite coated by CVD with a

---

* Nicalon fibers from Nippon carbon, Japan.

thick deposit of SiC, and pure aluminum (chemically etched prior to the experiment in order to remove the majority of the alumina layer). The substrates have been submitted or not to the K_2ZrF_6 surface treatment. The variations of the contact angle θ as a function of both temperature and time are shown in figures 1 and 2. Data from other authors taken from literature have been added to the original Rocher et al. data for the purpose of discussion.

When the K_2ZrF_6 surface treatment is not applied, the value of θ at the processing temperatures of AMCs, i.e. 700-800°C, remains very high (θ = 160°), a feature which is typical of a non-wetting behavior. It is only by raising temperature at about 900-950°C that the transition non-wetting/wetting takes place. Conversely, when the SiC-substrate has been treated with K_2ZrF_6 prior to the sessile drop experiment, wetting occurs as soon as aluminum melts. Moreover, lower θ values are observed when the amount of K_2ZrF_6 deposited on the substrate is increased (θ = 73° and 50° when the amount of K_2ZrF_6 is 9 and 12 $mg.cm^{-2}$, respectively). Finally, the contact angle value remains constant after only a few minutes of contact between the substrate and the liquid.

It is worthy of note that the θ values reported by Rocher et al. for substrates treated with K_2ZrF_6 and sessile drop experiments performed at low temperatures (i.e. 700-850°C) and a few minutes of contact, are similar to those measured (after 30 min of contact) with SiC-single crystal/pure aluminum couples by : (i) Köhler, above 1000°C and for a residual pressure of $2\text{-}8.10^{-4}$ Pa and (ii) Laurent, beyond 800°C and for a residual pressure of 10^{-4} - 5.10^{-5} Pa (11, 12).

Therefore, K_2ZrF_6 seems to activate both thermally and kinetically the decrease of the contact angle between a SiC-substrate and liquid aluminum.

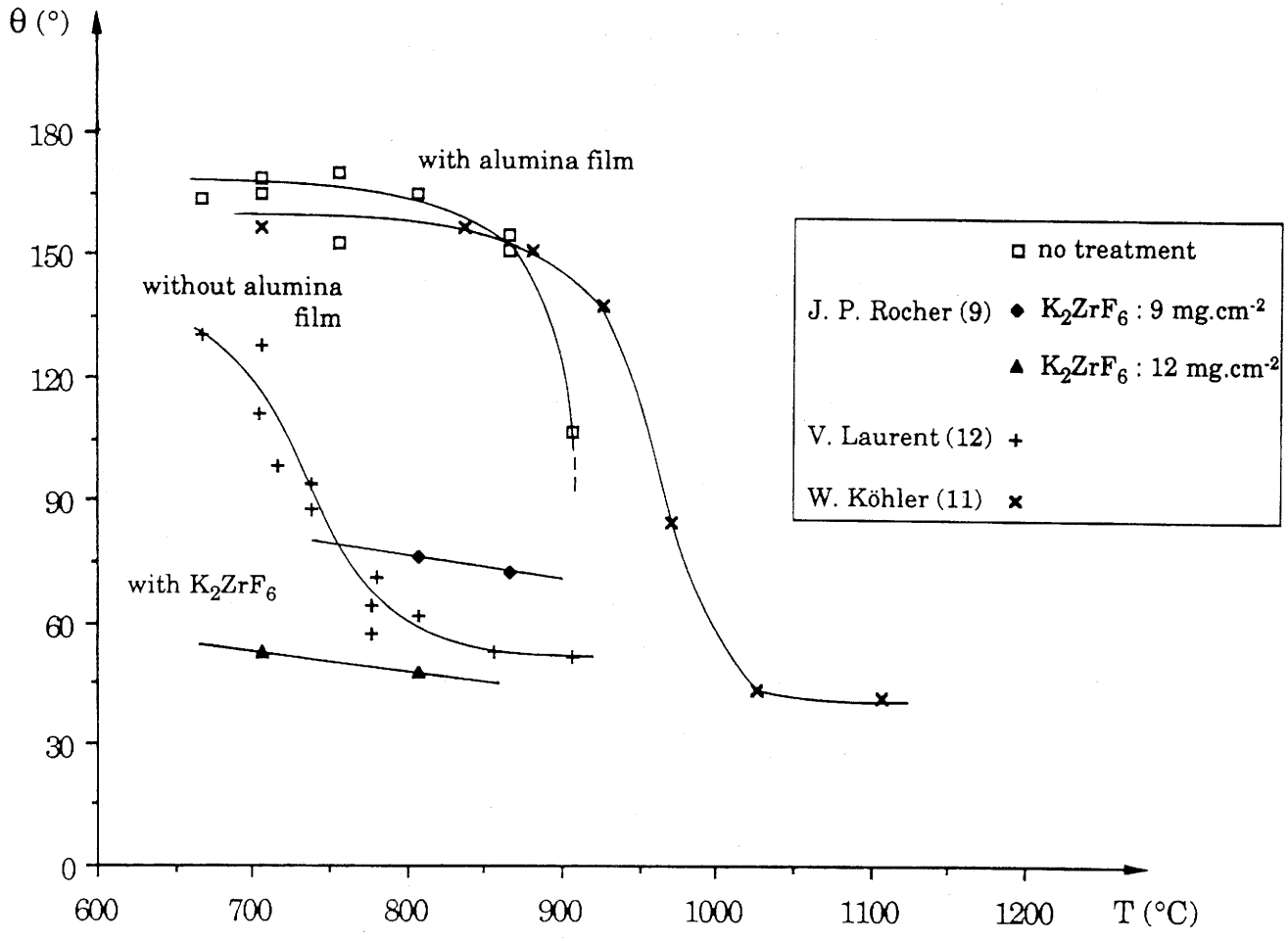

Figure 1 : Variations of the SiC/Al contact angle (θ) as a function of temperature (T), from sessile drop experiments

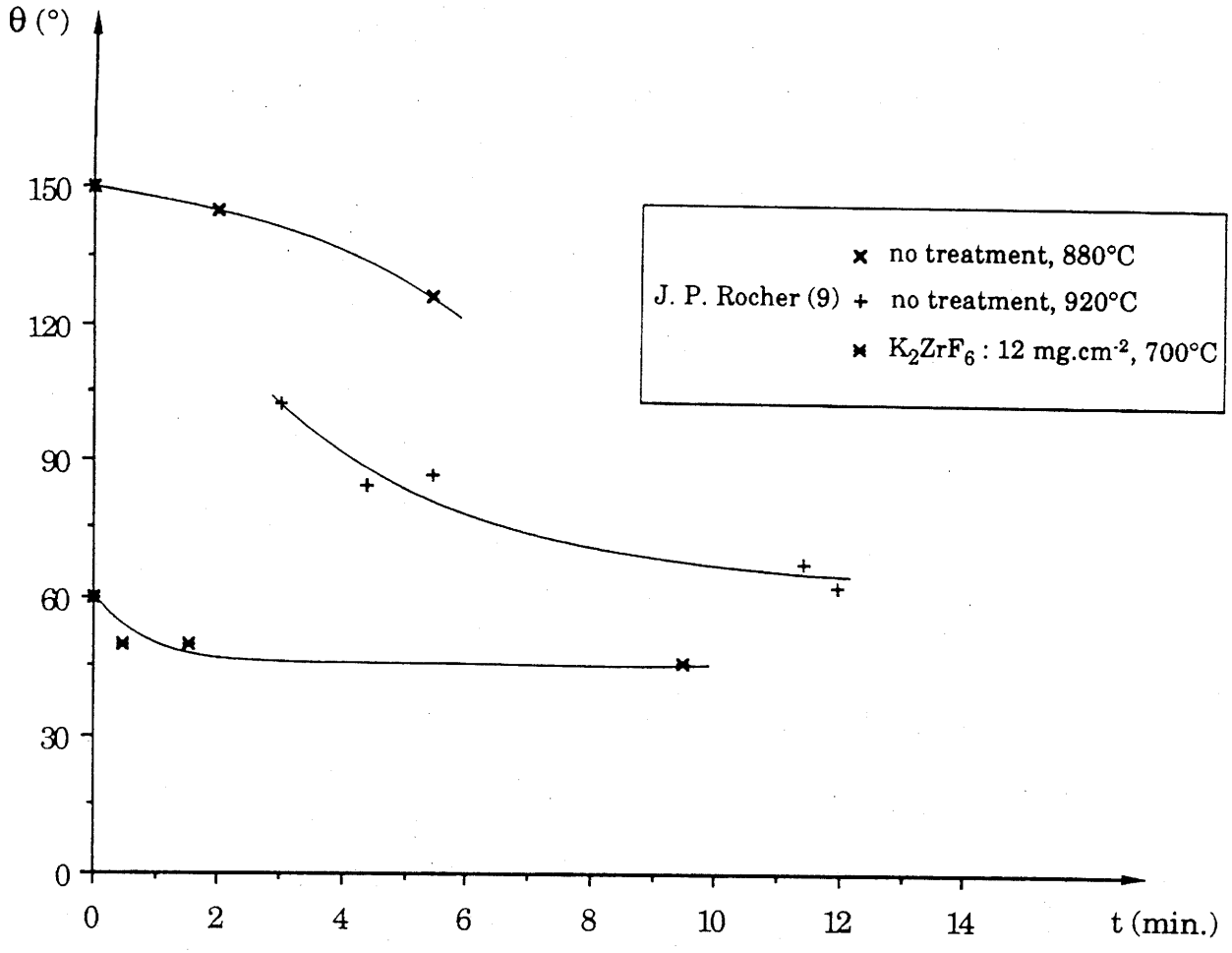

Figure 2 : Variations of the SiC/Al contact angle (θ) as a function of time (t), from sessile drop experiments

2.2 - Mechanisms

2.2.1 - Sessile drop experiment without K_2ZrF_6 treatment

Laurent et al. have shown that under particularly clean sessile drop experiment conditions (i.e. $P_T \leq 5.10^{-5}$ Pa ; $P_{O_2} \leq 10^{-15}$ Pa ; alumina layer separated mechanically from the aluminum sample just before the sessile drop experiment), the thin film of alumina still present on aluminum at the melting point and which prevents the wetting of the SiC substrate from taking place is reduced by aluminum according to the following equation (13) :

$$4\,Al_{(l)} + Al_2O_{3(s)} \rightleftharpoons 3\,Al_2O_{(g)} \qquad [1]$$

As soon as the true SiC/Al interface has been formed, the variations of the contact angle vs time are controlled by the dissolution of SiC in the liquid metal according to the following equation thought to be the rate limiting step in the formation of Al_4C_3 :

$$4\,Al_{(l)} + 3\,SiC_{(s)} \rightleftharpoons Al_4C_{3(s)} + 3\,(Si)_{Al} \qquad [2]$$

and whose kinetics obey an exponential law with respect to temperature.

As a matter of fact, the sessile drop experiment conditions used by both Rocher (9) and Köhler (11), i.e. a vacuum corresponding to a higher residual total pressure (one order of magnitude) and oxygen partial pressure, do not modify the general shape of the $\theta = f(T)$ curve, as shown in figure 1. However, for isothermal contacts of same durations : (i) the deoxidation process is shifted towards the high temperatures (by about 200°C) and (ii) the slope of the $\theta = f(T)$ curve (related to the thermal dependence of the SiC dissolution in liquid aluminum) is higher at 950°C than at 750°C.

2.2.2 - Sessile drop experiments and lab-scale preform impregnation with K_2ZrF_6 treatment

2.2.2.1 - Dislocation of the alumina film

Reaction mechanisms related to the interaction between K_2ZrF_6 and liquid aluminum, have been already suggested by Lundin (14) or Bushe and Semenov (15) to take into account the wetting enhancement phenomena observed in their processes used to fabricate aluminum-steel bimetallic materials. They proposed the following **overall** equations :

$$3\,K_2ZrF_6 + 4\,Al \rightleftharpoons 6KF.4AlF_3 + 3\,Zr \qquad [3]$$

or

$$3\,K_2ZrF_6 + 4\,Al \rightleftharpoons 6KF + 4AlF_3 + 3\,Zr \qquad [3']$$

In the present process, when either (i) liquid aluminum at 800°C comes in contact with a fibrous preform which has been pretreated with K_2ZrF_6 and preheated at about 650°C or (ii) an aluminum drop/SiC plane substrate (pretreated with K_2ZrF_6) couple is heated at a temperature slightly above the melting point of the metal, the fluoride species are first in contact with alumina present at the metal surface. Therefore, the first reaction which might take place is thought to involve **fluoride species and alumina**. It could be written, with reference to equation [3] as :

$$3\,"2KF,ZrF_4"\, + 2\,Al_2O_3 \rightleftharpoons "6KF,4AlF_3" + 3\,ZrO_2 \qquad [4]$$

on the basis of the following considerations. As a matter of fact, K_2ZrF_6 undergoes a peritectic melting at a temperature of 592°C, as shown in figure 3 (16). Thus, it is assumed that K_2ZrF_6, at a temperature corresponding to our experiments, e.g. 700°C, is totally decomposed into a mixture of a liquid phase and K_3ZrF_7 :

$$2\,"KF,ZrF_4" = x\,L\,(KF, ZrF_4) + y\,K_3ZrF_7$$

where L (KF, ZrF_4) is the liquid in equilibrium with K_3ZrF_7 at 700°C in the KF-ZrF_4 phase diagram and x + y = 1. In the following, this mixture resulting from the

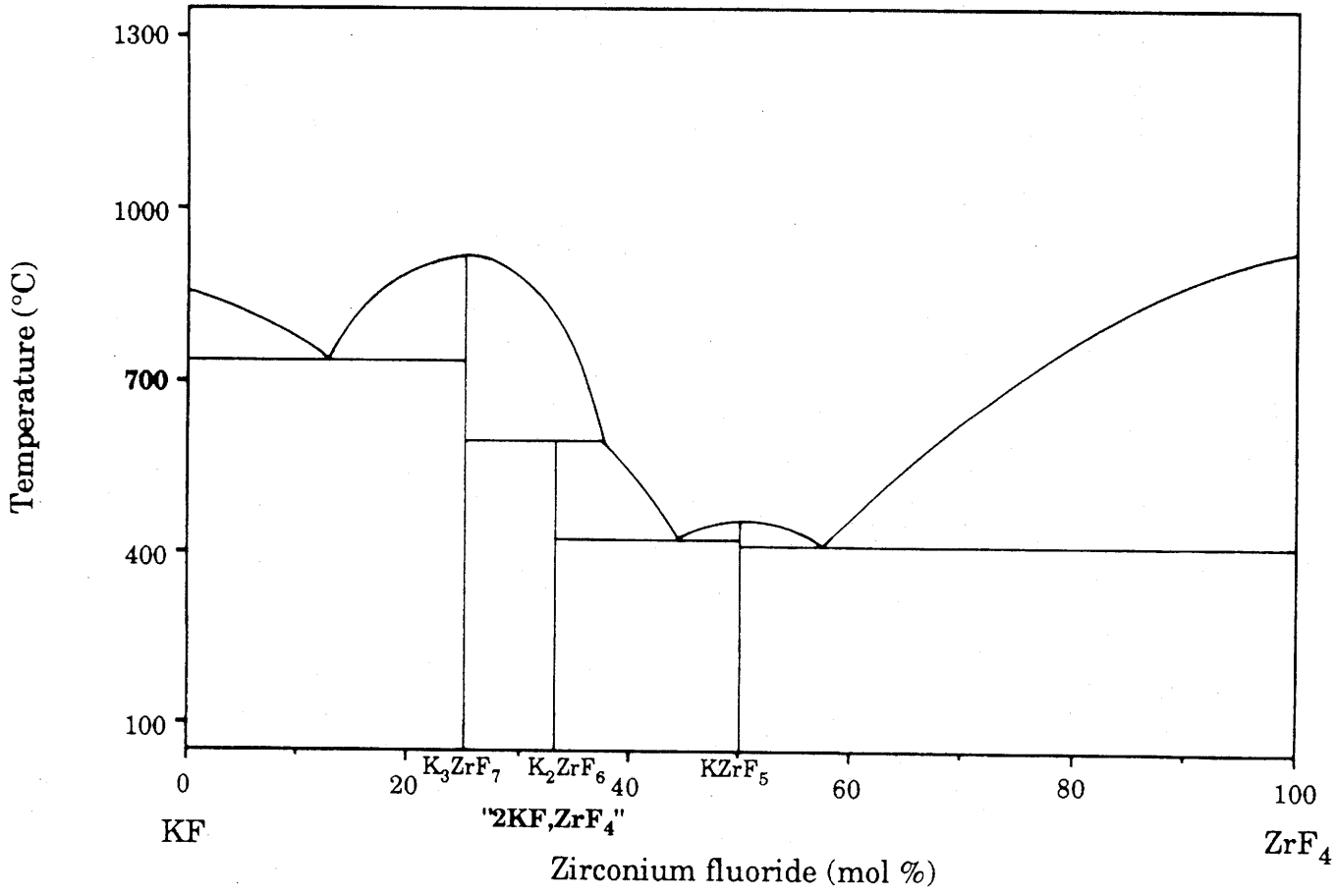

Figure 3: The calculated KF-ZrF_4 binary phase diagram (16)

decomposition of K_2ZrF_6 will be referred to as "$2KF,ZrF_4$". In a similar manner, "$6KF,4AlF_3$" will be used for the mixture of liquid phase and K_3AlF_6 corresponding to that specific composition (see equations [3] and [4]) at the same temperature in the $KF-AlF_3$ phase diagram, as shown in figure 4 (10) :

$$\text{"}6KF,4AlF_3\text{"} = x'\ L\,(KF, AlF_3) + y'\ K_3AlF_6$$

where L (KF,AlF_3) is the liquid in equilibrium with K_3AlF_6 at 700°C and $x' + y' = 1$.

On the basis of a thermodynamic study which has been published elsewhere (10), the Gibbs free energies of formation of both "$2KF,ZrF_4$" and "$6KF,4AlF_3$" as well as the Gibbs free energy variation corresponding to equation [4] were calculated. These calculations have shown that the chemical reaction between alumina and the products of decomposition of K_2ZrF_6 at 700°C is indeed **highly favored** since $\Delta G^\circ[4] = -\ 282.6\ kJ.mol^{-1}$ at 700°C.

In order to verify this conclusion, a 3 K_2ZrF_6 - 2 Al_2O_3 mixture was prepared in a dry glove box and set in a platinum tube which was then sealed under an atmosphere of dry argon. After heat treatment and cooling, an X-ray diffraction analysis showed that the only crystallized phases in the reaction product were K_3AlF_6; $KAlF_4$ and ZrO_2. This result is in full agreement with the thermodynamic calculations and equation [4] since "$6KF,4AlF_3$" gives a K_3AlF_6 + 3 $KAlF_4$ mixture after cooling at room temperature, as shown in figure 4.

Conversely, zirconia formed according to equation [4] could react immediately with aluminum at 700°C according to the following equation :

$$3\,ZrO_2 + 4\,Al \rightleftharpoons 2\,Al_2O_3 + 3\,Zr \qquad [5]$$

since the variation of the Gibbs free energy corresponding to equation [5], $\Delta G^\circ[5] = -\ 1.8\ kJ.mol^{-1}$, is slightly negative.

Thus, during a first step, the **thin alumina film** on the surface of liquid aluminum (known to prevent the wetting of the substrate) is **dislocated** at 700-800°C

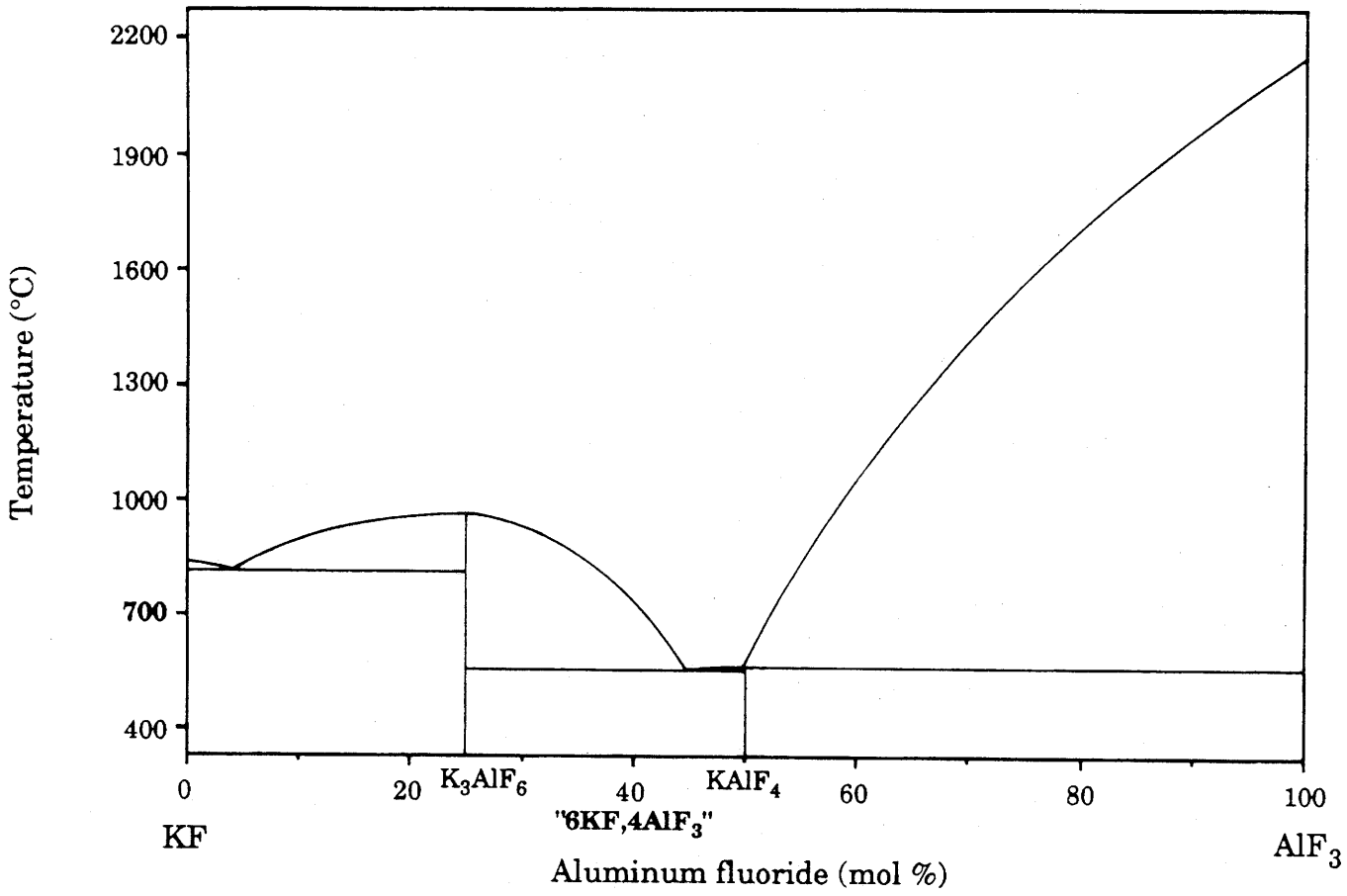

Figure 4: The calculated KF-AlF_3 binary phase diagram (10)

as the result of the chemical reactions corresponding to equations [4] and [5], allowing thus the liquid metal to come in contact with the K_2ZrF_6 deposit.

2.2.2.2 - Dissolution of the alumina film

In a second step, the alumina film is **totally dissolved** by the "$6KF,4AlF_3$" mixture formed as a result of the addition of equations [4] and [5], i.e. the following overall equation corresponding to another writting of equations [3] and [3'] taking into account the physical states at 700°C of the various species which are involved :

$$3\ "KF,ZrF_4" + 4\ Al \rightleftharpoons "6KF,4AlF_3" + 3\ Zr \qquad [3"]$$

This statement is based on the results of a thermodynamic study of the reciprocal ternary system $KF\text{-}AlF_3\text{-}Al_2O_3\text{-}K_2O$ and related binary systems, which have been published in details elsewhere (10). From these results, the vertical section "$6KF,4AlF_3$"-Al_2O_3 has been calculated and is shown in figure 5. As a matter of fact, it appears from figure 5 that for alumina concentrations corresponding to our experiments, i.e. about **a few mol. Al_2O_3 %**, the oxide can be totally dissolved for temperatures higher than 520°C (this alumina concentration corresponds to a film of alumina 100 Å in thickness and to a K_2ZrF_6 coating of a few $mg.cm^{-2}$).

2.2.2.3 - Local temperature rise

In a last step, zirconium formed according to equation [3"] can further react with aluminum which is in excess to lead to the formation of **intermetallic compounds**, according to the following equation :

$$3\ Zr + 9\ Al \rightleftharpoons 3\ Al_3Zr \qquad [6]$$

Reactions [3"] and [6] which might take place simultaneously are very exothermic since $\Delta H[3"] = -306.4\ kJ.mol^{-1}$ and $\Delta H[6] = -487.2\ kJ.mol^{-1}$ respectively. This heat

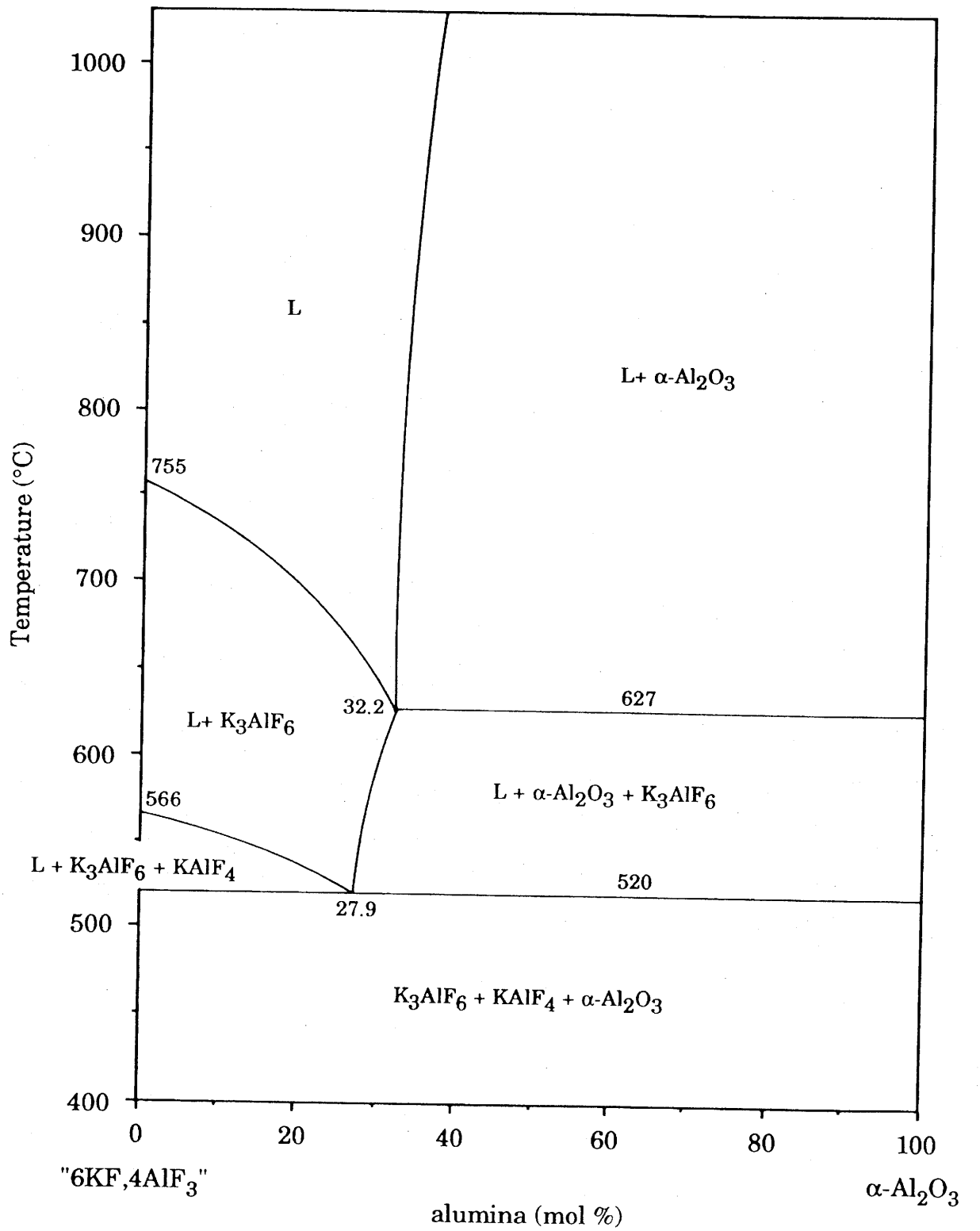

Figure 5 : The vertical section "$6KF,4AlF_3$"–α–Al_2O_3 from the $KF–AlF_3–Al_2O_3–K_2O$ ternary reciprocal system (10)

evolution yields a **local temperature rise** either at the fiber/matrix or liquid aluminum drop/substrate interfaces which is thought to be particularly significant for preforms due to (i) the high inner pore surface and (ii) the important amount of K_2ZrF_6. In section 3, a model will be presented allowing the calculation of temperature in a porous fiber preform during an impregnation experiment according to the K_2ZrF_6-process, when exothermic reactions (such as those already mentioned) take place. It will be shown that a temperature increase as high as 150°C may occur thus justifying the experimental observations reported in section 2.1.

2.3 - Discussion

It clearly appears from figure 5 that an excess of fluoride mixture "$6KF,4AlF_3$" coming in contact to a thin layer of solid alumina will yield a homogeneous liquid phase at those temperatures corresponding to preform impregnations. This liquid, formed in situ between silicon carbide and liquid aluminum, modifies significantly the **wetting ability** of the ceramic material.

In a totally different field and processing technique, the influence of K_2ZrF_6 on the ability of steel sheets to be wetted by liquid aluminum has been reported by Lundin (14). When a K_2ZrF_6 powder was poured on the surface of a liquid aluminum bath, it melts and forms a **very fluid liquid** which spreads out on the entire bath surface (like oil dropped on the surface of water). Furthermore, when this liquid was generated at the interface between a sheet of steel coated with K_2ZrF_6 and a bath of aluminum in which the sheet was dipped, it was observed that this liquid tends to move up towards the bath surface where it spreads out.

During our impregnation experiments on fiber preforms, performed in air by gravity casting, it was also observed that a fluid liquid resulting from the interaction between the K_2ZrF_6 treated preform and aluminum has been formed.

Due to metal flow, density difference and surface tension considerations, it was located logically in the dead head of the casting. After cooling, X-ray diffraction analysis showed that the product mainly consists of a mixture of K_3AlF_6; $KAlF_4$ and alumina compounds, in agreement with the reaction mechanisms discussed in sections 2.2.2.

As a matter of fact, the molten mixture "$6KF,4AlF_3$"-Al_2O_3 considered in our K_2ZrF_6-process is analogous to the molten **cryolitic mixture** Na_3AlF_6-Al_2O_3, used in the electrolytic fabrication of aluminum according to the Hall-Héroult process, from a chemical point of view. Thus, since the physical properties of the "$6KF,4AlF_3$"-Al_2O_3 molten mixture are not known, we will used in the following discussion those of the related sodium-based molten mixtures which are well established (and will be given between parentheses) (17).

The "$6KF,4AlF_3$"-Al_2O_3 liquid, which is non miscible with liquid aluminum and has a lower density ($\simeq$ 2.1 and 2.38 $g.cm^{-3}$ respectively) will move up towards the free surface of the metal, across the drop of aluminum (in a sessile drop experiment) or the aluminum dead head (in gravity casting impregnation), from the SiC/Al interface(s) where it has been formed. The surface tension of liquid aluminum (oxidized, 865 $erg.cm^{-2}$) is higher than the surface tension of the molten cryolitic mixture (in air, 140 $erg.cm^{-2}$) (17,18). Therefore, as discussed by Carter and Jones, the "$6KF,4AlF_3$"-Al_2O_3 liquid will spread out on the surface of the drop (or of the bath) (19). As a result, the alumina film initially present at the surface of liquid aluminum will be totally dissolved and replaced by a film of cryolitic liquid whereas the **true SiC/Al interface** is formed. When the experiments are performed in air, this cryolitic film protects the aluminum bath against any further oxidation.

In conclusion, the formation of the true SiC/Al interface at temperatures close to 800°C (taking into account the evolution of heat related to exothermic reactions) associated with that of a liquid cryolitic-type phase at the surface of liquid aluminum, seem to justify the low contact angle values which have been measured

for SiC substrates pretreated with K_2ZrF_6 (and which are, as a matter of fact, close to those measured by Laurent under very clean conditions at the same temperatures). The same phenomena could also explain the dramatic enhancement of the abilility of K_2ZrF_6-pretreated fiber preforms to be impregnated by liquid aluminum.

3 - EFFECT OF THE K_2ZrF_6 TREATMENT ON THE IMPREGNATION PARAMETERS OF A POROUS FIBROUS PREFORM

3.1 - Impregnation modelling

Quenisset et al. have recently modelled, on the basis of a numerical approach, the impregnation of a porous fiber preform by liquid aluminum alloy according to the **squeeze casting** process (20). The aim of their work was to study the effect of various parameters on : (i) the maximum impregnation depth referred to as z_M and (ii) the minimum pressure in the metal at pore entrance necessary to allow the impregnation of the preform at z_M, referred to as P_m. Among the parameters which have been considered were processing parameters (i.e. temperatures of both the liquid metal and porous preform, impregnation rate) as well as material parameters (i.e. volume fraction, density, specific heat and thermal conductivity for both the reinforcement and the matrix, preform permeability, viscosity and surface tension of the liquid metal and finally contact angle between the reinforcement and the liquid alloy).

The modelling was based on the general equations of heat and mass transfers combined with simplified boundary conditions. It was derived for **unidirectional preforms** assumed to be of semi infinite volume and made of a **hexagonal packing of cylindrical fibers** lying parallel (longitudinal direction L) or perpendicular (transverse direction T) to the impregnation direction. It was further

assumed that impregnation proceeds at constant speed U and stops (at $z = z_M$ from the preform surface) when temperature at the impregnation front reaches the liquidus temperature of the alloy. Finally, the model took into account capillary effect as well as the occurrence of heat sources during impregnation.

3.2 - Impregnation of porous SiC-fiber preforms

The Quenisset modelling was used in present work to **compare** the values of the impregnation parameters (mainly P_m and z_M) of porous SiC-preforms depending on whether they have been pretreated or not with K_2ZrF_6 prior to impregnation.

3.2.1 - Preform modelling and impregnation conditions

The fiber preforms which have been used by Rocher (21) to establish the feasibility of the K_2ZrF_6-process were made of a stack of SiC-fabrics* partly densified with SiC according to a CVI-technique which has been described in details elsewhere (22). Their residual open porosity was of the order of 20%. Obviously, such materials have a 2D-texture with large pores between adjacent fibrous layers. However, since the purpose of our study was simply to emphasize the effect of a K_2ZrF_6-pretreatment on the impregnation ability of a SiC-preform with respect to liquid aluminum, we assumed that such preforms could be modelled, in first approximation, as an **hexagonal array of SiC fibrous cylinders with the same overall open porosity**, i.e. 20%. The diameter of these equivalent cylinders, calculated from the mean value of the experimentally determined preform pores sizes and the relation between the pore diameter (D_p) and the cylinder diameter (D_c) in an hexagonal array (i.e. $V_f / (1-V_f) = D_p / D_c$, V_f=80%), was found to be 480 μm, i.e.

---

* Nicalon fibers from Nippon carbon

of the same order of magnitude than that of the SiC-infiltrated tows actually measured on a cross section of the preforms used by Rocher et al. in their impregnation experiments.

The physical characteristics of the equivalent fibrous cylinders and the liquid metal, introduced in the calculations, were those of the Nicalon fibers and **pure aluminum** respectively. The value given to the temperature of the liquid metal was 800°C and that of the equivalent preform 650°C, at the beginning of the impregnation process. The impregnation rate was assumed to be U = 0.5 $cm.s^{-1}$ on the basis of the impregnation rates actually observed for the K_2ZrF_6-treated SiC-preforms. Both (i) the exothermicity of reactions [3"] and [6], i.e. 3.3 $kJ.cm^{-3}$ of K_2ZrF_6 associated with an amount Q = 5 $mg.cm^{-2}$ of K_2ZrF_6 deposited on the surface of the equivalent SiC-cylinders and (ii) the contact angle decrease due to K_2ZrF_6 (θ = 75°), were taken into account. Since the surface tension of aluminum in presence of the cryolitic liquid film was unknown, that of pure aluminum (i.e. $\sigma = 865 - 0.2\ (T - 660)\ erg.cm^{-2}$, with T in °C) was used for all the calculations.

3.2.2 - Results and discussion

The results of the calculations are shown in table I. It clearly appears that the equivalent preform is impregnated much deeper and with much lower pressures when it has been pretreated with K_2ZrF_6. This dramatic improvement in the impregnation ability of the preform is due, as already mentioned in section 2.2, to (i) the occurrence of **exothermic reactions** related to K_2ZrF_6 and (ii) an enhancement of the wetting of SiC by liquid aluminum, i.e. a **decrease in the contact angle.**

In order to assess the respective contribution of (i) and (ii), the $z = f(P_z)$ curves, representing the variations of the impregnation depth as a function of the pressure in the metal at the preform surface, were calculated for the following sets of $\Delta H(kJ.cm^{-3})/Q(mg.cm^{-2}$ of $K_2ZrF_6)/\theta(°)$: (a) : 0/0/160 ; (b) : 0/0/75 ; (c) : 3.3/5/160 and

IMPREGNATION PARAMETERS	UNTREATED 1D-MODEL PREFORM $\Delta H = 0$ $\theta = 160°$	K_2ZrF_6-TREATED 1D-MODEL PREFORM $\Delta H = 3.3$ kJ.cm^{-3}, $Q = 5$ mg.cm^{-2} $\theta = 75°$
MODE-L IMPREGNATION		
z_M (cm)	1	∞ (no solidification of Al)
T (°C) at z_M	660 (aluminum m.p.)	807
P_z for z (MPa)	0.03 for z = 1 cm	<0 for z = 1 cm ; 0.004 for z = 20 cm
MODE-T IMPREGNATION		
z_M (cm)	0.6	∞ (no solidification of Al)
T (°C) at z_M	660 (aluminum m.p.)	807
P_z for z (MPa)	0.13 for z = 0.6 cm	0.06 for z = 0.6 cm ; 2.4 for z = 20 cm

Table 1 : Results of the calculations performed for 1D-model preforms treated (or not) with K_2ZrF_6 and representing in a first approximation 2D-SiC/SiC real preforms with a porosity of 20%

(d) : 3.3/5/75. As shown in figure 6, the variation of z as a function of P_z obey a linear law up to the solidification of the metal in the pore network ($z = z_M$). When the metal is solidified at the impregnation front, z can no longer increase whatever the pressure. It is worthy of note that a similar behavior has been experimentally observed by Fukunaga and Goda for a composite made of glass fibers and an aluminum matrix (23).

A comparison between the curves b_L ; b_T ; c_L and c_T, on the one hand, and the curves a_L ; a_T, on the other hand, leads to the following remarks :

(i) The main effect of the **exothermicity of the chemical reactions** involved in the K_2ZrF_6-process is to prevent an early solidification of the metal (actually observed at low depths for untreated preforms) as it flows in the preform and thus to allow the impregnation of large size preforms (as far as the required pressures P_z given by curves c_L and c_T are actually applied to the metal). As a matter of fact, the calculations have shown that the heat evolution due to the chemical reactions is large enough to maintain the liquid metal at about its initial temperature (i.e. 800°C) as it flows in the slightly colder preform (initial temperature : 650°C). Thus, the fluidity of the metal, which is directly related to its temperature, is kept constant. Furthermore, since the metal has not to be strongly over-heated, it leads after cooling at room temperature, to a high quality matrix. Conversely, the effect of the exothermicity of the chemical reactions on P_z, through the decrease in both the surface tension $\sigma(T)$ and viscosity $\mu(T)$ of the liquid metal, is limited, as shown in figure 6 for $z < 1$ cm (curves c_L, c_T and a_L, a_T).

(ii) The main effect of the **contact angle decrease** due to K_2ZrF_6 is to lower the value of the pressure P_z which has to be applied to the metal in order to achieve the impregnation of the preform at a given depth z (curves **a** and **b**). On the contrary, it has no influence on the maximum impregnation depth. The **pressure field** $P_z - P_a$, between the liquid metal at the preform surface (when the liquid front is at a depth

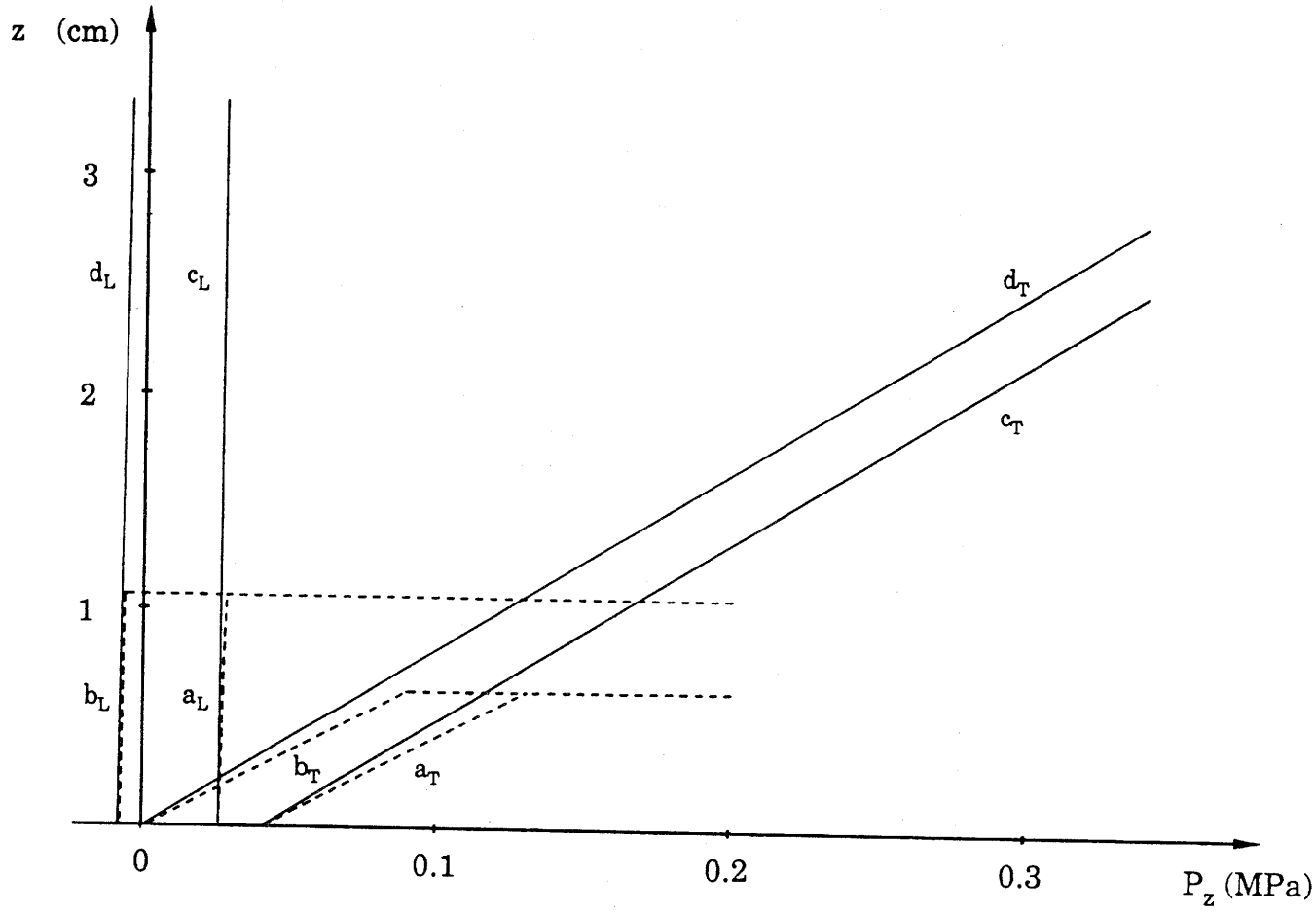

Figure 6 : Variations of the impregnation depth as a function of the pressure in aluminum for one dimensional model preforms (D = 480 μm). The curves are drawn for different ΔH ($kJ.cm^{-3}$)–θ (°) values : (a) : 0/160; (b) : 0/75; (c) : 3.3/160; (d) : 3.3/75 and for both mode-L and mode-T impregnations

z) and the portion of the preform not yet impregnated (where the pressure is P_a, with P_a = 100 kPa for experiments performed in air), results from two contributions : that of capillary forces, on the one hand, and that of frictional forces, on the other hand. It is given by the following equation :

$$P_z - P_a = P_\theta(\theta,V_f) \cdot \sigma(T) \cdot D^{-1} + K^{-1} \cdot U \cdot \int_0^z \mu(T)\, dz \qquad [7]$$

where P_θ is a dimensionless parameter which represents the capillary effect (function of both the contact angle and reinforcement volume fraction), D the diameter of the equivalent fibrous cylinders, K the preform permeability (proportional to D^2 when V_f is constant, with a proportionality coefficient different for impregnations in directions L and T) and U the impregnation rate. Thus, the effect of the contact angle decrease on the pressure field is not straightforward as discussed below.

In **mode T impregnation**, the effect of the capillary forces with respect to that of the frictional forces is small, particularly for large impregnation depths, due to the low transverse permeability of the model preform. Conversely, in **mode L impregnation**, the effects of the capillary forces and frictional forces are of the same order of magnitude. Under this latter condition and taking into account the fact that V_f, σ, D, U and μ are constant in our calculations, it comes out that the capillary force term is proportional to - cos θ and the frictional force term is constant. Since - cos θ is negative for a preform pretreated with K_2ZrF_6 (θ = 75°) and positive for an untreated preform (θ = 160°), the resulting value of P_z is lower in the former case than in the latter, as shown in figure 6.

As already mentioned, the contact angle decrease due to K_2ZrF_6 does not have any effect on the impregnation depth. As shown in figure 6, the solidification of the liquid metal occurs at the same depth z_M for (a) and (b). Therefore, for **preforms of large size**, the contact angle decrease has a beneficial effect on the impregnation of the preform only when an evolution of heat occurs simultaneously in order to

maintain liquid the aluminum, which is actually the case in the K_2ZrF_6-process. Under such conditions, a **spontaneous** impregnation of the preforms is possible **in mode-L** since P_z is negative (curve d_L) whereas this is not the case in mode-T due to the fact that the pressure lowering resulting from the contact angle decrease is too low as shown in figure 6 (curves d_T and c_T). Finally, for **preforms of small size**, the **single** effect of the contact angle decrease will be sufficient for allowing a spontaneous impregnation in mode-L (curves b_L vs a_L).

As far as **2D-SiC/SiC preforms** are concerned, their **actual** mode of impregnation has more common features with mode-L impregnation than with mode-T impregnation, due to the morphology of their pore network. It is worthy of note that rather thick 2D-SiC/SiC preforms (thickness : 1-1.5 cm) pretreated with K_2ZrF_6 have been successfully impregnated by aluminum without any pressure externally applied on the liquid, i.e. by simple gravity casting. Under such condition, the pressure on the preform is only the metallostatic pressure, i.e. that due to the weight of liquid aluminum (0.03 MPa in our experiments).

(iii) The **maximum impregnation depth** z_M depends directly on the temperature field since it is defined as the depth at which the temperature of the liquid front is equal to the melting point of aluminum. Thus, it is function of the reinforcement volume fraction V_f (both the specific heat and thermal conductivity of the composite depend on V_f), the temperatures of both the preform (before impregnation) T_F and the liquid aluminum T_{Al} as well as the occurrence of internal heat sources. The variations of z_M as a function of V_f were calculated for T_F = 650°C ; T_{Al} = 800°C and with the hypothesis that no internal heat source is present. They are shown in figure 7 from which it clearly appears that z_M is small (i.e. $z_M \leq 1$ cm) for high V_f values, in the model preform. Therefore, the use of the K_2ZrF_6-process, which results in exothermic chemical reactions as already discussed, is of particular interest for those preforms characterized by high V_f values which is indeed the case for the 2D-SiC/SiC preforms studied here (V_f = 0.8).

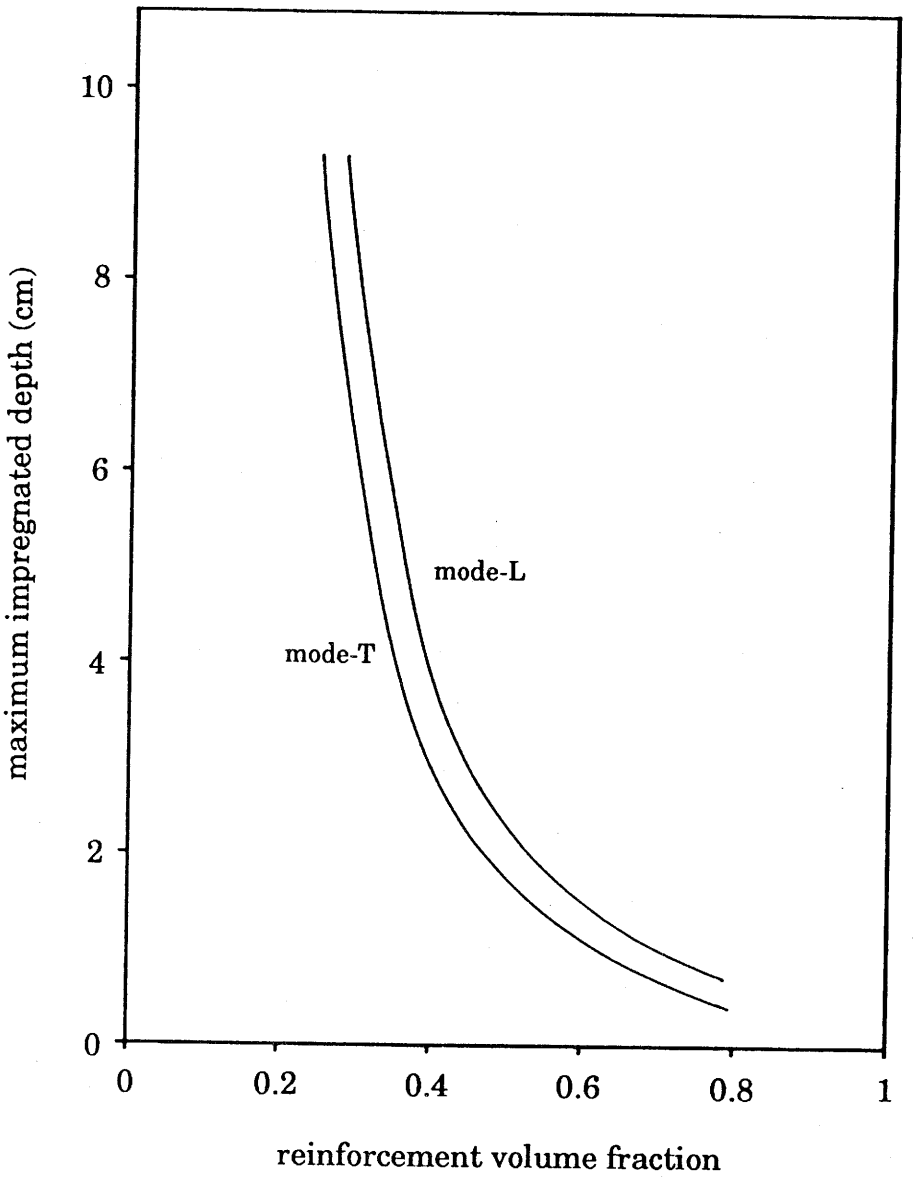

Figure 7 : Variations of the maximum impregnation depth z_M as a function of the reinforcement volume fraction for 1D-model preforms. The curves are drawn for T_F = 650°C ; T_{Al} = 800°C and no internal heat source

The **minimum amount of K_2ZrF_6** necessary to let **z_M reach an infinite value**, i.e. to maintain liquid the aluminum as it flows in a preform of infinite thickness, has been calculated for the model preform (for T_F = 650°C and T_{Al} = 800°C). The result of the calculations shows that only 0.45 mg of K_2ZrF_6 per cm^2 would be enough to keep aluminum just above its melting point (i.e. 660°C). However and as duscussed in section 2.2., such a temperature would not be sufficient to lower significantly the SiC/Al contact angle. A temperature of about 750°C, at which θ = 75° as shown in figure 1, seems to be more appropriate. The calculations have established that an amount of **3 mg K_2ZrF_6 per cm^2** would be necessary in order to maintain aluminum at 750°C as it flows in the model preform (with T_F = 650°C and T_{Al} = 800°C). It is noteworthy that this value : (i) corresponds to the maximum amount of K_2ZrF_6 which could be introduced in the model preform due to the available porosity (20%) and (ii) in close to that (5 $mg.cm^{-2}$) actually used for the impregnation of 2D-SiC/SiC preforms. As a matter of fact, larger K_2ZrF_6 amounts, that would require preforms of higher porosities, would lead to an excessive overheating of the system (T > 800°C) detrimental to the properties of the composite. In such a case, T_F could be lowered.

(iv) The variations of P_z as a function of θ is closely related to the **pressure threshold** above which pressure must be set in order to start the impregnation process, as shown in figure 6 (curves b_L, b_T and a_L, a_T). This pressure threshold is low for the model preforms due to the fact that the capillary force term is proportional to the reciprocal diameter of the fibrous cylinders which is large in the case considered here (D = 480 μm). This feature is also in agreement with the experimental data obtained for the real 2D-SiC/SiC preforms. On the other hand, the pressure threshold was expected to be much higher for untreated preforms made of **fibers smaller in diameter**. In order to verify this assumption, the variations of z as a function of P_z were calculated for a new model preform with the same overall porosity than real 2D-SiC/SiC preforms (i.e. 20%) but made of SiC fibrous cylinders

only **12.5 μm in diameter** (instead of 480 μm for the first model preforms and thus similar to the Nicalon fibers) and supposed to have been treated or not with the same amount of K_2ZrF_6 (per unit of volume). The results of the calculations are shown in figure 8 for the two model preforms. It is worthy of note that the ability of the preform made of small diameter fibers to be impregnated under low pressures depends entirely on the contact angle decrease due to K_2ZrF_6.

4 - CONCLUSION

The feasibility of the K_2ZrF_6-process, already established experimentally by Rocher et al. (21) has been justified theoretically in the present work. This process is based on a very simple procedure and products already used in light alloy casting. It has been shown that fiber preforms of rather low porosities and moderate thickness could be impregnated, when pretreated with K_2ZrF_6, under low pressures, i.e. by **gravity casting**. It is anticipated that its use in **squeeze casting** will allow the impregnation of large size preforms with pressures much lower than those presently utilized for untreated preforms.

ACKNOWLEDGEMENTS

This work has been supported, through a grant given to one of us (S.Schamm), by the French Ministry of Research and Technology.

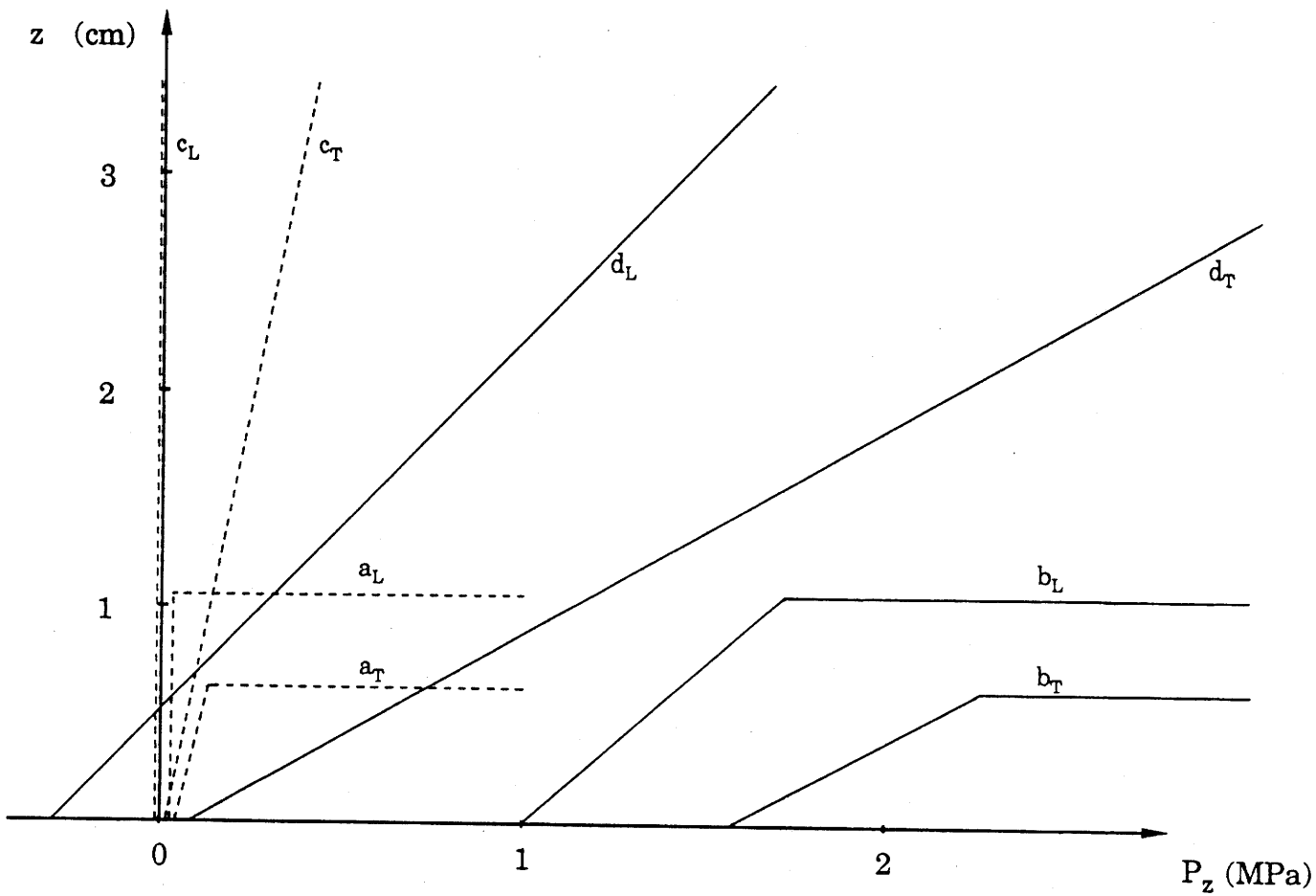

Figure 8 : Variations of the impregnation depth as a function of the pressure in aluminum for one dimensional model preforms :

(a) : untreated, D = 480 μm; (b) : untreated, D = 12.5 μm

(c) : pretreated with K_2ZrF_6, D = 480 μm ; (d) : pretreated with K_2ZrF_6, D = 12.5 μm

The curves are drawn for both mode-L and mode-T impregnations

REFERENCES

(1) - G. BLANKENBURGS, Australian Institute of Metals, 14 (1969) 236-241.

(2) - S. KOHARA, in Proceedings of Japan. US Conference on Composite Materials, Tokyo 1981, edited by K. Kawata and T. Akasaka (Japon Society for Composite Materials, 1981), 224-231.

(3) - M.F. AMATEAU, J. Composite Mater., 10 (1976) 279-296.

(4) - N. EUSTATHOPOULOS, J.C. JOUD, P. DESRE, J.M. HICTER, J. Mater. Sci., 9 (1974) 1233-1242.

(5) - A.R. CHAMPION, N.H. KRUEGER, H.S. HARTMANN, A.K. DHINGRA, in Proceedings of the 2nd Int. Conf. Composite Materials, Toronto 1978, edited by B. Noton et al. (TMS-AIME, 1978) 883-904.

(6) - T.W. CLYNE, M.G. BADER, G.R. CAPPLEMAN, P.A. HUBERT, J. Mater. Sci., 20 (1985) 85-96.

(7) - J.P. ROCHER, J.M. QUENISSET, R. PAILLER, R. NASLAIN, European Pat. 83901204-4.

(8) - R. NASLAIN, J.Y. ROSSIGNOL, P. HAGENMULLER, F. CHRISTIN, L. HERAUD, J.J. CHOURY, Rev. Chim. Miné., 18 (1981) 544.

(9) - J.P. ROCHER, J.M. QUENISSET, R. NASLAIN, submitted to J. Mater. Sci..

(10) - S. SCHAMM, L. RABARDEL, J. GRANNEC, C. BERNARD, O. RELAVE, R. NASLAIN, submitted to Calphad.

(11) - W. KÖHLER, Aluminium, 51 (1975) 443.

(12) - V. LAURENT, D. CHATAIN, N. EUSTATHOPOULOS, J. Mater. Sci. 22 (1987) 244-50.

(13) - V. LAURENT, Thesis, Institut National Polytechnique de Grenoble, 1988.

(14) - H. LUNDIN, US Patent 2, 686, 484 (1954).

(15) - N.A. BUSHE, M.E. SEMENOV, Liteinoe Proizv, 2 (1962) 15.

(16) - L. KAUFMAN, Calphad, 7 (1) (1983) 78-83.

(17) - C. GARCIA-CORDOVILLA, E. LOUIS, A. PAMIES, J. Mater. Sci., 21 (1986) 2787-2792.

(18) - K. GRJOTHEIM, C. KRÖHN, M. MALINOVSKY, K. MATIASOVSKY, J. THONSTAD, "Aluminium Electrolysis - Fundamentals of the Hall-Héroult Process". 2nd Edition, Aluminium-Verlag, Düsseldorf, 1982.

(19) - E.G. CARTER, D.C. JONES, Trans. Farad. Soc., 30 (1934) 1027-1038.

(20) - J.M. QUENISSET, R. FEDOU, F.A. GIROT, Y. LEPETITCORPS, Proc. Symp. on Advances in cast reinforced Met. Composites, 88th World Mat. Cong., Chicago, Sept. 25-30, 1988, pp. 133-38.

(21) - J.P. ROCHER, Thesis # 888, University of Bordeaux, 1986.

(22) - F. CHRISTIN, R. NASLAIN, C. BERNARD, Actes Conf. Int. CVD 7 (T.O. Sedwick and H. Lydtin, ed.), Los Angeles, The Electrochem. Soc.,Princeton, (1979) 499-514

(23) - H. FUKUNAGA, K. GODA, Bulletin of JSME, 27(228) (1984) 1245-1250.

CHAPITRE III

INTRODUCTION AU CHAPITRE III

Etant donnée la nette amélioration apportée par le procédé au K_2ZrF_6 sur l'aptitude à l'imprégnation de préformes céramiques poreuses par l'aluminium liquide (Chapitre II), il était important, dans la perspective d'une transposition industrielle, de définir la qualité de l'interface fibre-matrice. Cette interface, qui très souvent devient une interphase à cause de l'étendue des réactions chimiques entre fibre et matrice, est en effet l'endroit stratégique du composite où s'effectue le transfert des efforts reçus par la matrice aux fibres.

Pour cela, nous avons choisi d'évaluer l'affaiblissement mécanique de monofilaments SiC-CVD au cours des différentes étapes du procédé, i.e.

- après avoir déposé le fluorure à la surface du monofilament
- après traitement thermique du filament recouvert de fluorure
- après incorporation dans l'aluminium du filament traité par le fluorure

afin de définir la participation de chacune d'elles au processus de fragilisation.

Il est apparu, sur la base de l'analyse statistique de Weibull des résultats de traction, des observations au microscope électronique à balayage des faciès de rupture primaire et de la surface des monofilaments et des analyses X et Auger des produits de réaction, que essentiellement la dernière étape du procédé contribue à l'affaiblissement mécanique des monofilaments. La formation importante de cristaux de **carbure d'aluminium**, au cours de cette étape, est la cause de l'apparition d'entailles initiatrices de rupture à la surface des filaments.

L'étude physico-chimique du mécanisme de l'amélioration du mouillage, présentée au chapitre II, permet de comprendre que le fluorure $\mathbf{K_2ZrF_6}$ intervient de

manière indirecte dans le mécanisme de formation du carbure d'aluminium. Selon un processus exothermique de "nettoyage" de l'interface Al/SiC, il **active la cinétique de formation** du carbure d'aluminium qui résulte de la réaction directe entre le carbure de silicium et l'aluminium.

Soumis à "Composites Science and Technology"

COMPATIBILITY BETWEEN SiC-FILAMENTS AND ALUMINUM IN THE K_2ZrF_6 WETTING PROCESS AND ITS EFFECT ON THE FILAMENT FAILURE STRENGTH

S. SCHAMM[1], Y. LE PETITCORPS and R. NASLAIN[2]
Laboratoire de Chimie du Solide du CNRS, Université de Bordeaux I
351 Cours de La Libération, F-33405 Talence

ABSTRACT

The effect of the various steps of the K_2ZrF_6-process, used to enhance the wettability of SiC (or C) fibers by liquid aluminum, on the strength of the reinforcement, was studied on model materials. Lots of 45 uncoated SiC-CVD filaments (100 μm in diameter) were submitted to three treatments representative of the process : 1) coating with a K_2ZrF_6 layer of variable thickness, 2) annealing of the coated filaments at 650°C in sealed tubes and quenching, and 3) embedding the coated filaments in aluminum by hot pressing. After each step, the filaments were extracted chemically and tensile tested. The UTS data were treated statistically on the basis of a two-parameter Weibull function. Step 1 does not modify the filament strength. Step 2 results in a filament strength loss of about 20% and an increase in the Weibull modulus (from 8 to 20). Zirconium and oxygen were found to be present

---

Present addresses :
(1) CEMES-Laboratoire d'Optique Electronique du CNRS
29 rue J. Marvig, F-31055 Toulouse
(2) Laboratoire des Composites Thermostructuraux UM 47 du CNRS
3 Av. L. de Vinci, Europarc, F- 33600 Pessac

(based on AES analyses) at the filament surface but the size of the related critical flaws was too small to make their observation possible by SEM. Step 3 yields a more significant strength loss, depending on the amount of K_2ZrF_6 deposited in step 1, due to the formation of Al_4C_3 related to the chemical reaction between SiC and aluminum. The kinetics of growth of Al_4C_3 is faster than for untreated filaments mainly due to the cleaning effect of fluoride species on the SiC/Al interfaces. Thus, this latter filament strength loss is more an indirect consequence than an intrinsic feature of the process. It could be overcome by utilizing filaments coated with a soft material (e.g. pyrocarbon).

Key-words *K_2ZrF_6-PROCESS, SiC-FILAMENTS, ALUMINUM MATRIX COMPOSITES, SiC/Al COMPATIBILITY, FAILURE STRENGTH.*

1 - INTRODUCTION

It has been shown recently that the impregnation ability of porous preforms made of ceramic fibers (e.g. C or SiC-based Nicalon fibers) by liquid aluminum alloys is significantly improved when the preforms are pretreated with an aqueous solution of K_2ZrF_6 at (or near) its boiling point, according to a very simple procedure (1-2). As a matter of fact, various preforms, with different fiber types and morphologies, e.g. 2D-SiC(Nicalon) preforms consolidated with SiC by chemical vapor infiltration (CVI), have been successfully impregnated by liquid aluminum according to a gravity casting technique, when first pretreated with K_2ZrF_6 (3).

A detailed study of the chemical compatibility between the reinforcement and the matrix is considered as a necessary step in the development of any new metal matrix composite (MMC) in order to assess whether or not the chemical reactions which may occur between the two components during the composite processing result in a fiber strength loss. The chemical reactivity between aluminum and silicon carbide has been already the subject of many studies. The equilibria that may occur in the ternary Al-Si-C system were studied on the basis of thermodynamic calculations (4-6). The analysis and modelling of the Al/SiC interface were performed according to Auger electron spectroscopy (AES), electron energy loss spectroscopy (EELS), X-ray and UV photoelectron spectroscopies (XPS and UPS) (7-8). The identification of the reaction products formed at the SiC/Al interface was done by X-ray diffraction (XRD) as well as transmission electron microscopy (TEM) and scanning electron microscopy (SEM) (9-10). Finally, the effect of the interfacial chemical reaction on the failure strength of SiC-filaments was assessed through tensile tests (11). It can be concluded from these studies that the interactions occuring during the processing of SiC-Al composites between the reinforcement and the matrix result in the formation of Al_4C_3 and elemental silicon. Under tensile loading, the microcracking of the brittle aluminum carbide

layer surrounding each fiber is responsible for notch effects which may lower the fiber strength.

The aim of the present contribution is to study the chemical reactivity between K_2ZrF_6 and SiC, on the one hand, and that between SiC and aluminum in presence of K_2ZrF_6, on the other hand, as well as their effect on the reinforcement failure strength in both cases. Within this scope, tensile tests on β-SiC CVD-filaments coupled with a Weibull analysis of the data have been performed after each step of the K_2ZrF_6-process. Furthermore, the external surfaces of chemically extracted filaments and their failure surfaces were observed by SEM. Finally, the reaction products formed at the SiC-filament/aluminum matrix interface were analysed by SEM, AES and X-ray electron probe (EPMA) microanalyses in order to derive reaction mechanisms.

2 - EXPERIMENTAL

2.1 - Materials and chemical treatments

The successive steps of the elaboration of a SiC-fiber/aluminum matrix composite according to the K_2ZrF_6-process have been simulated, utilizing large diameter SiC-CVD filaments(*), i.e. : 1) precipitation of K_2ZrF_6 microcrystals on the filament surface from a K_2ZrF_6 aqueous solution at a temperature close to its boiling point and drying at 110°C, 2) treatment under vacuum at 650°C for 15 minutes of the coated filaments encapsulated in glass silica tubes (sealed under a residual pressure of 1.2 Pa) and quenching in air at room temperature, and 3) imbedding the filaments in a matrix of aluminum (> 99.5 % in purity) by hot pressing between two foils of metal (T = 700°C ; t = 5 min.; P = 2 MPa ; residual pressure in the bag : $1.3\ 10^{-3}$ Pa) according to a procedure which has been initially designed for

(*) from SIGMA (FRG)

titanium-matrix composites and described elsewhere (12). Furthermore, for each step, several lots of filaments corresponding to different amounts of K_2ZrF_6 deposited were used. The amount of K_2ZrF_6 deposited was assessed by weighing the filaments before and after the fluoride treatment and expressed as the mass of K_2ZrF_6 deposited per unit of filament surface ($mg.cm^{-2}$).

Within the scope of the present study, SiC-**CVD filaments** were thought to exhibit the following advantages with respect to yarn fibers (e.g. Nicalon fibers) : (i) CVD-filaments(*) are of large and regular diameter, i.e. 100 μm, whereas yarn fibers are made of hundreds of filaments whose diameter is small (15 μm for Nicalon fibers) and variable both along one given filament (dispersion : 5 %) and from one filament to the other (dispersion : up to 40 %), a feature rendering the deposition of a layer corresponding to a given amount of K_2ZrF_6 per unit of surface much easier for the CVD-filaments, (ii) due to their elaboration by CVD, large diameter SiC-filaments are only made of silicon and carbon (13) whereas yarn fibers spun from polycarbosilane (PCS) and pyrolysed contain a large amount of oxygen (14) and finally, (iii) the failure strength of SiC-CVD filaments is much higher than that of SiC yarn fibers and more uniform (for a 50 mm gauge length, the mean UTS $\bar{\sigma}$ and Weibull modulus m are respectively $\bar{\sigma}$ = 3500 MPa and m = 8 for the former and $\bar{\sigma}$ = 2000 MPa and m = 4-5 for the latter). An **uncoated** SiC-CVD filament, referred to as SiC(Σ) and which has been characterized elsewhere (15), was chosen for this study (rather than one from the SCS-i (with i = 2, 6, 8) series(**) known to have received a thick coating (at least 1 μm) of either pure carbon or a carbon-rich SiC + C mixture). The SiC(Σ) filament has a tungsten core and it is made of a SiC-CVD deposit containing 6 at.% of free silicon (from EPMA data utilizing a SiC single crystal, assumed to be stoichiometric, as a standard). AES depth profiling

(*) from SIGMA (FRG)
(**) from AVCO

analyses have shown that the Si/C atomic ratio remains constant near the filament surface (i.e. over at least 2 μm).

2.2 - Mechanical testing

The filaments, after having been submitted to the steps 1, 2 and 3 of the K_2ZrF_6-process mentioned above, were mechanically tested individually in tension (load cell : 500 N ; elongation rate : 1 $mm.min^{-1}$; pneumatic grips) at room temperature. An average of 45 filaments were tested for each experiment in order to take into account the statistical character of the filament failure. A paper holder, which has been described elsewhere (13), was used to facilitate the filament alignment in the grips, to define accurately the gauge length (40 mm in all the experiments) and to avoid any damaging due to handling.

Before the tensile tests, the filaments were extracted chemically from the materials in which they have been heat treated. The coating of K_2ZrF_6 (steps 1 and 2) was dissolved by maintaining the filaments in boiling water. The aluminum matrix (step 3) was dissolved with an aqueous solution of sodium hydroxide. Then, the filaments were dried and their diameter measured according to a laser diffraction procedure (0.95 mW He-Ne laser ; λ = 0.6328 μm).

In a few tensile tests, the filaments have been embedded in a silicone product in order to recover the filament fragments after rupture and to study by SEM the failure surfaces.

2.3 - Statistical treatment of the UTS data

The SiC-CVD filaments are known for their brittleness. Their strength is controlled by their population of defects consisting of (i) intrinsic defects usually of small size and due to processing, and (ii) surface defects often of larger size and due

to handling, mechanical abrasion or chemical reactions with the environment (including the effect of the composite processing technique). As a result, the values of the UTS of SiC-CVD filaments depend on the volume of sample tested and exhibit generally a rather large dispersion. The statistical character of the failure strength of brittle materials is usually taken into account on the basis of a two parameter Weibull distribution function, according to which the probability of failure P_R of a sample of volume V loaded at a stress level σ is given by the following equation (16) :

$$P_R = 1 - \exp\left[-V \left(\frac{\sigma}{\sigma_o}\right)^m \right] \qquad [1]$$

where σ_o is a scale factor and m the so-called Weibull modulus (which is used to characterize the distribution of the UTS values with respect to the mean value). When the sample is a cylinder, which is the case for a CVD-filament, as mentioned above : $V = \pi d^2 L/4$ (where d is the filament diameter and L the gauge length).

If the gauge length is constant, it can be shown that the variations of P_R as a function of σ obey the following relation :

$$\text{LnLn } 1/(1-P_R) = m \text{ Ln}\sigma + \text{constant} \qquad [2]$$

As a result, if the UTS data obey the Weibull distribution law, the variations of LnLn $1/(1-P_R)$ as a function of Lnσ must be linear and the slope of the corresponding straight line gives directly the value of m.

Several estimators can be used to calculate P_R. Regarding the large number of filaments tested for each lot (N = 45), the estimator which has been used, in the present study, was chosen as that given by the following equation :

$$P_R = \frac{i}{N+1} \qquad [3]$$

with i = 1,2,...45

Apart the Weibull modulus m, the other parameters derived from the statistical treatment of the UTS data which have been taken into account are :

$\sigma_{0.5}$, the median of the UTS values (corresponding to a probability of failure of 50 %), $\bar{\sigma}$ the arithmetic UTS mean value, S the standard deviation with respect to $\bar{\sigma}$, C_V the coefficient of variation defined by $C_V = S/\bar{\sigma}$ and which is known to depend only on the Weibull modulus m. The relation between C_V and m, which has been used here is that given by Street and Ferte in their study of boron CVD-filaments, i.e. (17):

$$C_V \simeq m^{-0.94} \qquad [4]$$

Finally, r is the correlation factor associated with a given Weibull LnLn $1/(1-P_R)$ = f(Lnσ) plot. The values of the Weibull modulus derived from equations [2] and [4] will be referred to as m [2] and m [4] respectively.

It is worthy of note that an overall length of SiC(Σ) filament of about **50 meters** has been used to perform the various experiments described in the present study. In order to take into account the occurrence of possible differences in the characteristics of the material along such a length, the continuous filaments was first cut into segments of equal length (i.e. about 80 mm). Then lots of 45 filaments were prepared in a **random** manner, submitted to the chemical/thermal treatments and finally tensile tested.

3 - RESULTS AND DISCUSSION

3.1 - Effects of the K_2ZrF_6-process steps on SiC-filaments UTS

Some of the Weibull plots, representative of the effect of the different K_2ZrF_6-process steps on the filament UTS are shown in figure 1 (when several curves have almost the same values of $\sigma_{0.5}$ and m, only one among them is represented). It appears that : (i) some of them are almost perfectly linear (corresponding to unimodal Weibull distributions) whereas others are not and will better fit bi-modal distribution as already noticed by Martineau et al. (13) and by Le

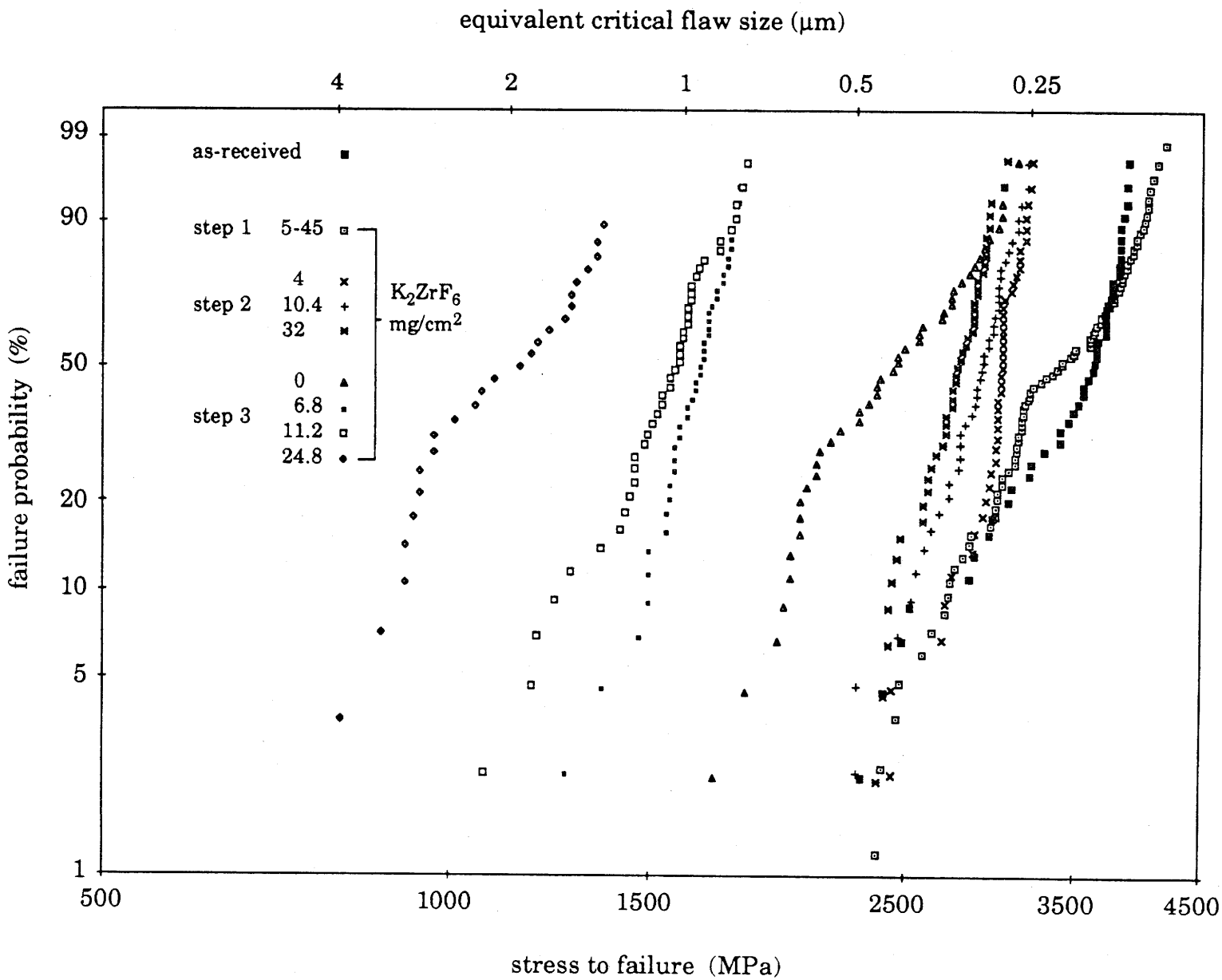

Figure 1 : Weibull plots for SiC(Σ)-CVD filaments at different stages of the K_2ZrF_6-process

Petitcorps et al. (15) in their studies of tungsten or carbon core CVD-filaments and (ii) generally speaking, the weibull plots are shifted towards the low UTS side depending on the nature of the treatment which has been applied to the filament. The various parameters derived from the statistical treatment of the UTS data are given in table 1. Finally, the variations of $\sigma_{0.5}$ measured after the steps 2 and 3, as a function of the amount of K_2ZrF_6 initially deposited on the filament surface, are shown in figure 2.

3.2 - Nature and size ot the critical defects

As shown in figure 3, **the critical defects**, i.e. the defects which have initiated the filament failure, are mainly located at the filament surface. This result suggests that the strength loss of the filament shown in figures 1 and 2 is due to the chemical interactions between the reinforcement and the products (i.e. K_2ZrF_6, Al_4C_3 and aluminum) in which it has been maintained at high temperatures (step 2 and 3). The few failure surfaces which have been observed by SEM exhibit the features typical of brittle materials already reported for other SiC-based fibers (e.g. the Nicalon fibers) (18). Surrounding the critical defect itself (arrows in figures 3 b, c, d), one observes successively : (i) a small mirror zone (slow crack propagation) and then (ii) a mist region and hackles (catastrophic crack propagation) which are located in a plane perpendicular to the fiber and load axis. Therefore, the filaments appear to have failed on **mode I.**

The surface defects, for the filaments submitted to the K_2ZrF_6-process step 3 (amount of K_2ZrF_6 : 6.8 $mg.cm^{-2}$), are numerous, rather small in average depth and homogeneously distributed on the filament surface (fig.3b). This feature is in agreement with the high value (i.e. about 16) of the Weibull modulus given in table 1. However, when the amount of K_2ZrF_6 deposited on the filament surface is increased prior to the step 3, i.e. 11.2 $mg.cm^{-2}$ for the fractography shown in figure 3c and

Treatment	K_2ZrF_6 (mg/cm^2)	$\sigma_{0.5}$ (MPa)	$\bar{\sigma}$ (MPa)	σ_0 (MPa)	S (MPa)	C_v	r	m[2]	m[4]	$\bar{d}$ (µm)	$\bar{\sigma}a^{1/2}$ ($MPa.m^{1/2}$)
As-received	-	3622	3444	1119	434	0.13	0.96	8.0	9.1	100	-
Step 1	5-45	3405	3376	1127	486	0.14	0.99	8.2	7.9	100	-
Step 2	0	3584	3472	1152	450	0.13	0.98	8.1	8.8	100	-
	1.8	3079	3047	1910	177	0.06	0.98	18.9	20.6	99.6	1.4
	4.0	3026	2989	1821	170	0.06	0.94	18.0	21.1	99.4	1.6
	6.4	2837	2764	1641	178	0.06	0.99	17.1	18.5	99.3	1.6
	10.4	2871	2864	1529	223	0.08	0.99	14.3	15.1	99.3	1.7
	16.8	2984	2945	1839	160	0.05	0.94	19.0	22.2	99.5	1.5
	32.0	2771	2748	1637	177	0.06	0.99	17.3	18.5	99.2	1.7
											$\overline{1.6}$
Step 3	0	2448	2446	681	383	0.16	0.98	7.0	7.2	99.4	1.3
	3.0	1592	1579	921	105	0.07	0.98	16.6	17.8	98.4	1.4
	6.8	1652	1635	919	115	0.07	0.99	15.6	16.8	97.8	1.7
	11.2	1578	1539	613	170	0.11	0.99	9.8	10.4	97.4	1.8
	24.8	1096	1108	293	173	0.16	0.97	6.8	7.2	95.8	1.6
											$\overline{1.6}$

Table 1: Parameters derived from the Weibull treatment for each step 1, 2 and 3 and for different amounts of K_2ZrF_6 deposited

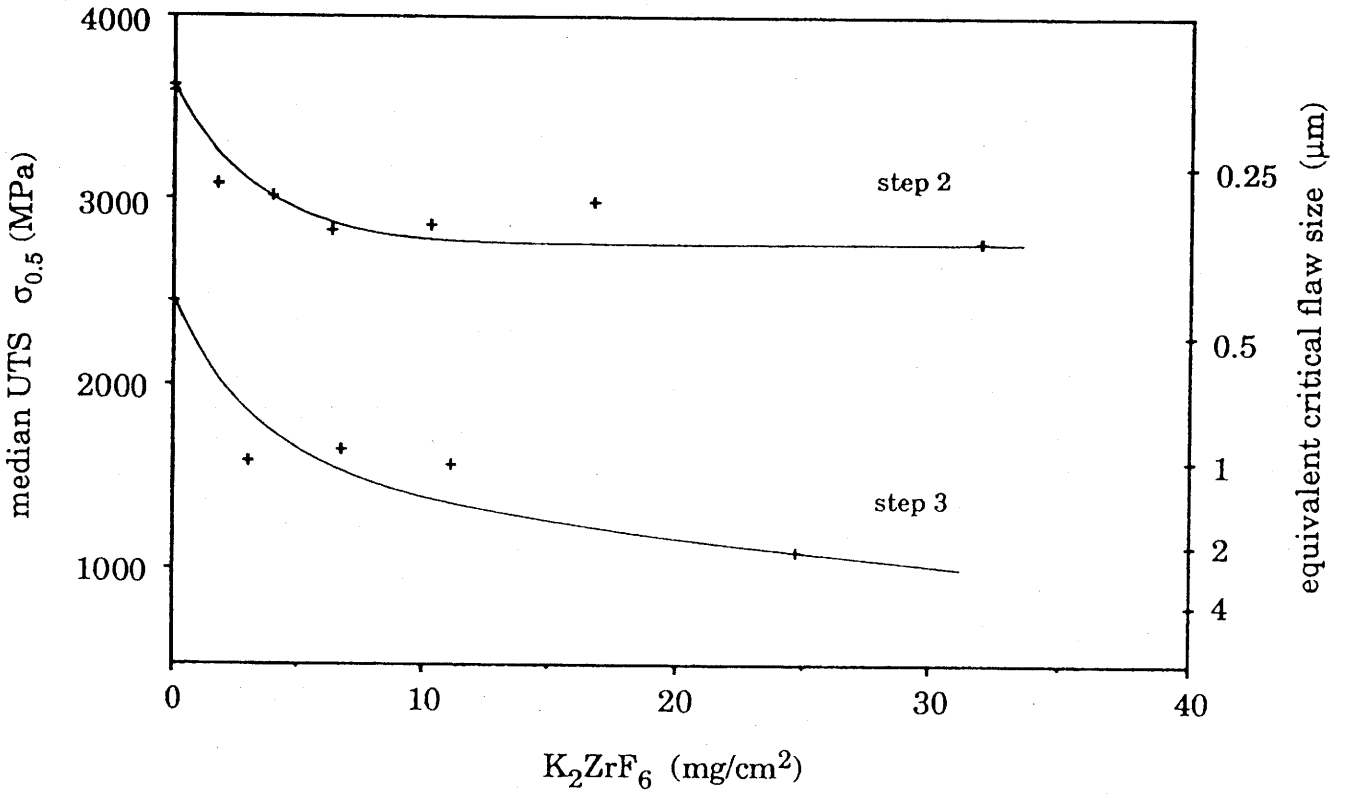

Figure 2 : Variations of the median UTS of SiC(Σ)-CVD filaments chemically extracted from K_2ZrF_6 (step 2) or aluminum (step 3) in the K_2ZrF_6-process

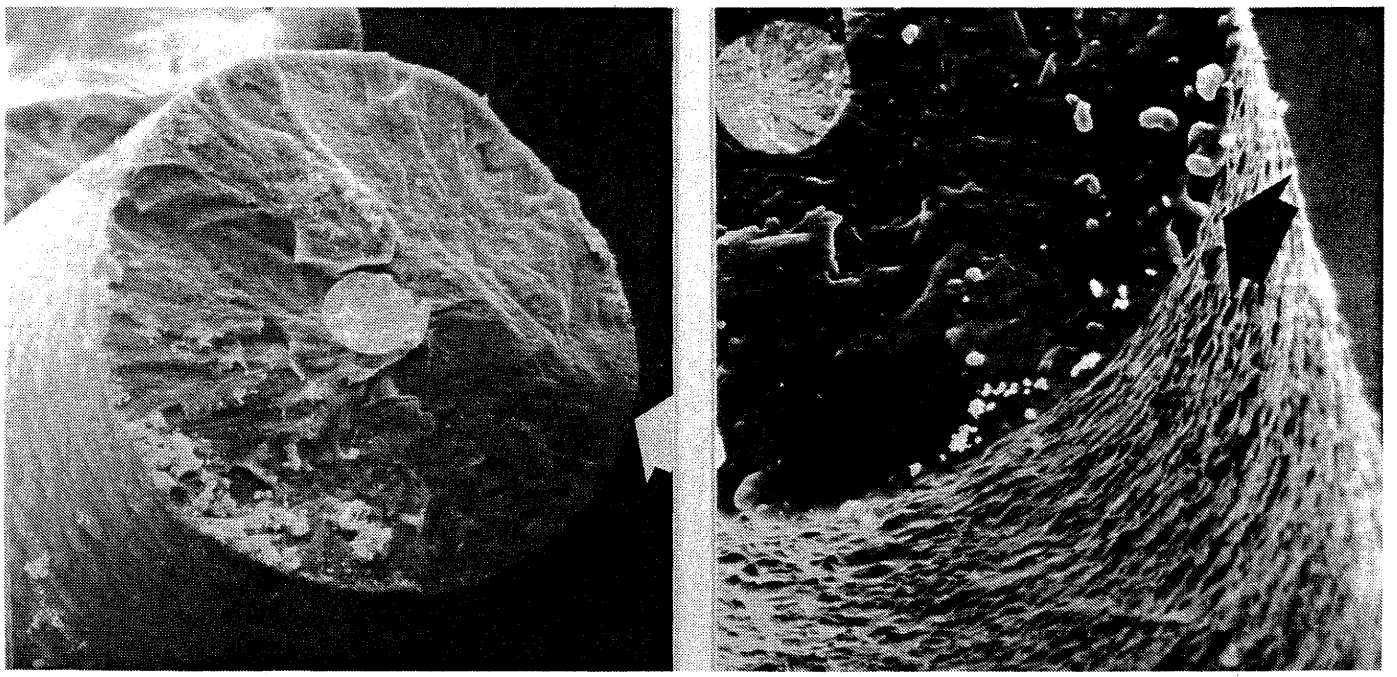

(a) X 700 ⌊⌋ 10 µm (b) X 1200 ⌊⌋ 10 µm

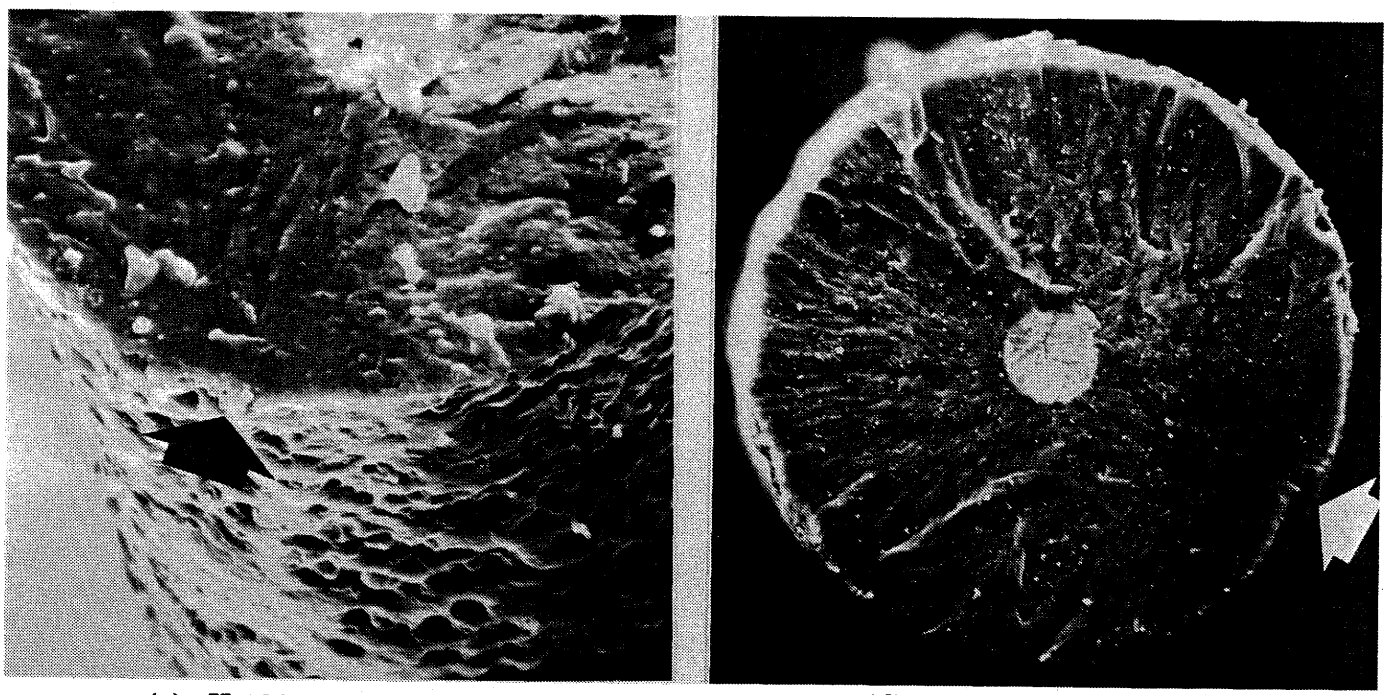

(c) X 1200 ⌊⌋ 10 µm (d) X 800 ⌊⌋ 10 µm

Figure 3 : SEM fractographic analysis of SiC(Σ)-filaments after tensile test and for different surface amounts of K_2ZrF_6 :

(a) extracted from K_2ZrF_6 after step 2 ; K_2ZrF_6 : 32 mg.cm^{-2}

(b), (c), (d) extracted from aluminum after step 3 for K_2ZrF_6 : 6.8; 11.2 and 24.8 mg.cm^{-2} respectively

24.8 mg.cm^{-2} for figure 3d, the defects are deeper and distributed in a less homogeneous manner. As a result, the Weibull modulus decreases (9.8 and 6.8, respectively) (table 1).

Although the surface of the filaments which have been submitted only to the step 2 of the K_2ZrF_6-process does not exhibit apparent defects (fig.3a), the fact that the corresponding Weibull moduli are high (m = 15-20) suggests : (i) that the filament surface has been chemically altered in a similar homogeneous way and (ii) that the surface defects are too small in size to be seen on the SEM micrograph (table 1).

The **size of the critical flaw** (i.e. the equivalent critical flaw radius a_c) could be derived from the UTS value utilizing fracture mechanics, e.g. the critical stress intensity factor in mode I, K_{IC}, according to the following equation already used by Andersson and Warren in their study of Nicalon-type fibers (14,19) :

$$K_{IC} = 1.12\,\sigma\,(\pi a_c)^{1/2} \simeq 2\,\sigma\,a_c^{1/2} \qquad [5]$$

This approach supposes that the value of K_{IC} is known. Although K_{IC} can be derived from a detailed fractographic analysis (i.e. by measuring the critical flaw and mirror radii), as recently used by Sawyer et al. for various fibers derived from polymeric precursors (18), this possibility was not exploited here lacking enough reliable fractographic data. Conversely, a value of $K_{IC} \simeq 3$ MPa.m$^{1/2}$, given by Andersson and Warren for β-SiC (the SiC modification present in SiC(Σ) filaments) was used, as a first approximation and taking into account the following remark. It is clearly apparent from figure 3 that the surface defects responsible for the filament strength loss are due to a chemical attack. As a matter of fact, this chemical attack results in a decrease in the filament diameter which is very slight for step 2 but significant and variable for step 3 (table 1). Therefore, it is not irrealistic to compare the order of magnitude of the thickness of material consumed by the chemical reaction, defined as $(\bar{d} - 100)/2$ (where $\bar{d}$ is the actual mean filament diameter and

100 the initial diameter), to that of the defect critical size (a_c). As a matter of fact and as shown in table 1, the product $\overline{\sigma}\ [(\overline{d} - 100)/2]^{1/2}$ appears to be constant and equal to 1.6 MPa.$m^{1/2}$. This value would lead to "K_{IC}" value of 3.2 MPa.$m^{1/2}$.

The equivalent critical flaw radius scale derived from that of UTS, on the basis of equation [5] and for $K_{IC} \simeq 3$ MPa.$m^{1/2}$, is shown in figures 1 and 2. It is noteworthy that the order of magnitude of the critical flaw size is 0.3 μm for the filaments submitted to step 2. This small value could explain that the defects are not apparent from the SEM micrograph shown in figure 3a.

3.3 - Discussion of the effect of step 1 on filament UTS

The simple precipitation of K_2ZrF_6 microcrystals, from a saturated hot aqueous solution (i.e. at about 80°C), on the filament surface does not significantly lower the mean UTS of the filaments, as shown in figure 1 and table 1. Furthermore, the amount of K_2ZrF_6 deposited on the filament has no noticeable effect on the UTS value. As a result, the single Weibull plot given in figure 1 is representative of all the data obtained after the step 1 treatment.

As shown in figure 4, for two different surface amounts of K_2ZrF_6, the deposit is not strongly adherent to the filament surface. It has been even partly detached from the substrate (fig.4b) when the filament was broken into small fragments for the purpose of the SEM analysis although it was initially continuous and homogeneous in thickness. At the beginning of the precipitation process (fig.4a), the deposit is not continuous, as could be expected for a nucleation step. The K_2ZrF_6 crystals are different in both size and morphology : (i) the smallest crystals are acicular with their long edge parallel to the filament surface whereas (ii) some of the largest ones have a hexagonal habit with the hexagonal axis perpendicular to the filament axis. This growth of hexagonal shaped crystals seems to be later on favored in thicker continuous deposits as they are shown on figure 4c. K_2ZrF_6

(a) X 700

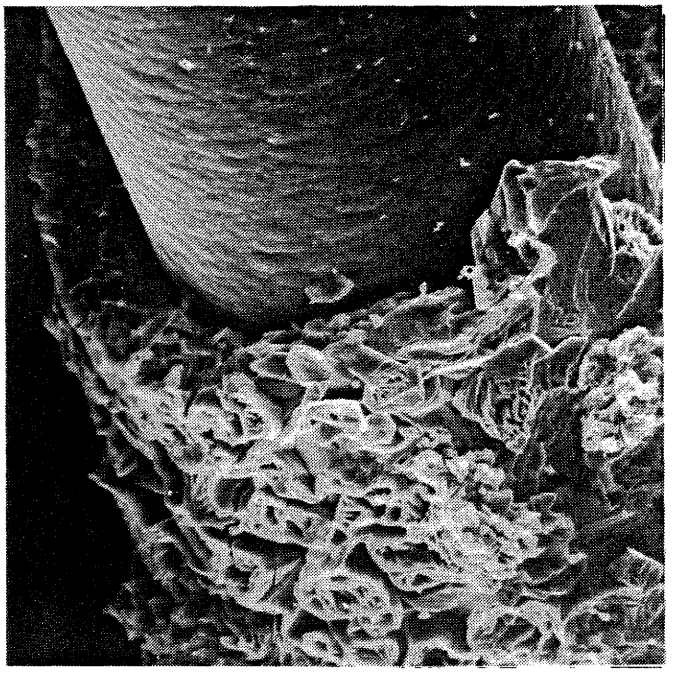

(b) X 700

10 μm

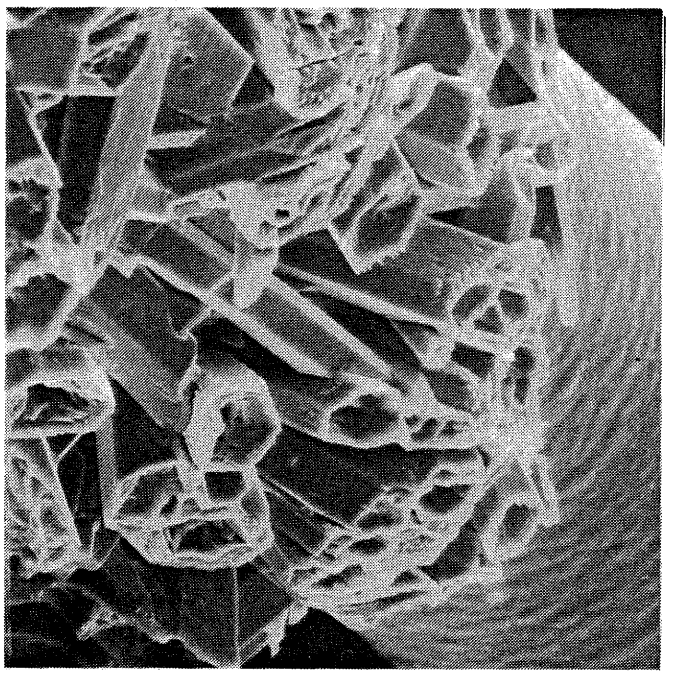

(c) X 700

Figure 4 : Morphology of the K_2ZrF_6 deposited in step 1

(a) 1 $mg.cm^{-2}$ of K_2ZrF_6

(b) 11 $mg.cm^{-2}$ of K_2ZrF_6

(c) well-developed K_2ZrF_6 crystals of hexagonal shape

crystallize in the orthorhombic structure and the fact that the parameters b (11.40 Å) and a (6.58 Å) are in a ratio of about $\sqrt{3}$ gives the structure a pseudo-hexagonal character (20).

3.4- Discussion of the effect of step 2 on filament UTS

The median UTS of filaments, which have been submitted to the step 2 of the K_2ZrF_6-process, decreases first sharply as a function of the surface amount of fluoride deposited on the filament prior to the heat treatment, **then it remains constant**, at a level of **80 % of the initial value**, even for K_2ZrF_6 amounts as large as 30 $mg.cm^{-2}$, as shown in figure 2. Chemical interactions between the filament surface and K_2ZrF_6 during the exposure at 650°C are thought to be responsible for the filament strength loss.

As shown in figure 5, the K_2ZrF_6 deposit resulting from the step 2 treatment is no longer made of well facetted crystals (fig.4) but appears **to have melted** during the annealing at 650°C (the molten state appearance being kept by quenching at room temperature). Furthermore and as already mentioned in section 3.3, the deposit is not strongly bonded to the filament surface, a feature which is in agreement with the fact that the strength loss due to this treatment is only limited. The molten state appearance of the deposit is consistent with the related $KF\text{-}ZrF_4$ phase diagram given by Kaufman (21) according to which K_2ZrF_6 (or 2 $KF.ZrF_4$) undergoes at 590°C a peritectic decomposition :

$$K_2ZrF_6 \rightleftharpoons K_3ZrF_7 + \text{Liquid} \qquad [6]$$

Assuming that the main features of the phase diagram, which has been established for a pressure of one atmosphere, are kept when the pressure is lowered to 3.7 Pa (the residual pressure in the sealed glass silica tubes), the occurrence of the

X 450 ⌊⌋ 10 μm

Figure 5 : Morphology of the K_2ZrF_6 deposit after (i) annealing at 650°C for 15 min in silica tubes sealed under vacuum (residual pressure : 1.2 MPa) and (ii) quenching at room temperature

peritectic equilibrium [6] combined with quenching explains the morphology of the deposit shown in figure 5.

The AES depth profile analysis given in figure 6 shows that chemical interactions have taken place during the annealing treatment at the filament surface. As a result, both **oxygen and zirconium** are present near the surface. Although a detailed thermodynamic study has not been performed, chemical reactions between SiC or/and Si (the filament contains 6 at % of free silicon), on the one hand, and K_3ZrF_7 or/and the liquid phase resulting from equation [6], on the other hand, could have occurred at 650°C yielding some diffusion of zirconium in the filament. As a matter of fact, the calculation of the Gibbs free energy variation of the two following reactions :

$$K_3ZrF_7 + SiC \rightleftharpoons ZrC + 3\,KF + \overline{SiF_4}\uparrow \qquad [7]$$

$$K_3ZrF_7 + 2\,Si \rightleftharpoons ZrSi_2 + 3\,KF + \overline{SiF_4}\uparrow \qquad [8]$$

gives rise to SiF_4 equilibrium partial pressures respectively of the order of 10^{-6} and 10^{-4} Pa. These low values support the assumption that reactions [7] and [8] are not well developed in the conditions of our experiments.

The **presence of oxygen** is probably due to different sources of contamination : (i) the initial filament surface contains some oxygen (see insert in fig.6) presumably as SiO_2 which will be dissolved in the fluoride liquid arising from the peritectic equilibrium [6], (ii) some residual water has been undoubtedly encapsulated with the filaments in the sealed silica tube (either as adsorbed species on the silica wall or/and entrapped into the K_2ZrF_6 deposit). This water, whatever its origin, may give rise to the hydrolysis of K_3ZrF_7 at 650°C and the formation of zirconia according to the following equation :

$$K_3ZrF_7 + 2\,\overline{H_2O}\uparrow \rightleftharpoons ZrO_2 + 3\,KF + 4\,\overline{HF}\uparrow \qquad [9]$$

whereas HF may act as a transport agent to extract oxygen from the silica wall of

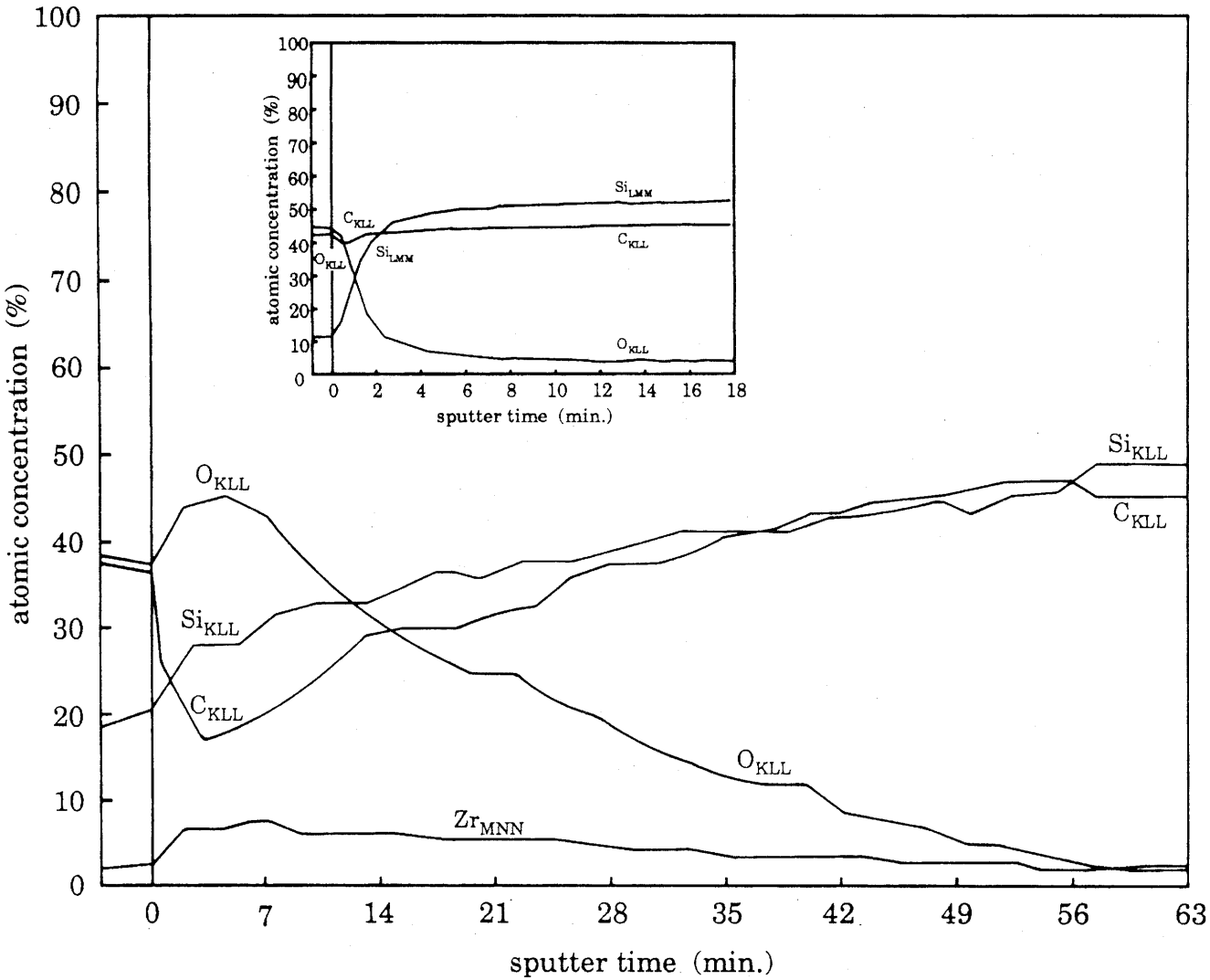

Figure 6 : AES depth profile analysis of silicium, carbon, oxygen and zirconium near the SiC-filament surface for a filament extracted from K_2ZrF_6 (step 2).
Insert : AES analysis of the as-received SiC(Σ) filaments.
Sputter rate : 15 and 2 (insert) nm.min^{-1} (standard : Ta_2O_5)

the tubes :

$$4\,HF + SiO_2 \rightleftharpoons SiF_4 + 2\,H_2O \qquad [10]$$

It thus appears that the interactions that may have occurred between the SiC-filament, the K_2ZrF_6 deposit and the silica container during the step 2 of the K_2ZrF_6-process are complex. However, they must have been (i) of relatively low intensity since the resulting filament strength loss is limited, i.e. only about 20% and (ii) homogeneous over the filament surface regarding the increase in Weibull modulus (i.e. from 8 to 20).

3.5 - Discussion of the effect of step 3 on filament UTS

As shown in figure 2 and table 1, the step 3 of the K_2ZrF_6-process results in a filament strength loss which is **more significant** than that observed for the step 2. Moreover, the residual filament strength regularly decreases as the amount of K_2ZrF_6 deposited on the filament during step 1 increases. However, it should be mentioned that **untreated** filaments submitted to step 3 undergo a strength loss which is of the order of 30%. Finally, as far as the amount of K_2ZrF_6 deposited in step 1 is less than 10 $mg.cm^{-2}$ the SiC-filaments have a residual UTS which is still of the order of 50% that of the as-received reinforcement.

The mechanism responsible for the filament strength loss has been identified from experiments performed under very **severe interaction conditions**. Namely, pure liquid aluminum was poured on SiC(Σ) filaments coated with a thick layer of K_2ZrF_6 (i.e. 8 $mg.cm^{-2}$ corresponding to a thickness of about 20 μm) and the whole maintained at 800°C for 15 min. After cooling, the aluminum matrix was dissolved in a methanol solution of bromine and the extracted filaments were observed in SEM and analysed by EPMA.

As shown in figure 7 (a, b, c), the surface of the extracted filament is covered with small hexagonal crystals, made of carbon and aluminum combined in an atomic ratio Al/C close to 4/3 (on the basis of EPMA data) and thus identified to the **aluminum carbide** Al_4C_3. The nature of the crystals was confirmed by an AES depth profile analysis performed on the composite before chemical extraction (fig.8). The fact that Al_4C_3 is found at the filament surface is in agreement with the conclusions drawn by many authors according to which SiC-based reinforcements react with liquid aluminum to form Al_4C_3 crystals having their roots in the reinforcements and silicon which is dissolved in the liquid (22) :

$$3\,SiC + 4Al \rightleftharpoons Al_4C_3 + 3\,Si \qquad [11]$$

Al_4C_3 could also result from a reaction between SiC and the mixture of fluorides "6KF,4AlF_3" formed as aluminum reacts with "2KF,ZrF_4" during the K_2ZrF_6-process (2), according to the following equation :

$$\text{"6KF, 4AlF}_3\text{"} + 3\,SiC \rightleftharpoons Al_4C_3 + 6\,KF + 3\,\underline{SiF_4}\downarrow \qquad [12]$$

In fact, the equilibrium partial pressure of SiF_4 deduced from the evaluation of the Gibbs free energy variation of reaction [12] (700°C) is very low, i.e. 10^{-12} Pa. Therefore, we assume that reaction [12] doesn't proceed.

When in a next step, the Al_4C_3-coated SiC-filament is treated with an aqueous solution of sodium hydroxide, the aluminum carbide crystals are dissolved leaving pits at the filament surface (fig.7d). Therefore, the surface defects, discussed in section 3.1 and which are responsible for the filament strength loss after the step 3, are **Al_4C_3 crystal prints in the filament surface** due to chemical reaction [11] and to the NaOH-chemical extraction procedure. These defects act as stress concentrators (notch effect) at the filament surface, their effect on the filament UTS depending on the thickness of the Al_4C_3 layer (fig.2).

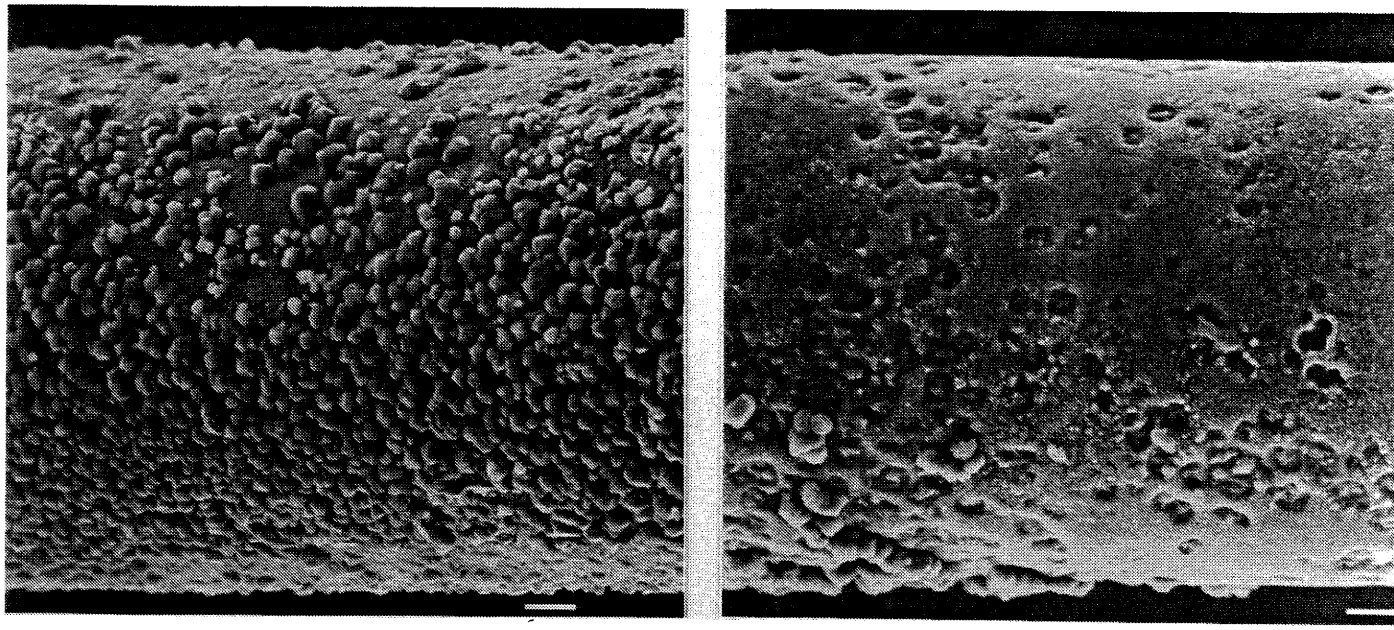

(a) X 700 10 μm (d) X 700

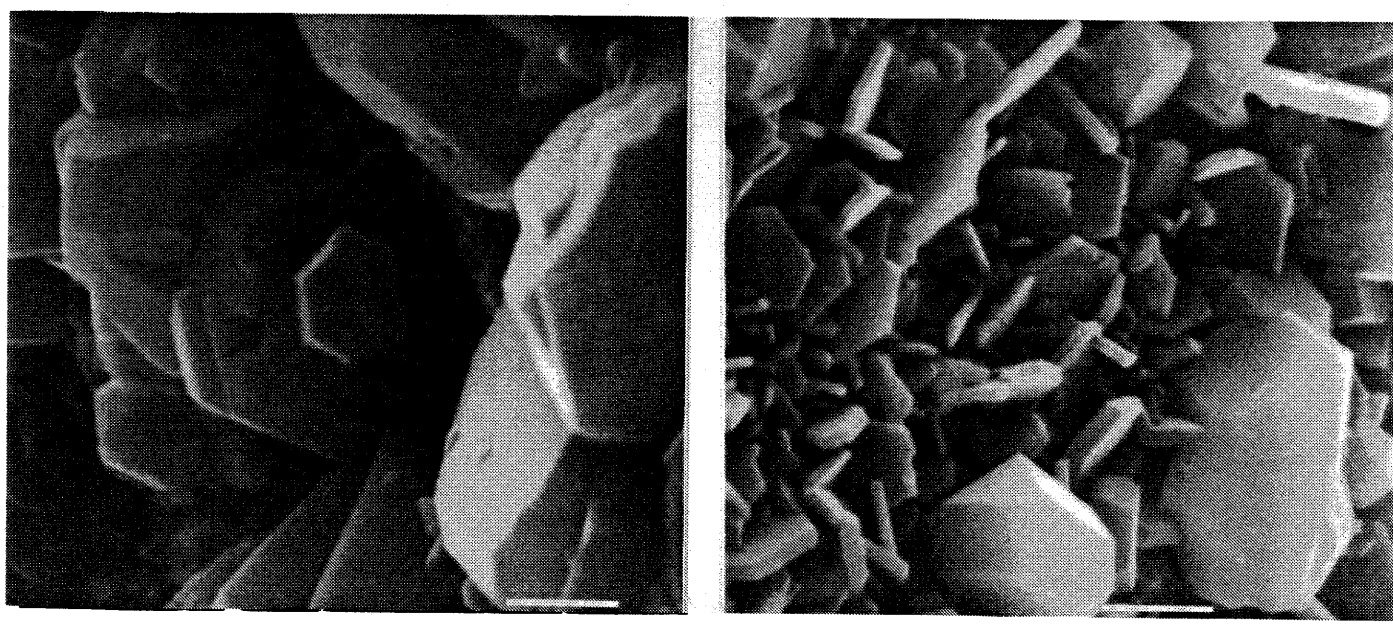

(b) X 15000 1 μm (c) X 15000

Figure 7 : SEM micrographs of a SiC(Σ)-filament coated with K_2ZrF_6, maintained in liquid aluminum for 15 min at 800°C then treated with: a methanol solution of bromine (a, b, c) and an aqueous solution of sodium hydroxide (d). The crystals are Al_4C_3. Their dissolution in NaOH leaves pits at the filament surface.

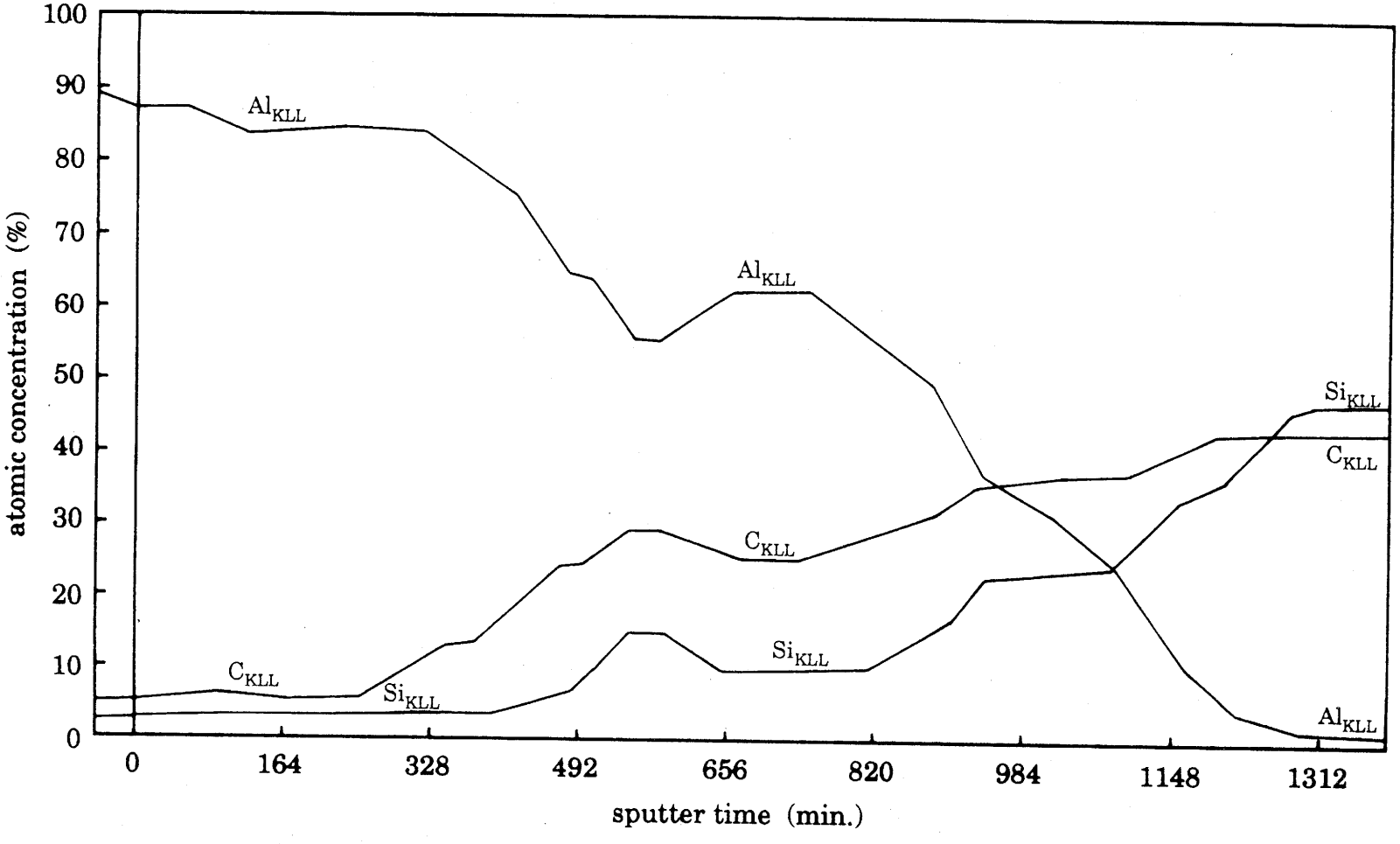

Figure 8 : AES depth profile analysis of silicium, carbon and aluminium near the SiC/Al interface, for a SiC-filament covered with K_2ZrF_6 (8 mg/cm^2) and maintained 15 min in aluminum at 800°C. Sputter rate : 25 nm.min^{-1} (standard Ta_2O_5)

It is worthy of note that the same experiment performed with **untreated** SiC(Σ) filaments (step 3) results in the formation of less aluminum carbide, as already mentioned, and thus to a lower filament strength loss. Therefore, it seems that the K_2ZrF_6-process **increases the kinetics of growth of Al_4C_3** which is anyhow a normal product of the interaction between liquid aluminum and a SiC reinforcement. This activation phenomenon can be explained on the basis of the following features of the K_2ZrF_6-process, which have been discussed in details elsewhere (2); the K_2ZrF_6-process : (i) allows a better contact between the SiC reinforcements and liquid aluminum since it enhances their wetting ability and dissolves the alumina film covering the metal (this oxide film may act as a diffusion barrier when no fluoride treatment is applied) and (ii) increases the SiC/Al interface temperature due to the exothermicity of the reactions which are involved.

4 - CONCLUSIONS

It has been shown that the K_2ZrF_6-process does not significantly lower the failure strength of SiC-reinforcement by itself (the strength loss due to the fluorides species under conditions representative of a casting procedure is of the order of 20% only). On the other hand, it has been observed that the kinetics of growth of Al_4C_3, which is a normal product of the interaction between SiC and Al, is increased with an additional loss of strength of the reinforcement. This indirect consequence of the K_2ZrF_6 treatment is thought to be mainly related to the cleaning effect of the fluoride species on the SiC/Al interfaces. Obviously, the notch effect due to the failure of the brittle Al_4C_3 layer on the SiC-filament surface, in SiC/Al composites processed according to the K_2ZrF_6-process, could be : (i) reduced by an optimization of the fluoride layer thickness and casting parameters and (ii) even supressed by utilizing SiC-filaments coated with a layer of a soft material (e.g. pyrocarbon) acting as a mechanical fuse (23-24). Therefore, in addition to the simplicity of the procedure

according to which it can be used to produce aluminum matrix composites, the K_2ZrF_6-process does not significantly alter by itself the strength of the reinforcement, under optimized conditions.

ACKNOWLEDGEMENTS

This work has been supported, through a grant given to S.Schamm, by the French Ministry of Research and Technology. The authors acknowledge the assistance of M. Lahaye for the X-Ray and Auger electron spectroscopy analyses.

REFERENCES

(1) - J.P. ROCHER, J.M. QUENISSET, R. PAILLER, R.N. NASLAIN, Brev. Eur. 83901204-4.

(2) - S. SCHAMM, R. FEDOU, J.P. ROCHER, J. M. QUENISSET, R. NASLAIN, to be submitted to Metallurgical Transactions

(3) - J.P. ROCHER, Thesis ≠ 888, Univ. Bordeaux, June 23, 1986.

(4) - R. WARREN, C.H. ANDERSSON, Composites, 15 (2) (1984) 101-111.

(5) - J.C. VIALA, P. FORTIER, C. BERNARD, J. BOUIX, Proceedings of the first European Conference on Composite Materials, Bordeaux 1985, Ed. A.R. Bunsell, P. Lamicq, A. Massiah, 583-588.

(6) - K. KANNIKESWARAN, R.Y. LIN, Journal of Metals, 39 (9) (1987) 17-19.

(7) - V.M. BERMUDEZ, Appl. Phys. Lett. 42 (1) (1983) 70-72.

(8) - L. PORTE, J. Appl. Phys. 60 (2) (1986) 635-638.

(9) - T. ISEKI, T. KAMEDA, T. MARUYAMA, J. Mater. Sci. 19 (1984) 1962-1968.

(10) - S. TOWATA, S. YAMADA, J. Japan Inst. Metals, 47 (2) (1983) 159-165.

(11) - H. TEZUKA, S. SAITO, A. KOHIYAMA, N. IGATA, Annual Report of the Engineering Research Institute , Faculty of Engeenering, University of Tokyo, 46 (1987) 135-141.

(12) - R. PAILLER, P. MARTINEAU, M. LAHAYE, R. NASLAIN, Rev. Chim. Minérale 18 (1981) 520-543.

(13) - P. MARTINEAU, M. LAHAYE, R. PAILLER, R. NASLAIN, M. COUZI, F. CRUEGE, J. Mater. Sci. 19 (1984) 2731-2748.

(14) - C.H. ANDERSSON, R. WARREN, Composites, 15 (1) (1984) 16-24.

(15) - Y. LE PETITCORPS, M. LAHAYE, R. PAILLER, R. NASLAIN, Composites Science and Technology 3 (1988) 31-55

(16) - W.J. WEIBULL, Appl. Mech. 18 (1951) 293-297.

(17) - K.N. STREET, J.P. FERTE, Proc. ICCM-1, Geneva/Boston, 1975, Ed. E. Scala, E. Anderson, I. Toth, B.R. Noton, Vol.1, 137-163.

(18) - L.C. SAWYER, M. JAMIESON, D. BRIKOWSKI, M.I. HAIDER, R.T. CHEN, J. Am. Ceram. Soc., 70 (11) (1987) 798-810.

(19) - M.Kh. SHORSHOROV, L.M USTINOV, A.M. ZIRLIN, V.I. OLEFIRENKO, L.V. VINDGRADOV, J. Mater. Sci. 14(1979) 1850-1861.

(20) - H. BODE, G. TEUFER, Acta. Cryst. , 9 (1956) 929-933

(21) - L. KAUFMAN, Calphad 7 (1) (1983) 78-83.

(22) - V. LAURENT, Thesis, Grenoble, Nov. 4, 1988.

(23) - J.A. CORNIE, R.J. SUPLINKAS, A.W. HAUZE, Ceram. Eng. Sci. Proc., 1 (1980) 728-743

(24) - S.R. NUTT, F.E. WAWNER, "Metal Matrix Composite II", NASA Conference publication, 2252 (1982) 27-42.

CONCLUSIONS GENERALES

CONCLUSIONS GENERALES

Ce travail s'inscrivait dans le cadre général des recherches conduites au Laboratoire de Chimie du Solide du CNRS sur les **matériaux composites à matrice d'alliages légers** en vue : (i) de développer des procédés d'élaboration originaux au plan scientifique et technique tout en étant réaliste au plan industriel, (ii) de préciser les interactions physico-chimiques entre fibre et matrice aux températures d'élaboration et d'utilisation du matériau et (iii) de rechercher les corrélations susceptibles d'exister entre le comportement mécanique global du matériau et les aspects physico-chimiques, notamment interfaciaux.

La présente étude fait suite au travail de thèse de **J. P. ROCHER** qui avait été consacré à la mise au point d'un procédé de prétraitement des renforts fibreux à base de carbone ou de carbure de silicium - **le procédé au K_2ZrF_6** - en vue d'améliorer leur **aptitude au mouillage** par les alliages d'aluminium et de développer une méthode d'élaboration des composites correspondants qui puisse être aisément transférée au plan industriel. Rappelons que dans son principe, le procédé repose sur une précipitation de microcristaux de K_2ZrF_6, à partir d'une **solution aqueuse** à température proche de l'ébullition, à la surface des fibres. Ainsi prétraité, le renfort fibreux devient mouillable ($\theta < 90°$) par les alliages d'aluminium (à 700-800°C) et peut être imprégné selon les techniques habituelles de la fonderie des alliages légers (e. g. par coulée par gravité). Enfin, un autre avantage du procédé réside dans le fait qu'il fait appel à des produits qui étaient déjà utilisés comme **flux de désoxydation** et qu'il peut être mis en oeuvre **à l'air**.

Notre étude, à caractère fondamental, avait pour objectif d'identifier les mécanismes physico-chimiques impliqués dans la mise en oeuvre du procédé au K_2ZrF_6 et d'établir s'ils modifiaient le pouvoir renforçant des fibres de façon significative. Elle nous a permis ainsi : (1) d'expliquer l'efficacité du procédé en termes d'amélioration du mouillage dans le système SiC/Al, (2) de définir la participation du fluorure double K_2ZrF_6 ou/et des produits dérivés à l'affaiblissement mécanique de renforts filamentaires modèles de carbure de silicium et (3) d'attribuer, par une approche numérique, à chacun des paramètres physiques associés au procédé, un rôle spécifique dans l'amélioration de l'aptitude à l'imprégnation par l'aluminium liquide de préformes modèles à base de SiC.

(1) - En ce qui concerne les **bases physico-chimiques** susceptibles de rendre compte de l'**amélioration du mouillage**, nous avons montré que le schéma réactionnel suivant peut être proposé :

$$3\ "2KF,ZrF_4" + 4\ Al \rightleftharpoons "6KF,4AlF_3" + 3\ Zr \qquad [1]$$

$$9\ Al + 3\ Zr \rightleftharpoons 3\ Al_3Zr \qquad [2]$$

Il est en effet très favorisé d'un point de vue thermodynamique puisqu'à 973 K les variations d'enthalpie libre de Gibbs des réactions [1] et [2] sont respectivement - 306,4 et - 487,2 $kJ.mol^{-1}$. Ce schéma réactionnel reprend en partie les mécanismes qui avaient été antérieurement proposés par **LUNDIN** ainsi que par **BUSCHE** et **SEMENOV** pour rendre compte du rôle que pouvait jouer K_2ZrF_6 dans l'élaboration de feuilles bimétalliques acier/aluminium. Nous avons dû, dans l'écriture de la réaction [1], les modifier pour tenir compte du fait qu'aux températures considérées, K_2ZrF_6 est décomposé avec formation d'un liquide et de K_3ZrF_7 (le mélange étant représenté par "$2KF,ZrF_4$"). De même, au niveau du second membre, la notation "$6KF,4AlF_3$" a été utilisée pour représenter le mélange - liquide + K_3AlF_6 - qui se forme aux

températures considérées (et dont la solidification conduit à K_3AlF_6 + $KAlF_4$, après retour à l'ambiante).

Les réactions [1] et [2] sont **très exothermiques** ce qui justifie le rougeoiment qui est observé lorsqu'une préforme fibreuse prétraitée au K_2ZrF_6 est mise en contact avec un bain d'aluminium liquide. Les calculs ont en effet montré qu'une préforme modèle (ayant une porosité de 20% comparable à celle d'une préforme fibreuse 2D-SiC/SiC réelle) ainsi prétraitée et préchauffée à 650°C subissait une **élévation de température de 150°C** lorsqu'elle était imprégnée par de l'aluminium liquide coulé à 800°C.

Par ailleurs, la réaction [1] conduit à la formation de fluorures doubles d'aluminium et de potassium, **en partie liquide**, qui ont la propriété de **dissoudre la couche d'alumine** qui recouvre la surface de l'aluminium liquide et inhibe le mouillage de la céramique par le métal. Pour établir cette importante propriété, nous avons dû, dans un premier temps, procéder à une étude expérimentale des mélanges K_3AlF_6-Al_2O_3 par ATD et diffraction des rayons X et, dans un second temps, calculer une partie du diagramme de phases du **système ternaire réciproque KF-AlF_3-Al_2O_3-K_2O** (sur la base de la théorie CIS pour décrire la phase liquide). Ce travail nous a permis de tracer la section verticale "6KF,4AlF_3"-Al_2O_3 et de montrer que le mélange de fluorures doubles "6KF,4AlF_3" : (i) était susceptible de dissoudre la pellicule d'alumine dès 520°C et (ii) formait avec l'alumine (pour quelques % d'alumine en moles) un **liquide cryolithique homogène et très fluide à 800°C** (comparable à celui, à base de sodium, utilisé dans la fabrication par electrolyse de l'aluminium).

Lors de l'imprégnation d'une préforme fibreuse de SiC, prétraitée par K_2ZrF_6 et préchauffée à 650°C, le liquide cryolithique qui se forme au niveau des interfaces fibre/matrice quitte ces dernières (en raison de sa fluidité et de sa plus faible densité) pour se rassembler à la surface du métal liquide en entrainant avec lui, sous forme dissoute, l'alumine et permet le **contact direct SiC/Al**. Dans ces conditions, nous

avons pu conclure, en nous appuyant notamment sur une étude récente due à V. LAURENT, que la **dissolution du carbure de silicium dans le métal liquide** (étape limitante de la formation de Al_4C_3 par réaction entre SiC et l'aluminium liquide) était à l'origine du mouillage du renfort fibreux.

Il apparaît donc qu'au niveau des processus physico-chimiques susceptibles de justifier l'efficacité du procédé au K_2ZrF_6 deux phénomènes jouent un rôle particulièrement important : (i) l'**exothermicité** des réactions interfaciales entre K_2ZrF_6 et l'aluminium et (ii) la formation de **fluorures doubles KF-AlF_3 qui dissolvent l'alumine** en formant un liquide cryolithique drainant l'oxygène vers la surface de l'aluminium liquide. L'extraction de l'oxygène permet ensuite la formation des interfaces vraies SiC/Al, l'abaissement de l'angle de contact (qui passe de 160° à 75° en présence de K_2ZrF_6 à 750°C) étant lié à la formation de Al_4C_3.

(2) - En ce qui concerne **l'affaiblissement mécanique** du renfort qui pourrait résulter de la mise en oeuvre du procédé au K_2ZrF_6, l'étude que nous avons poursuivie sur un **matériau modèle** (filament CVD de SiC de grand diamètre antérieurement étudié au Laboratoire par R. PAILLER, P. MARTINEAU et Y. LE PETITCORPS) a permis d'identifier la contribution de chacune des étapes du procédé. Il a paru logique d'utiliser comme critère la résistance à rupture en raison de la sensibilité de cette propriété mécanique aux modifications de l'état de surface de l'éprouvette (pouvant résulter, par exemple, d'une réaction chimique interfaciale avec l'aluminium). Toutes les mesures ont fait l'objet d'**un traitement statistique** (loi de distribution de Weibull à deux paramètres) ce qui nous a conduit à tester, pour chaque étape, une quarantaine d'éprouvettes monofilamentaires.

Les résultats de notre étude ont clairement montré que : (i) l'opération de précipitation des cristaux de K_2ZrF_6, à partir de la solution aqueuse à 80-100°C, à la surface des filaments et (ii) le recuit à 650°C des filaments prétraités, n'affaiblissaient

que **très légèrement** la résistance à rupture des filaments (20% au plus). En revanche, en présence d'aluminium, le traitement est sensiblement plus dégradant et nous avons pu justifier cet effet et le relier à des causes physico-chimiques.

En effet, l'observation au MEB des faciès de rupture primaire et de la surface des filaments, une fois extraits de la matrice d'aluminium (dissoute par une solution aqueuse de soude), montre que des **piqûres** se sont formées en surface lors du maintien en température (résultant de l'élaboration du composite SiC/Al par compression à chaud). Ces piqûres se sont révélées être les empreintes laissées, après dissolution, par des **microcristaux de Al_4C_3** (dissous, comme l'aluminium, par la soude). L'emploi d'un réactif plus sélectif, i.e. d'une solution de méthanol bromé, a permis de dissoudre la matrice d'aluminium tout en conservant les cristaux de Al_4C_3 dont la composition a été établie à la fois par microsonde de Castaing et spectrométrie d'électrons Auger. Ainsi, l'affaiblissement de résistance mécanique des filaments résulte d'un **effet d'entaille** exercé sur le filament par les cristaux fragiles de Al_4C_3 formés en surface aux dépens de SiC et dont les racines pénètrent, sous la forme de coins, en profondeur. L'affaiblissement de la résistance des fibres de carbone ou de carbure de silicium, dû à une réaction avec l'aluminium, est un phénomène par ailleurs bien établi.

Il est essentiel de noter que le fluorure K_2ZrF_6, ou/et ses produits de réaction avec l'aluminium, n'interviennent **directement que de façon faible** dans l'affaiblissement de la résistance à rupture du renfort. En revanche, sur la base de l'effet de nettoyage de l'interface SiC/Al (i.e. extraction de l'alumine qui la contamine) et de l'effet thermique (lié à l'exothermicité des réactions), les fluorures contribuent à **activer la cinétique de formation de Al_4C_3** et ont, de ce fait, un rôle indirect sur l'affaiblissement mécanique du renfort (la formation de Al_4C_3 dans les composites n'ayant pas fait l'objet du traitement au K_2ZrF_6 pouvant se trouver ralenti par un effet de barrière dû à l'alumine).

(3) - En ce qui concerne, enfin, l'**amélioration de l'aptitude à l'imprégnation** du renfort fibreux par l'aluminium, liée au procédé au K_2ZrF_6, nous avons cru approprié de faire appel à une modélisation numérique qui avait été développée par **J. M. QUENISSET** et ses collaborateurs pour les préformes unidirectionnelles. Afin de ne pas trop nous éloigner des préformes 2D-SiC/SiC, élaborées par densification CVI d'un empilement de tissus de fibres Nicalon et qui avaient servi de base à l'étude expérimentale de **J. P. ROCHER**, nous avons défini une **préforme modèle** constituée d'un empilement hexagonal de cylindres fibreux de SiC, ayant la même porosité (i.e. 20%) que les préformes 2D-SiC/SiC. Cette condition a conduit à donner à ces cylindres un diamètre de 480 µm qui est bien du même ordre de grandeur que le diamètre des mèches de fibres Nicalon imprégnées de SiC par CVI, dans les préformes réelles. En revanche, il est clair que la préforme modèle ne restitue pas la morphologie effective du réseau de pores des préformes 2D-SiC/SiC. Cette partie de notre étude a donc essentiellement un caractère comparatif.

Sur la base de l'**approche numérique** qui a été développée pour la préforme modèle, supposée avoir été traitée (ou non) par K_2ZrF_6 puis imprégnée par l'aluminium dans des conditions identiques à celles effectivement utilisées pour les préformes 2D-SiC/SiC, il apparait que les deux principaux phénomènes physico-chimiques i.e. l'exothermicité des réactions [1] et [2] et l'abaissement de l'angle de contact, ont une influence distincte sur les paramètres d'imprégnation :

- d'une part, l'**exothermicité des réactions** permet d'augmenter de manière significative la profondeur de préforme imprégnée, qui peut même dans certains cas devenir infinie. En effet, la chaleur dégagée in situ par les réactions [1] et [2] compense le refroidissement du métal (la température de la préforme est de 650°C seulement), supposé être coulé à 800°C, au fur et à mesure qu'il progresse dans la préforme en évitant sa solidification prématurée. L'apport de chaleur dû à l'exothermicité des réactions [1] et [2] est particulièrement bénéfique pour les

préformes caractérisées par des fractions volumiques élévées de fibres (pour lesquelles le métal se solidifie à une profondeur inférieure au cm quand elles n'ont pas été traitées par K_2ZrF_6).

- d'autre part, l'**abaissement de l'angle de contact** permet de diminuer la pression d'imprégnation qu'il est nécessaire d'appliquer au métal pour qu'il atteigne, avant de se solidifier, une profondeur acceptable au sein de la préforme (i.e. quelques cm).

- le calcul a montré, enfin, qu'une **quantité minimale de K_2ZrF_6**, de l'ordre de 3 $mg.cm^{-2}$, était nécessaire pour maintenir l'aluminium à une température, i.e. 750°C, où il est suffisamment fluide et où l'angle de contact a une valeur suffisamment faible (θ=75°). Il est intéressant de noter que cette quantité correspond au remplissage complet de la porosité de la préforme par K_2ZrF_6 et qu'elle est proche de l'optimum établi expérimentalement (5 $mg.cm^{-2}$) pour la préforme réelle. De même, les calculs ont montré qu'il était possible d'identifier des conditions d'imprégnation pour lesquelles : (i) la **profondeur** d'imprégnation devenait **infinie** ou/et (ii) l'imprégnation pouvait se faire sans appliquer **aucune pression extérieure** sur le métal, autre que la pression métallostatique due au métal lui-même (imprégnation spontanée).

En résumé, la présente étude a permis, nous semble-t-il, d'atteindre les objectifs qui lui avaient été fixés dans la mesure où : (i) les bases physico-chimiques justifiant l'efficacité du procédé ont été dégagées et (ii) l'influence du procédé sur le pouvoir renforçant des fibres a été précisée. Le procédé au K_2ZrF_6 apparait ainsi de **mise en oeuvre particulièrement simple** puisqu'il peut s'opérer à l'air et ne fait appel qu'à des produits déjà utilisés comme flux désoxydant en fonderie d'alliages légers. De plus, il a été prouvé qu'il s'applique à des préformes fibreuses à base de carbure de silicium ou de carbone, de forme complexe, quelle que soit leur porosité. Le procédé, par l'exothermicité des réactions qu'il implique et l'abaissement de l'angle de

contact, permet l'**imprégnation spontanée**, e. g. par coulée par gravité, et complète des préformes. Cependant, il a également pour conséquence d'activer la formation du **carbure d'aluminium** aux interfaces fibre/matrice et, de **manière indirecte**, d'affaiblir ainsi de façon significative le pouvoir renforçant des fibres.

Sans pour autant remettre en cause l'intérêt du procédé au K_2ZrF_6, une voie permettant d'éviter l'effet négatif qui vient d'être noté, (et qui est intrinsèquement lié à la réactivité des systèmes C/Al et SiC/Al), serait (i) de faire appel à un renfort comportant un **revêtement compliant** (e. g. de pyrocarbone), en partie consommable, qui protègerait le renfort contre l'effet d'entaille dû aux cristaux de Al_4C_3 (des filaments CVD-SiC(C) existent dans le commerce) et (ii) d'envisager un refroidissement rapide (pour minimiser la durée du contact à haute température entre SiC et Al) tel que ceux qui sont mis en oeuvre en **imprégnation par forgeage liquide**. Dans ce dernier cas, on peut penser, sur la base des conclusions de la présente étude, que les pressions de forgeage liquide (qui sont actuellement de 50 à 100 MPa) pourraient être considérablement abaissées.

ANNEXE I

APPLICATION DE LA THEORIE CIS (CONFORMAL IONIC SOLUTION) AUX SYSTEMES TERNAIRES RECIPROQUES

L'étude expérimentale des systèmes polyconstitués est en général très consommatrice de temps. De plus, la difficulté d'une telle étude augmente très rapidement avec le nombre des espèces considérées. Il est donc utile de pouvoir estimer les propriétés thermodynamiques de ces systèmes.

Afin de mieux comprendre le comportement des solutions ionisées qui jouent un rôle essentiel dans certaines technologies, comme par exemple le procédé électrolytique de Hall-Héroult, des concepts généraux et des théories sur les systèmes de sels fondus ont été développés. Ainsi, grâce à la théorie CIS, l'expression analytique de l'énergie libre de Gibbs de mélange de la phase liquide peut être décrite, ce qui permet de calculer à priori le diagramme de phases de tels systèmes (1). La théorie CIS est une théorie de mécanique statistique qui tiend compte de façon rigoureuse des interactions électrostatiques entre les ions de même charge constituant un mélange de sels fondus. Elle ne fait intervenir, dans les expressions qui décrivent les propriétés thermodynamiques de ces mélanges, que les données thermodynamiques des sels constituants purs et de leurs mélanges binaires. La théorie CIS et son extension empirique aux systèmes constitués de charges différentes conduit à des diagrammes calculés, en général en très bon accord avec les mesures expérimentales, comme par exemple, ceux des systèmes AlF_3-LiF-NaF, AlF_3-CaF_2-LiF, AlF_3-CaF_2-NaF et CaF_2-LiF-NaF intervenant dans le procédé électrolytique de Hall-Héroult (2-9).

Blander et Yosim ont appliqué la théorie CIS au plus simple des systèmes ternaires réciproques (10). Un tel système est constitué de deux cations A^+, B^+ et de deux anions C^-, D^-, de charge unitaire, auxquels correspondent les sels AC, BC, AD et BD. La théorie CIS est une théorie de perturbation dans laquelle les sels constituants et leurs mélanges sont générés à partir d'un sel "test" hypothétique utilisé comme référence. Reprenons le développement de Blander et Yosim. Soient λ le paramètre de taille caractéristique du sel "test" et λ_1, λ_2, λ_3, λ_4 ceux des sels AC, BC, AD et BD respectivement. On définit alors les quatre paramètres de perturbation g_i tels que :

$$g_i = \frac{\lambda}{\lambda_i} \qquad i=1, 2, 3, 4$$

Selon la statistique de Boltzmann, l'intégrale de configuration du sel "test", qui est un arrangement de N cations et N anions de même charge auquel est associé l'énergie potentielle U, s'écrit :

$$Z = \frac{1}{(N!)^2} \int..\int \exp(-U/kT)\,(d\tau)^{2N}$$

$(d\tau)$ = combinaison des éléments de volume des 2N ions

k = constante de Boltzmann

Pour une configuration ionique donnée du sel "test ", U peut s'exprimer selon la somme des interactions au sein de paires d'ions (c: cation, a: anion) par la relation :

$$U = \sum_{c}^{N}\sum_{a}^{N} u_{ca} + \sum_{c}\sum_{c<c'} u_{cc'} + \sum_{a}\sum_{a<a'} u_{aa'}$$

L'écriture c<c' et a<a' signifie que chaque paire cation-cation, anion-anion est prise en compte une seule fois. A cause de la forte tendance locale à la neutralité

électrique, les configurations pour lesquelles deux ions de même signe sont proches voisins sont peu probables et ne contribuent que de façon négligeable à l'intégrale de configuration. Des mesures de diffraction des rayons X et des neutrons sur des sels fondus ont confirmé cette hypothèse. En conséquence, la majeure variation de Z qui est due à la variation de la taille des ions du sel "test" peut être reliée aux sommes des rayons cation-anion et aux paramètres de perturbation g_i. Ainsi, dans les configurations les plus probables, $u_{cc'}$ et $u_{aa'}$ sont indépendants des g_i.

Définissons maintenant un mélange d'ions (Conformal Ionic Mixture) tel que l'énergie d'interaction u_{ca} pour toute paire cation-anion qu'il contient s'exprime sous la forme d'une somme de deux termes : un premier terme $h_{ca}(r)$, qui dépend uniquement de la distance entre les centres cation-anion, r, telles que l'interaction coulombienne, l'interaction ion-multipole, et un second terme $f_{ca}(g_i r)$ qui dépend de la taille des ions à travers le produit $g_i r$, tel que le potentiel répulsif de sphères dures utilisé par Reiss (1). Alors, pour un "mélange ionique conforme" tel que celui des ions A^+, B^+, C^- et D^- :

$$u_{ca} = f_{ca}(g_i r) + h_{ca}(r)$$

$$h_{ca}(r) = h_1(r) = h_2(r) = h_3(r) = h_4(r)$$

où 1, 2, 3 et 4 désignent respectivement les paires AC, BC, AD et BD

$$U_m = \sum_c^{N_A}\sum_a^{N_C} f_{ca}(g_1 r) + \sum_c^{N_B}\sum_a^{N_C} f_{ca}(g_2 r) + \sum_c^{N_A}\sum_a^{N_D} f_{ca}(g_3 r) + \sum_c^{N_B}\sum_a^{N_D} f_{ca}(g_4 r)$$

$$+ \sum_c^{N}\sum_a^{N} h_{ca}(r) + \sum_c \sum_{c<c'} u_{cc'} + \sum_a \sum_{a<a'} u_{aa'}$$

et $$Z_m = \frac{1}{N_A!\, N_B!\, N_C!\, N_D!} \int..\int \exp(-U_m/kT)\,(d\tau)^{2N}$$

où $N = N_A + N_B = N_C + N_D$ (condition de neutralité électrique) et N_A, N_B, N_C, et N_D désignent les nombres de moles d'ions A^+, B^+, C^- et D^-. Or l'énergie libre de Gibbs du mélange, G_m, est liée à la fonction de partition* par la relation classique :

$$- G_m/kT = \ln Z_m$$

Le développement au deuxième ordre de G_m autour de la valeur lnZ du sel "test" conduit à :

$$\ln Z_m = (\ln Z_m)_{g=1} + \sum_{i=1}^{4} \left(\frac{\ln Z_m}{g_i}\right)_{g=1} (g_i-1) + \sum_{i=1}^{4}\sum_{j=1}^{4} 1/2 \left(\frac{^2 \ln Z_m}{g_i\, g_j}\right)_{g=1} (g_i-1)(g_j-1)$$

l'écriture $(\ )_{g=1}$ signifie la valeur limite lorsque tous les g_i approchent l'unité avec,

$$(\ln Z_m)_{g=1} = \left[\ln\left(\frac{(N!)^2}{N_A!\, N_B!\, N_C!\, N_D!} \frac{1}{(N!)^2} \int..\int \exp(-U_m/kT)\, (d\tau)^{2N}\right)\right]_{g=1}$$

$$= - (N_A \ln X_A + N_B \ln X_B + N_C \ln X_C + N_D \ln X_D) + \ln Z$$

la formule de Stirling a été utilisée pour le développement des factorielles et les fractions ioniques sont définies par :

$$X_A = \frac{N_A}{N_A+N_B} = \frac{N_A}{N} = 1-X_B$$

$$X_C = \frac{N_C}{N_C+N_D} = \frac{N_C}{N} = 1-X_C$$

---

* Rigoureusement, la fonction de partition est le produit de l'intégrale de configuration et de l'intégrale cinétique. Cependant, la partie cinétique sera volontairement ignorée pour la brièveté du calcul étant donné qu'elle s'élimine systématiquement au moment du résultat final où l'on ne prend en compte que la différence entre les valeurs des grandeurs thermodynamiques du mélange et de ses constituants.

De la même façon pour le sel pur i (i=1, 2, 3, 4) :

$$U_i = \sum_c^N \sum_a^N f_{ca}(g_i r) + \sum_c^N \sum_a^N h_{ca}(r) + \sum_c \sum_{c<c'} u_{cc'} + \sum_a \sum_{a<a'} u_{aa'}$$

$$Z_i = \frac{1}{(N!)^2} \int..\int \exp(-U_i/kT)\,(d\tau)^{2N}$$

et le développement de l'énergie libre de Gibbs G_i autour de la valeur du sel "test" est :

$$-G_i/kT = \ln Z_i = \ln Z + \left(\frac{\ln Z_i}{g_i}\right)_{g=1} (g_i-1) + 1/2 \left(\frac{^2 \ln Z_i}{g_i^2}\right)_{g=1} (g_i-1)^2 + ...$$

De longs calculs de dérivation et de nombreuses simplifications d'écriture conduisent finalement aux expressions suivantes pour les énergies libres de Gibbs par mole de sel pur i, G_i, et par mole de mélange, G_m (10) :

$$-G_i/RT = \ln Z + \frac{F}{Z'}(g_i-1) + 1/2 \left[\frac{1}{Z'}(J + \mathcal{N}K + \mathcal{N}L + \mathcal{N}^2 M) - (\frac{F}{Z'})^2 \right] (g_i-1)^2$$

$$-G_m/RT = \ln Z - X_A \ln X_A - X_B \ln X_B - X_C \ln X_C - X_D \ln X_D$$

$$+ \sum_c \sum_a X_c X_a \left\{ \frac{F}{Z'}(g_i-1) + 1/2 \left[\frac{1}{Z'}(J + \mathcal{N}K + \mathcal{N}L + \mathcal{N}^2 M) - (\frac{F}{Z'})^2 \right] (g_i-1)^2 \right\}$$

$$- X_C X_D\, 1/2 \left[\frac{1}{Z'}(\mathcal{N}L + \mathcal{N}^2 M) - (\frac{F}{Z'})^2 \right] \left[X_A (g_1-g_3)^2 + X_B (g_2-g_4)^2 \right]$$

$$- X_A X_B\, 1/2 \left[\frac{1}{Z'}(\mathcal{N}L + \mathcal{N}^2 M) - (\frac{F}{Z'})^2 \right] \left[X_C (g_1-g_2)^2 + X_D (g_3-g_4)^2 \right]$$

$$+ X_A X_B X_C X_D\, 1/2 \left[\frac{\mathcal{N}^2 M}{Z'} - (\frac{F}{Z'})^2 \right] (g_1 + g_4 - g_2 - g_3)^2$$

$\mathcal{N}$ désigne le nombre d'Avogadro

$Z' = (\mathcal{N}!)^2 Z$

F, J, K, L et M sont des intégrales de la forme :

$$(1/kT) \text{ ou } (1/kT)^2 \int..\int \exp(-U_m/kT)\,(d\tau)^{2N}$$

et résultent des dérivations $\left(\frac{Z_i}{g_i}\right)_{g_i=1}$ et $\left(\frac{^2 Z_i}{g_i\, g_j}\right)_{g_i=1}$

Dans le développement de G_m, l'expression :

$$\ln Z + \sum_c \sum_a X_c X_a \left\{ \frac{F}{Z'}(g_i-1) + 1/2 \left[\frac{1}{Z'}(J + \mathcal{N}K + \mathcal{N}L + \mathcal{N}^2 M) - \left(\frac{F}{Z'}\right)^2 \right](g_i-1)^2 \right\}$$

peut aussi s'écrire :

$$\ln Z + \sum_c \sum_a X_c X_a \left\{ -G_i/RT - \ln Z \right\}$$

$$= \ln Z - \sum_c \sum_a X_c X_a \,(-G_i/RT) - \ln Z \qquad \text{puisque } \sum_c \sum_a X_c X_a = 1$$

Par ailleurs, l'expression extrapolée de G_m dans le cas où le mélange est constitué de deux sels uniquement, par exemple les sels AC et AD , notés 1 et 3 respectivement, est :

$$-G_m^{1-3}/RT = -X_C \ln X_C - X_D \ln X_D - X_C\, G_1/RT - X_D\, G_3/RT$$
$$- X_C X_D\, 1/2 \left[\frac{1}{Z'}(\mathcal{N}L + \mathcal{N}^2 M) - \left(\frac{F}{Z'}\right)^2 \right] (g_1-g_3)^2$$

que l'on peut aussi écrire :

$$G_m^{1-3} = RT\,(X_C \ln X_C + X_D \ln X_D) + X_C\, G_1 + X_D\, G_3 + \Delta G_{1-3}^E$$

où ΔG_{1-3}^E est l'énergie libre de Gibbs d'excès de formation du mélange 1-3 référée aux sels 1 et 3. De la même façon, on pourrait définir ΔG_{1-2}^E, ΔG_{2-4}^E et ΔG_{3-4}^E.

Compte-tenu de ces deux remarques, l'expression simplifiée de l'énergie libre de Gibbs du mélange des ions A^+, B^+, C^- et D^- devient :

$$G_m = RT\,(X_A \ln X_A + X_B \ln X_B + X_C \ln X_C + X_D \ln X_D) + \sum_c \sum_a X_c\, X_a\; G_i$$
$$+ X_A\, \Delta G^E_{1\text{-}3} + X_B\, \Delta G^E_{2\text{-}4} + X_C\, \Delta G^E_{1\text{-}2} + X_D\, \Delta G^E_{3\text{-}4}$$
$$- X_A\, X_B\, X_C\, X_D\; P\; (g_1 + g_4 - g_2 - g_3)^2$$

avec $P = 1/2 \left[\frac{N^2 M}{Z'} - \left(\frac{F}{Z'}\right)^2 \right]$

et rappelons que 1, 2, 3 et 4 désignent les sels AC, BC, AD et BD respectivement.

Seul le dernier terme de cette expression ne peut se déduire de la théorie CIS. Cependant, par comparaison avec le terme correspondant de la théorie du quasi-réseau (11), il est pris proportionnel à ΔG^2 (10) où ΔG est l'énergie libre de Gibbs standard associée à la relation d'échange :

$$AC + BD \quad AD + BC \qquad [1]$$

Le coefficient de proportionnalité est -1/2ZRT. Z est le nombre de coordination du quasi-réseau. Ce dernier terme rend compte du mélange non aléatoire des ions dans la solution étant donnée la relation [1].

Alors, puisque :

$$\sum_c \sum_a X_c\, X_a\; G_i = X_A\, X_C\, G_{AC} + X_A\, X_D\, G_{AD} + X_B\, X_C\, G_{BC} + X_B\, X_D\, G_{BD}$$
$$= X_A\, X_C\, [\Delta G_{AC} + G^\circ_A + G^\circ_C)\,] + X_A\, X_D\, [\Delta G_{AD} + G^\circ_A + G^\circ_D\,]$$
$$+ X_B\, X_C\, [\Delta G_{BC} + G^\circ_B + G^\circ_C\,] + X_B\, X_D\, [\Delta G_{BD} + G^\circ_B + G^\circ_D\,]$$
$$= \sum_c \sum_a X_c\, X_a\; \Delta G^\circ_i + X_A G^\circ_A + X_B G^\circ_B + X_C\, G^\circ_C + X_D G^\circ_D$$

l'énergie libre de Gibbs de formation par mole de mélange de la phase liquide du système ternaire réciproque AC, BC, AD, BD référée aux éléments simples A, B, C et D pris dans leur état standard s'exprime par la relation :

$$\Delta G_m = G_m - X_A G^\circ_A - X_B G^\circ_B - X_C G^\circ_C - X_D G^\circ_D$$

$$= RT\,(X_A \ln X_A + X_B \ln X_B + X_C \ln X_C + X_D \ln X_D)$$

$$+ \sum_c \sum_a X_c X_a \Delta G^\circ_i + X_A \Delta G^E_{1\text{-}3} + X_B \Delta G^E_{2\text{-}4} + X_C \Delta G^E_{1\text{-}2} + X_D \Delta G^E_{3\text{-}4}$$

$$- X_A X_B X_C X_D \Delta G[1]^2/2ZRT$$

La théorie CIS a été étendue de façon empirique par M. L. Saboungi et M. Blander aux systèmes ternaires réciproques constitués d'ions de charges différentes (4). Comme T. Forland l'avait déjà proposé, avec succès, dans le cas des systèmes binaires, il s'agit de remplacer dans l'expression de l'énergie libre de Gibbs d'excès les fractions ioniques (X) par les fractions d'équivalents (Y) , tout en conservant les fractions ioniques dans l'expression du terme de mélange idéal. Soit le système ternaire réciproque $A_{qC}C_{qA}$-$A_{qD}D_{qA}$-$B_{qC}C_{qB}$-$B_{qD}D_{qB}$ (noté ultérieurement AC-AD-BC-BD) basé sur le mélange des ions A^{+qA}, B^{+qB}, C^{+qC}, D^{+qD}, et auquel est associé la relation d'échange :

$$(q_A q_C)^{-1}\,AC + (q_B q_D)^{-1}\,BD \quad (q_A q_D)^{-1}\,AD + (q_B q_C)^{-1}\,BC \qquad [2]$$

Les fractions d'équivalents sont définies par :

$$Y_A = \frac{q_A N_A}{q_A N_A + q_B N_B} = \frac{q_A N_A}{N} = 1\text{-}Y_B$$

$$Y_C = \frac{q_C N_C}{q_C N_C + q_D N_D} = \frac{q_C N_C}{N} = 1\text{-}Y_D$$

où N_A, N_B, N_C et N_D sont les nombres de moles d'ions A^{+q_A}, B^{+q_B}, C^{-q_C} et D^{-q_D}

$N = q_A N_A + q_B N_B = q_C N_C + q_D N_D$ traduit la condition d'électroneutralité

L'énergie libre de Gibbs de formation de la phase liquide contenant N moles d'équivalents s'exprime selon la relation :

$$N\,\Delta G_m = RT \sum_c \sum_a N_{ca} \ln a_{ca}$$

où ΔG_m est l'énergie libre de Gibbs par mole d'équivalent

N_{ca} est le nombre de moles de l'espèce ca avec ca = AC, AD, BC, BD

a_{ca} est l'activité de chaque composé, définie selon :

$$a_{AC} = X_A^{q_C} X_C^{q_A} \ln\gamma_{AC}$$

$$a_{AD} = X_A^{q_D} X_D^{q_A} \ln\gamma_{AD}$$

$$a_{BC} = X_B^{q_C} X_C^{q_B} \ln\gamma_{BC}$$

$$a_{BD} = X_B^{q_D} X_D^{q_B} \ln\gamma_{BD}$$

γ_{ca} est le coefficient d'activité du composé ca

Donc,

$$\Delta G_m = RT/N \left[N_{AC} \ln X_A^{q_C} X_C^{q_A} + N_{BC} \ln X_B^{q_C} X_C^{q_B} \right.$$

$$\left. + N_{AD} \ln X_A^{q_D} X_D^{q_A} + N_{BD} \ln X_B^{q_D} X_D^{q_B} \right] + RT/N \sum_c \sum_a N_{ca} \ln \gamma_{ca}$$

Le premier terme, entropie de configuration du mélange idéal, s'exprime en fonction des fractions ioniques :

$$\Delta G_m^{id} = RT/N \left[(q_C N_{AC} + q_D N_{AD}) \ln X_A + (q_C N_{BC} + q_D N_{BD}) \ln X_B \right.$$

$$\left. + (q_A N_{AC} + q_B N_{BC}) \ln X_C + (q_A N_{AD} + q_B N_{BD}) \ln X_D \right]$$

$$= RT/N \, (N_A \ln X_A + N_B \ln X_B + N_C \ln X_C + N_D \ln X_D)$$

et le second terme, énergie libre de Gibbs d'excès du mélange référée aux éléments purs A, B, C et D, s'exprime en fonction des fractions d'équivalents par extrapolation du formalisme de la théorie CIS :

$$\Delta G_m^{id} = \sum_c \sum_a Y_c \, Y_a \, \Delta G^{\circ}_{ca}/q_a \, q_c$$

$$+ Y_A \, \Delta G^E_{AC\text{-}AD} + Y_B \, \Delta G^E_{BC\text{-}BD} + Y_C \, \Delta G^E_{AC\text{-}BC} + Y_D \, \Delta G^E_{AD\text{-}BD}$$

$$- Y_A \, Y_B \, Y_C \, Y_D \, \Delta G[2]^2/2ZRT$$

BIBLIOGRAPHIE

(1) - H. Reiss, J. L. Katz, O. J. Kleppa, J. Chem. Phys. 36 (1962)144

(2) - M. Blander, L. E. Topol, Inorg. Chem. 5 (1966) 1641

(3) - M. L. Saboungi, M. Blander, High Temp. Sci. 6 (1974) 37

(4) - M. L. Saboungi, M. Blander, J. Am. Ceram. Soc. 58 (1975) 1

(5) - M. L. Saboungi, P. Cerisier, J. Electrochem. Soc. 121 (1974) 1258

(6) - T. Foosnaes, T. Ostvold, H. A. Oye, Acta Chem. Scand. A32 (1978) 973

(7) - M. L. Saboungi, C. Bale, P. L. Lin, M. Blander, A. Pelton, Extended Abstract N°.157, Vol.79-2, The Electrochemical Society (1979)

(8) - M. L. Saboungi, P. L. Lin, P. Cerisier, A. Pelton, Met. Trans. 11B (1980) 493

(9) - M. L. Saboungi, H. Schnyders, M. S. Foster, M. Blander, J. Phys. Chem. 78 (1974) 1091

(10) - M. Blander, S. J. Yosim, J. Chem. Phys. 39 (1963) 2610

(11) - M. Blander, M. Braunstein, Ann. N. Y. Acad. Sci. 79 (1960) 838

(12) - T. Forland, Norg. Tek. Vitenskapsakad., Ser.2, N°.4 (1957)

ANNEXE II

ESTIMATION DES GRANDEURS THERMODYNAMIQUES D'UN SYSTEME A PARTIR DE SON DIAGRAMME DE PHASES EXPERIMENTAL

Un diagramme d'équilibre de phases permet de représenter les domaines de phases stables d'un système pour des conditions données de pression, température et composition. Jusqu'aux années cinquante, les diagrammes de phases ont été essentiellement établis à partir de mesures expérimentales par les métallurgistes ou les céramistes . Parallèlement mais indépendamment, les chimistes mesuraient les grandeurs thermodynamiques de ces phases. Ce n'est que depuis environ quinze ans que l'approche thermodynamique du diagramme de phases a pris son essor. L'état stable d'un système polyconstitué étant associé au minimum de son énergie libre de Gibbs à pression et température constantes, il est possible de calculer à partir des grandeurs thermodynamiques d'un système son diagramme de phases moyennant une description analytique adaptée de ces grandeurs. Ces deux approches du diagramme de phases permettent, une fois mises en cohérence, une description intégrée de l'ensemble des propriétés d'un système.

En dehors des systèmes binaires métalliques les plus usités, le nombre de systèmes pour lesquels il existe à la fois une détermination expérimentale et calculée du diagramme de phases est encore limité. Aussi, lorsque les grandeurs thermodynamiques d'un système ne sont pas disponibles, il est possible de les estimer à partir du diagramme de phases expérimental quand il existe. Les valeurs ainsi obtenues ne sont qu'indicatives et elles devront être confirmées par l'expérience.

Illustrons cette démarche à partir du diagramme de phases expérimental du système binaire Ga-Sb représenté à la figure 1. Ce système est constitué de deux éléments Ga et Sb de structures notées respectivement α et γ , du composé défini GaSb de structure notée β et enfin d'une phase liquide notée L. Il s'agit de déterminer la variation d'énergie libre de Gibbs qui accompagne la réaction :

$$(1\text{-}X)\ (Ga)_L + X\ (Sb)_L \ \Delta\ (Ga_{1-X}Sb_X)_L \qquad \text{(noté } L_X\text{)}$$

Son expression est:

$$\Delta G^{L_X} = G^{L_X} - X\, G^{L_X}_{Sb} - (1\text{-}X)\, G^{L_X}_{Ga}$$

$$= RT\,[X \ln X + (1\text{-}X) \ln(1\text{-}X)] + \Delta G^{L_X}_{xs} \qquad [1]$$

où X est la fraction molaire en Sb; $G^{L_X}_{Sb}$ et $G^{L_X}_{Ga}$ sont les énergies libres de Gibbs de Sb et Ga purs liquides; $\Delta G^{L_X}_{xs}$ est l'énergie libre de Gibbs d'excès de formation de la phase liquide; elle peut être modélisée sous la forme :

$$\Delta G^{L_X}_{xs} = X\,(1\text{-}X)\, g(X, T) \qquad [2]$$

où g est une fonction polynômiale de X et de T.

Le diagramme isobare, isotherme, énergie libre de Gibbs-composition (noté ΔG-X) d'un système est un outil pratique pour visualiser et comprendre les problèmes de stabilité et d'énergie des différentes phases en équilibre. Comme il est montré à la figure 2, le diagramme ΔG-X du système Ga-Sb, à 800K par exemple, permet de retrouver les limites de phases expérimentales. Etant donné que la grandeur énergie libre de Gibbs ne peut être connue en valeur absolue, seules les variations des énergies libres de Gibbs des différentes phases du système par rapport à une référence qui dans ce cas est commune, à savoir Ga et Sb purs, liquides, sont

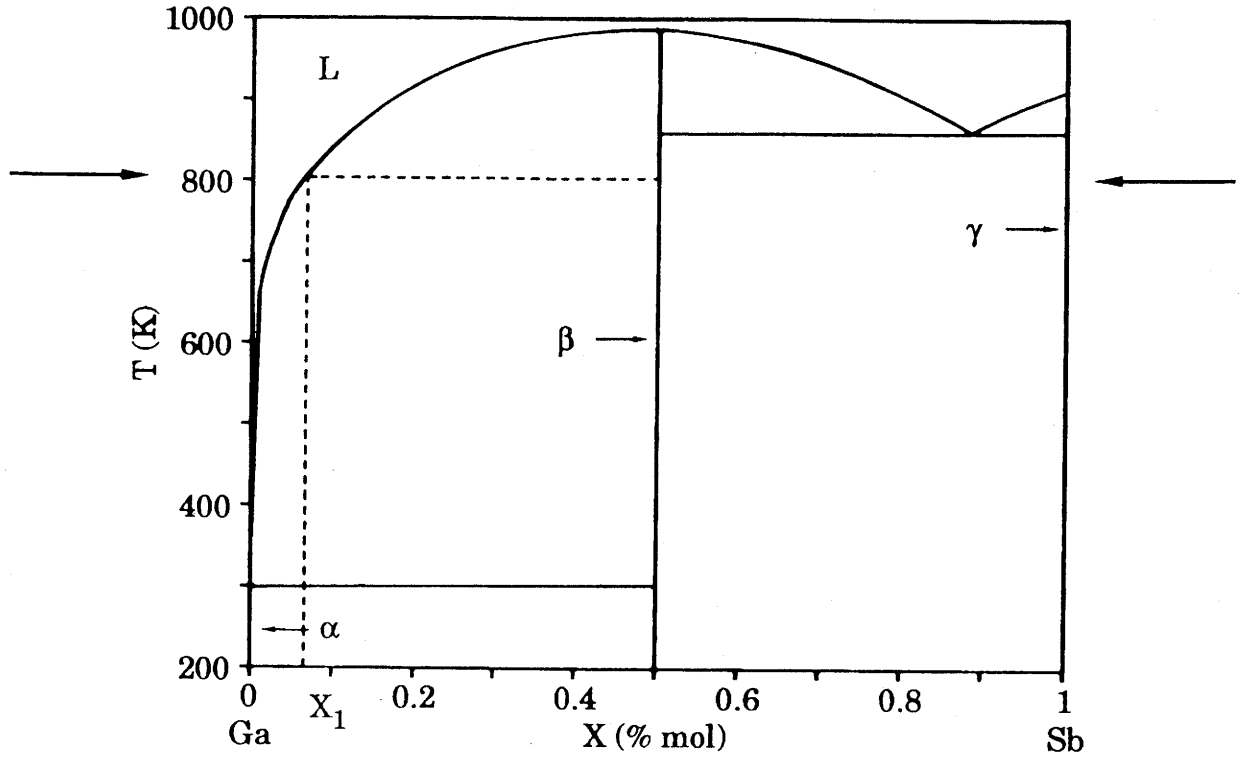

Figure 1: Diagramme de phases du système binaire Ga-Sb

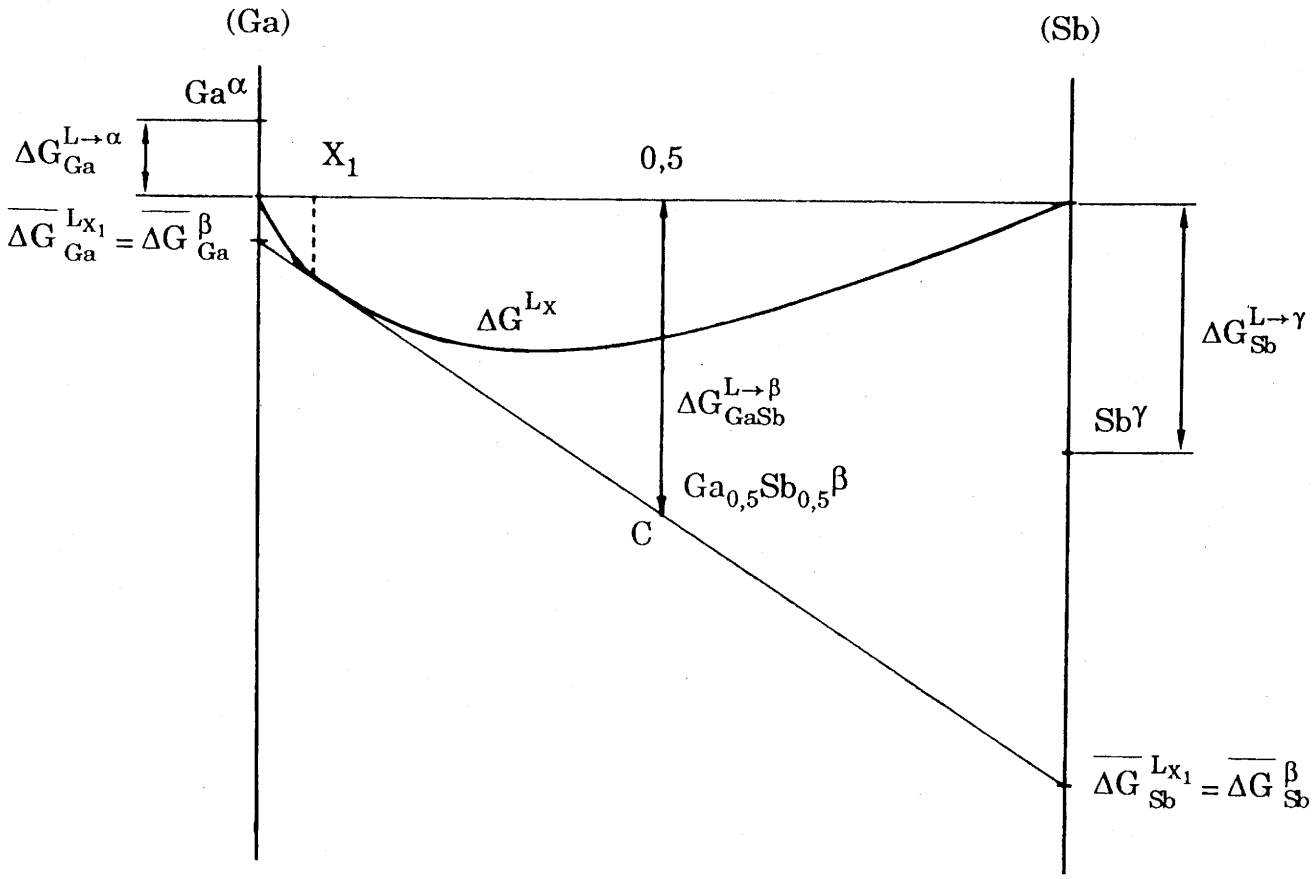

Figure 2: Diagramme ΔG-X du système binaire Ga-Sb à 800K

indiquées sur ce diagramme. Elles sont définies par les relations :

$$\Delta G^{L_X} = G^{L_X} - X\, G_{Sb}^{L_X} - (1-X)\, G_{Ga}^{L_X}$$

$$\Delta G_{Ga}^{L\rightarrow\alpha} = G_{Ga}^{\alpha} - G_{Ga}^{L}$$

$$\Delta G_{Sb}^{L\rightarrow\gamma} = G_{Sb}^{\gamma} - G_{Sb}^{L}$$

$$\Delta G_{GaSb}^{L\rightarrow\beta} = G_{GaSb}^{\beta} - 0{,}5\, G_{Ga}^{L} - 0{,}5\, G_{Sb}^{L}$$

L'équilibre

$$L_{X_1} \rightleftharpoons (GaSb)_{\beta} \qquad [3]$$

observé à 800K sur le diagramme de phases expérimental est illustré sur le diagramme ΔG-X par la tangente à la courbe ΔG^{L_X} à la composition X_1 menée à partir du point C qui correspond à l'énergie de formation du composé défini $Ga_{0,5}Sb_{0,5}$ (fig.2). Ce tracé traduit l'égalité des potentiels chimiques des éléments Ga et Sb à 800K dans les deux phases en équilibre. Elle peut s'exprimer par les relations :

$$\overline{\Delta G}_{Ga}^{L_{X_1}} = \overline{\Delta G}_{Ga}^{\beta} \qquad [4]$$

$$\overline{\Delta G}_{Sb}^{L_{X_1}} = \overline{\Delta G}_{Sb}^{\beta} \qquad [5]$$

En effet, par définition, le potentiel chimique ou énergie libre de Gibbs molaire partielle des éléments Ga et Sb dans une phase δ ($\delta = L_{X_1}, \beta$), de composition X, exprimé par rapport aux potentiels chimiques de référence (Ga et Sb purs, liquides) s'écrit:

$$\overline{\Delta G}_{Ga}^{\delta} = \Delta G^{\delta} - X \left(\frac{\partial \Delta G^{\delta}}{\partial X}\right)_{P,T} \qquad [6]$$

$$\overline{\Delta G}_{Sb}^{\delta} = \Delta G^{\delta} + (1-X) \left(\frac{\partial \Delta G^{\delta}}{\partial X}\right)_{P,T} \qquad [7]$$

Il résulte de ces expressions que l'intersection avec les axes notés (Ga) et (Sb) (fig.2) de la tangente à la courbe ΔG^{δ} correspond aux potentiels chimiques respectifs $\overline{\Delta G}^{\delta}_{Ga}$ et $\overline{\Delta G}^{\delta}_{Sb}$.

La combinaison des équations [1], [2], [4], [5], [6] et [7] conduit à :

$$\overline{\Delta G}^{L_{X_1}}_{Ga} = RT \ln(1-X_1) + X_1^2\, g(1-X_1, T) + X_1 (1-X_1) \left(\frac{\partial g}{\partial X}\right)_{X=1-X_1} \qquad [8]$$

$$\overline{\Delta G}^{L_{X_1}}_{Sb} = RT \ln X_1 + (1-X_1)^2\, g(X_1, T) + X_1 (1-X_1) \left(\frac{\partial g}{\partial X}\right)_{X=X_1} \qquad [9]$$

Quand aux variations d'énergie libre de Gibbs associées au passage de Ga et Sb purs, liquides, à Ga et Sb dans un état métastable de structure β, elles peuvent être représentées à l'aide d'une fonction polynômiale de T identique à celles que l'on utilise pour représenter les transitions entre phases stables :

$$\Delta G_{Ga}^{L\rightarrow\beta} = A + B\,T + \ldots \qquad [10]$$

$$\Delta G_{Sb}^{L\rightarrow\beta} = A' + B'\,T + \ldots \qquad [11]$$

Ainsi, l'égalité des expressions [8] et [10] d'une part et, [9] et [11] d'autre part, qui traduit la condition de l'équilibre [3], fournit deux équations dont les inconnues sont les paramètres de la fonction g et les paramètres A, B, A' et B'. La détermination complète de la fonction ΔG^{L_X} suppose donc que l'on écrive et que l'on résolve un système d'équations du type [8,10] et [9,11], dont le nombre doit être égal à celui des inconnues, à partir de l'observation du diagramme de phases expérimental à différentes températures. Dans le cas ou il existe des informations expérimentales suffisamment nombreuses, il est maintenent envisageable d'opérer à partir de programmes d'optimisation plus sophistiqués bien que utilisant les mêmes règles de base.